การพัฒนาอนุพันธ์ 8-ไฮดรอกซี-9-อิมินิลจูโลลิดีนเพื่อใช้เป็นฟลูออเรสเซนต์เซ็นเซอร์

นายธนพงศ์ เลิศพิริยะสกุลกิจ

วิทยานิพนธ์นี้เป็นส่วนหนึ่งของการศึกษาตามหลักสูตรปริญญาวิทยาศาสตรมหาบัณฑิต
สาขาวิชาปิโตรเคมีและวิทยาศาสตร์พอลิเมอร์
คณะวิทยาศาสตร์ จุฬาลงกรณ์มหาวิทยาลัย
ปีการศึกษา 2558
ลิขสิทธิ์ของจุฬาลงกรณ์มหาวิทยาลัย

DEVELOPMENT OF 8-HYDROXY-9-IMINYLJULOLIDINE DERIVATIVES AS FLUORESCENT
SENSORS

Mr. Thanaphong Lertpiriyasakulkit

A Thesis Submitted in Partial Fulfillment of the Requirements

for the Degree of Master of Science Program in Petrochemistry and Polymer Science

Faculty of Science

Chulalongkorn University

Academic Year 2015

Thesis Title   DEVELOPMENT OF 8- HYDROXY- 9-
                     IMINYLJULOLIDINE DERIVATIVES AS FLUORESCENT
                     SENSORS
By   Mr. Thanaphong Lertpiriyasakulkit
Field of Study   Petrochemistry and Polymer Science
Thesis Advisor   Assistant Professor Anawat Ajavakom, Ph.D.

Accepted by the Faculty of Science, Chulalongkorn University in Partial Fulfillment of the Requirements for the Master's Degree

....Dean of the Faculty of Science
(Associate Professor Polkit Sangvanich, Ph.D.)

THESIS COMMITTEE

....Chairman
(Assistant Professor Warinthorn Chavasiri, Ph.D.)

....Thesis Advisor
(Assistant Professor Anawat Ajavakom, Ph.D.)

....Examiner
(Chatr Panithipongwut, Ph.D.)

....External Examiner
(Assistant Professor Nantanit Wanichacheva, Ph.D.)

ธนพงศ์ เลิศพิริยะสกุลกิจ : การพัฒนาอนุพันธ์ 8-ไฮดรอกซี-9-อิมินิลจูโลลิดีนเพื่อใช้เป็นฟลูออเรสเซนต์เซ็นเซอร์ (DEVELOPMENT OF 8-HYDROXY-9-IMINYLJULOLIDINE DERIVATIVES AS FLUORESCENT SENSORS) อ.ที่ปรึกษาวิทยานิพนธ์หลัก: ผศ. ดร. อนวัช อาชวาคม, 124 หน้า.

การพัฒนาฟลูออเรสเซนต์เซนเซอร์ที่มีความจำเพาะกับไอออนของโลหะนั้นกลายเป็นสิ่งที่มีความจำเป็นอย่างยิ่ง ในงานวิจัยนี้ได้มุ่งเน้นในการดัดแปลงและพัฒนาตัวรับรู้ทางฟลูออเรสเซนต์ โดยได้เลือกใช้อนุพันธ์จูโลลิดีนเป็นหน่วยให้สัญญาณฟลูออเรสเซนต์เชื่อมต่อปฏิกิริยาแบบชิพเบสกับอนุพันธ์ของไดพิโคริลเอมีนแทนที่บนวงอะนิลีนที่ตำแหน่งต่างๆ ได้แก่ ออร์โท (J2P), เมทา (J3P) และพารา (J4P) ตามลำดับ ซึ่งทำหน้าที่เป็นหน่วยควบคุม จากผลการทดลองในสภาวะที่มีตัวทำละลายผสมน้ำ/เมทานอล ในอัตราส่วน 1:9 โดยปริมาตร พบว่าสารประกอบ J2P, J3P และ J4P มีค่าการดูดกลืนแสงสูงสุด (λ_{ab}) ที่ช่วงความยาวคลื่น 380, 415 และ 420 นาโนเมตร ตามลำดับ นอกจากนี้ยังพบว่าสารประกอบ J2P ให้การตอบสนองแบบขยายสัญญาณฟลูออเรสเซนต์อย่างมีนัยสำคัญกับไอออนของอลูมิเนียมเพียงชนิดเดียว โดยการเปล่งแสงฟลูออเรสเซนต์สูงสุดปรากฏที่ช่วงความยาวคลื่น 490 นาโนเมตร มีประสิทธิภาพการคายแสงเท่ากับ 0.156 และมีค่าคงที่การรวมตัว (K_a) เท่ากับ 2.25×10^5 M^{-1} นอกจากนี้เมื่อเปลี่ยนสภาวะตัวทำละลายผสมเป็น น้ำ/ไดเมทิลซัลฟอกไซด์ (5:95 โดยปริมาตร) ปรากฏว่าสารประกอบ J2P ให้การตอบสนองอย่างมีนัยสำคัญกับไอออนของแมกนีเซียมเพียงชนิดเดียว โดยพบการเปล่งแสงฟลูออเรสเซต์สูงสุดที่ช่วงความยาวคลื่น 470 นาโนเมตร มีประสิทธิภาพการคายแสงที่ช่วงความยาวคลื่นดังกล่าว เท่ากับ 0.096 และมีค่าคงที่ของการรวมตัว (K_a) ระหว่าง J2P กับ Mg^{2+} เท่ากับ 4.00×10^4 M^{-1} จากผลการศึกษาพบว่ารูปแบบของการรวมตัวระหว่างลิแกน J2P กับไอออนโลหะทั้งสองเกิดขึ้นในอัตราส่วน 1:1 พร้อมทั้งให้ค่าการตรวจวัดต่ำสุด (LOD) สำหรับไอออนอลูมิเนียมและไอออนแมกนีเซียมที่สภาวะดังกล่าวเท่ากับ 0.17 ไมโครโมลาร์ และ 1.32 ไมโครโมลาร์ ตามลำดับ จากผลการศึกษาคาดว่าปรากฏการณ์การขยายสัญญาณฟลูออเรสเซนต์ของโมเลกุลนั้นเกิดผ่านกลไก Chelation-enhanced fluorescence (CHEF).

สาขาวิชา   ปิโตรเคมีและวิทยาศาสตรพอลิเมอร์ ลายมือชื่อนิสิต ....

ปีการศึกษา 2558   ลายมือชื่อ อ.ที่ปรึกษาหลัก ....

5772006723 : MAJOR PETROCHEMISTRY AND POLYMER SCIENCE

KEYWORDS: FLUORESCENT SENSOR / FLUORESCENT SENSOR FOR MAGNESIUM ION / FLUORESCENT SENSOR FOR ALUMINIUM ION / JULOLIDINE- BASED FLUORESCENT SENSOR / IMINE-BASED FLUORESCENT SENSOR

THANAPHONG LERTPIRIYASAKULKIT: DEVELOPMENT OF 8- HYDROXY- 9- IMINYLJULOLIDINE DERIVATIVES AS FLUORESCENT SENSORS. ADVISOR: ASST. PROF. ANAWAT AJAVAKOM, Ph.D., 124 pp.

The development of fluorescent sensor which is specify toward metal ion become important. In this work, the fluorescent sensor containing julolidine derivative as a fluorophore linked with the control part using of dipicolylamine derivative substituted on aniline ring at *ortho*- (J2P), *meta*- (J3P) and *para*- (J4P) position, respectively, were successfully developed and synthesized via Schiff base reaction. According to the experimental results under the mixed solvent condition of H_2O/methanol (1:9, v/v), the maximum absorption bands of compounds J2P, J3P and J4P were observed at 380, 415 and 420 nm, respectively. Moreover, in the presence of aluminum ion (Al^{3+}), the fluorescent signals of compound J2P significantly enhanced. The maximum emission intensity appeared at 490 nm along with the fluorescence quantum yield as 0.156. The association constant (K_a) was calculated as 2.25×10^5 M^{-1}. Furthermore, when the solvent condition was changed to H_2O/DMSO (5:95, v/v), compound J2P provided significant response toward only magnesium ion (Mg^{2+}). The strongest fluorescent signal was observed at 470 nm with the fluorescence quantum yield as 0.096. The K_a value of the coordination between J2P and Mg^{2+} is 4.00×10^4 M^{-1}. The stoichiometric complexation between J2P ligand and both metal ion supported the formation of 1:1 and the detection limits (LOD) for Al^{3+} and Mg^{2+} detection under above conditions were 0.17 µM and 1.32 µM, respectively. In addition, the fluorescence enhancing phenomenon was extrapolated to occur through the Chelation- enhanced fluorescence (CHEF) mechanism.

Field of Study: Petrochemistry and   Student's Signature ....

                       Polymer Science   Advisor's Signature ....

Academic Year: 2015

ACKNOWLEDGEMENTS

CONTENTS

LIST OF FIGURE

LIST OF SCHEME

LIST OF TABLE

CHAPTER I

INTRODUCTION

1.1 Introduction of Julolidine

Julolidine is a heterocyclic aromatic compound of which tricyclic structure is composed of one aromatic ring and tertiary amine linked two aliphatic rings as shown in **Figure 1.1.**
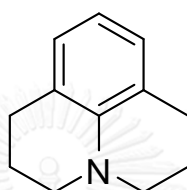
Figure 1.1 Basic structure of julolidine.

Julolidine was successfully synthesized by Pinkus in 1892 [1]. Since then this compound and its derivatives have found many interesting applications such as chemiluminescence substances [2], photoconductive materials [3], chromogenic substrates in analytical redox reactions [4], dye intermediates [5], potential antidepressants and tranquilizers [6], nonlinear optical materials [7], and color stability improving agent for red organic light-emitting diodes (OLEDs) [8].

In 1955, Glass and co-workers [9] demonstrated a method for one pot synthesis of julolidine using tetrahydroquinoline coupling with trimethylene chlorobromide in acidic condition under the high temperature up to 150-160 °C (**Figure 1.2**) to obtain julolidine in high product yield.
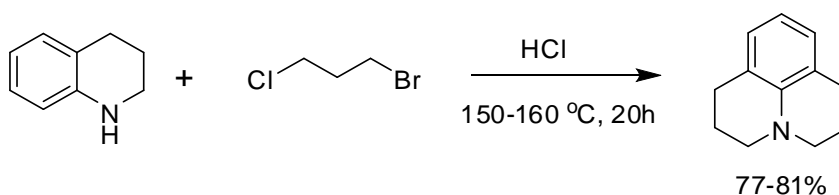
Figure 1.2 The synthetic scheme of julolidine by Glass and co-workers [9].

In 2015, Labed and team [10] reported a new method for preparation of julolidine using iridium-complexes [Cp*IrCl$_2$]$_2$ to catalyze a coupling reaction between tetrahydroquinoline and propane-1,3-diol (**Figure 1.3**). The results show that the condition using [Cp*IrCl$_2$]$_2$ as a catalyst and diphenylphosphinobenzoic acid (DPPBA) as a ligand provides a high conversion toward julolidine. Moreover, when the reaction time was raised up to 36 h., the isolated yield of julolidine increased to 91%.

Figure 1.3 The synthesis scheme of julolidine by Labed and team [10].

In 2001, Kauffinan and team [11] reported an inexpensive method to synthesize julolidine derivatives containing hydroxyl group. In this report, julolidine was successfully synthesized by coupling *m*-anisidine with bromo-3-chloropropane followed by treatment of HBr as a catalyst in demethylation step to gain 8-Julolidinol (**JD-OH**) in moderate yield (**Figured 1.4**). Moreover, 9-formyl-8-hydroxyjulolidine (**1**) was formed by using phosphoryl chloride in DMF via Vilsmeier reaction mechanism.

Figure 1.4 The synthesis scheme of **JD-OH** and julolidine **1** [11].

In 1996, Katritzky and co-workers [12] reported a method to synthesize and characterize julolidine derivatives by the reaction of *N,N*-bis[(benzotriazol-1-yl)methyl]aniline17 (**2**) with 1-vinyl-2-pyrolidinone using *p*-toluenesulfonic acid monohydrate as a catalyst to gain julolidine **3** in high yield as shown in **Figure 1.5.**
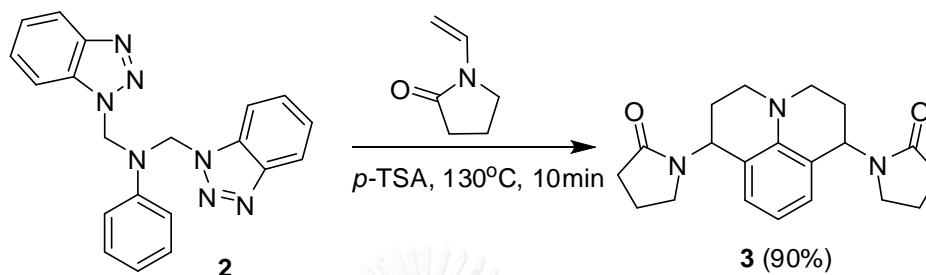
Figure 1.5 The synthesis scheme of julolidine derivative **3** [12].

In 2011, Yuan and colleagues [13] demonstrated that julolidine 8-hydroxyjulolidine could be prepared by combination of the reaction between *m*-anisidine and bromo-3-chloropropane and reaction with HI for the demethyation step to obtain the target product of 70% yield (**Figure 1.6**). In addition, this target was further modified for the fluorescent sensor **4** that came up with the high selectivity toward chlorate ions.
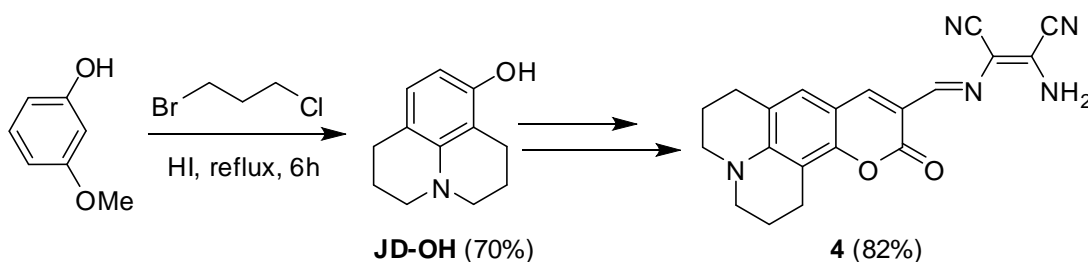
Figure 1.6 The synthetic scheme of julolidine derivative **4** [13].

In 2014, Zhang and co-workers [14] developed a synthetic procedure of 8-hydroxy julolidine-9-carboxaldehyde (**1**) using two step reaction. Sodium carbonate was applied to the reaction between 3-aminophenol and 1-bromo-3-chloropropane followed by the formulation reaction using POCl$_3$ in DMF (**Figure 1.7**). Moreover, compound **1** was used to synthesize the fluorescent sensor **FP** which was highly selective toward fluoride ions.
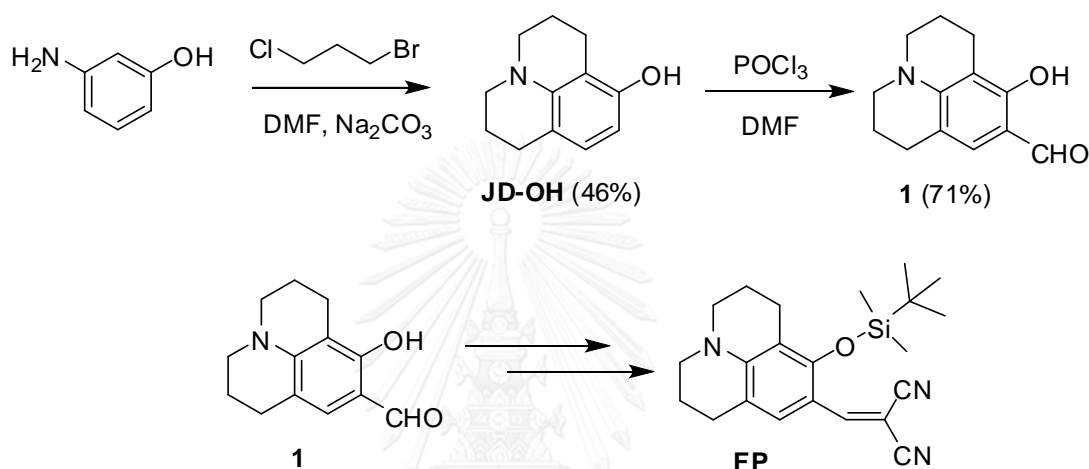
Figure 1.7 The synthetic scheme of julolidine derivative **FP** [14].

Due to its small and highly rigid julolidine core structures, its derivatives can be used in several applications especially in the fluorescent sensing ones. Nowadays, many reports demonstrated that julolidine can be used and developed as fluorogenic and chromogenic moiety in the fluorescent sensing applications [15-16]. Not only does a julolidine derivative can increase a solubility of fluorescent sensor [17] but also exhibit a strong fluoregenic properties in aqueous media [18].

1.2 Introduction of fluorescence and fluorometry

Fluorescence is one of the luminescence, phenomena that emits the light in visible region. A molecule which composes of a large **π**-conjugation and a highly rigid structure can exhibit a fluorescence signal. According to its potential properties

including low detection limit, rapid detection, high sensitivity and selectivity, inexpensive and also easy to use, fluorescence becomes one of the interesting techniques and is wildly used in both quantitative and qualitative applications for several types of analytes such as metal ions [19-20], amino acids [21], nitroaromatic compounds [22] and biological substrates [23-24]. The changes of fluorescence signal and its optical properties, which is measured by fluorescence spectrometer, provide important information to describe an interaction mechanism and also some special properties between fluorescent sensor and analyte.

Fluorescence is a photon emission process that occurs when a molecule absorbs photons from UV-visible light, known as excitation, and then rapidly emits light photons when the excited molecule returns to their ground state. The phenomenon is usually illustrated by the Jablonski diagram, which offers a convenient representation of the excited state structure and the relevant transitions, for possible various molecular processes. From Franck-Condon principle, most molecules absorb light more rapidly (10^{-15} s) than molecular vibration (10^{-8} s). A simplified Jablonski diagram shown in **Figure 1.8**, demonstrates that this causes electrons to become excited to second electronic state (S_2), then the electrons lose the energy by internal conversion (vibration or rotation) evacuate to first excited state (S_1). After that, the fluorescence signal is observed when the electrons relax to singlet ground electronic state (S_0) via photon emission (radiative decay). The time required to complete the whole process takes only around nano-second.
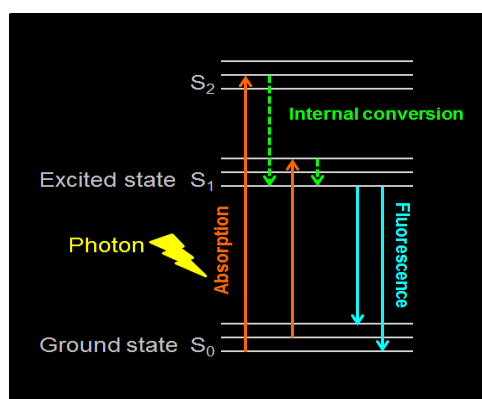
Figure 1.8 Jablonski diagram of the fluorescence processes [25].

1.3 Introduction of fluorescent chemosensor

The fluorescent sensors actually consist of three components as shown in **Figure 1.9** fluorophore, which exhibits the fluorogenic properties and provides the fluorescence signal; receptor or control part, which specifies toward analyte; and spacer or linker. The interaction between fluorescent sensor and analyte causing the change of fluorescence signal, the fluorescence intensity measured, can be divided into three cases; the "Turn off" fluorescent sensor, the fluorescence intensity drops obviously in the presence of the analyte; the "Turn on" fluorescent sensor, the fluorescence intensity significantly enhanced in the presence of the analyte; and the shift of fluorescence emission wavelength after addition of analyte. The change of fluorescence intensity can be described in general mechanism including Chelated-enhanced fluorescence (CHEF), photo-induced electron transfer (PET), excited state intramolecular proton transfer (ESIPT), photo-induced charge transfer (PCT), fluorescence (FÖrster) resonance energy transfer (FRET), and excimer/exciplex formation or extinction. An important feature of the fluorescent sensors is the signal transduction of the analytes leading to the readout that can happen in a very short time (less than nanoseconds) and without any other assistances. This makes real-time and real-space detection of the analyte possible as well as the imaging associated with analyte distribution [26].
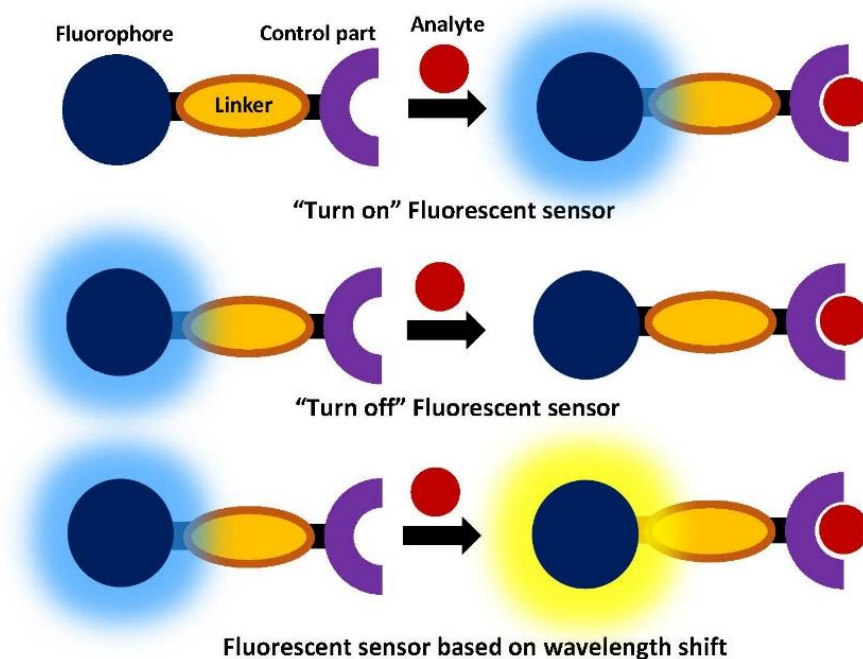
Figure 1.9 Schematic illustration of a sensor device.

1.4 The systematic operation of fluorescent chemosensor

1.4.1 Photo-induced electron transfer (PET)

PET process is one of the important fluorescence quenching mechanisms that is relevant to the intramolecular electron transfer occurring when the highest occupied molecular orbital (HOMO) energy level of receptor is between the lowest unoccupied molecular orbital (LUMO) and HOMO of fluorophore. When the light energy is applied to fluorophore, the electrons in the ground state commonly move from HOMO to LUMO energy level then the electron at HOMO of receptor can transfer to half-filled HOMO of fluorophore whereas the electrons at LOMO of fluorophore move to half-filled HOMO of receptor. The electron transfer process releases an energy in non-radiative region resulting in the fluorescence quenching of the molecule. Nevertheless, the fluorescent sensor, which is composed of the appropriate receptor in the system and its HOMO located between LUMO and HOMO of fluorophore leading the electron at the HOMO of receptor to move directly to HOMO of fluorophore (**Figure1.10**).

Accordingly, excited electrons at the LUMO of fluorophore move to HOMO of receptor instead of that of fluorophore causing the disappearance of fluorescence signal.
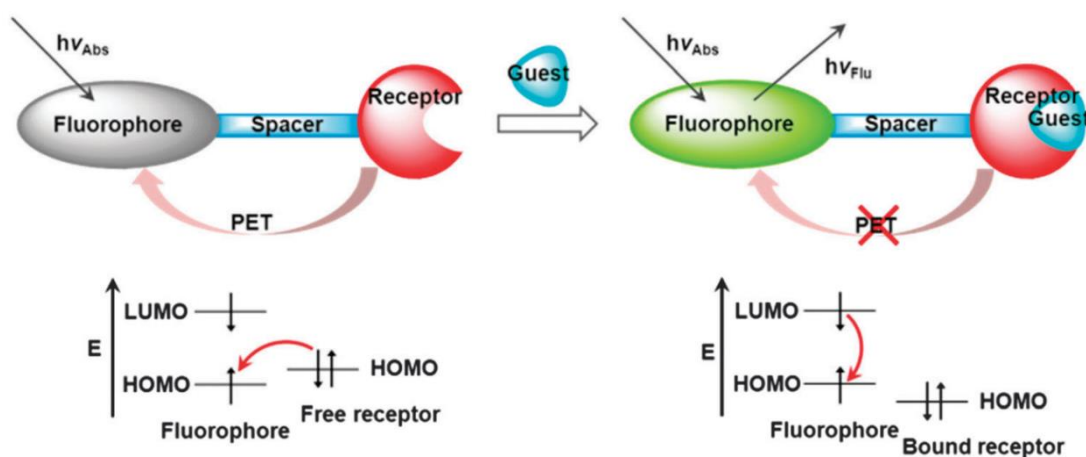
Figure 1.10 Photoinduced electron transfer (PET) [27].

1.4.2 Excited state intramolecular proton transfer (ESIPT)

ESIPT process is investigated in aromatic molecule containing a phenolic hydroxy group that can form an intramolecular hydrogen bond with the nearby hetero atom in the same molecule. The mechanism of ESIPT can be used to describe some of photophysical properties of molecules which exhibit an interesting characteristics, such as fluorescent solar concentrators [28], ultraviolet stabilization [29], stimulated radiation production [30], environmental probes in biomolecules [31], information storage devices [32] and organized assemblies [33]. The appearance of a second band to the red region of the normal band in the fluorescence spectrum is observed when ESIPT process occurs in electronically excited singlet states. The emission from S_1 state of the molecule to thermodynamically most stable S_0 state generates a normal band spectrum. According to ESIPT process, the emission from the tautomerization of molecule provides the second band of fluorescence spectrum as shown in **Figure 1.11**.
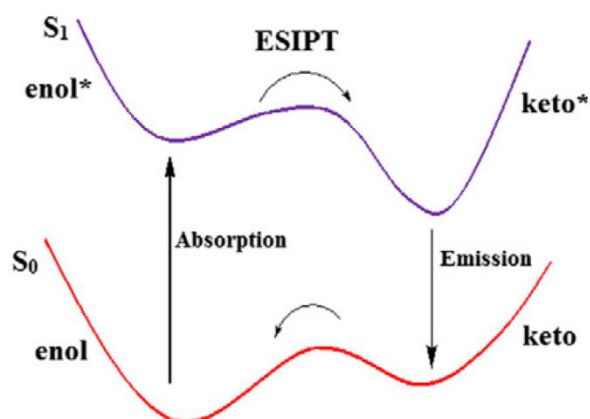
Figure 1.11 Energy diagram of excited state intramolecular proton transfer (ESIPT) [34].

1.5 The fluorescent chemosensor based on C=N isomerization inhibition

The imine-based fluorescent sensor is a fluorescent sensor that is composed of imine bond (C=N) linking between fluorophore and control part [35-36]. The characteristic behavior of an imine bond is the rotation between *cis-* and *tran-* conformation. The rotation of such bond leads to a large relaxation energy at non-radiative region causing a non-fluorescence type of electronic energy decay to ground state. The chelation between imine-based fluorescent sensor and metal ion that actually uses both lone pair electron on nitrogen atom at C=N and other heteroatoms from control part or fluorogenic moiety causing the inhibition of C=N isomerization (**Figure 1.12**). This inhibition not only increases the rigidity of molecule, but also decreases the energy decay from non-radiative region allowing the fluorescence enhancement via CHEF mechanism [37-38].
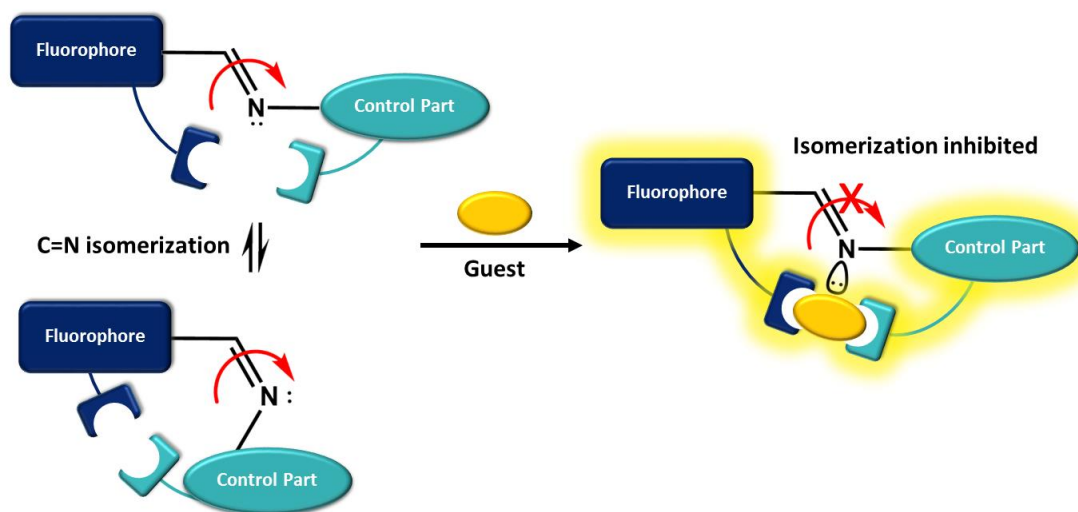
Figure 1.12 Schematic illustration of the imine-based fluorescent sensor [39].

1.6 Applications of fluorescent chemosensors

Small fluorescent molecular sensors have become essential chemosensors, due to their special properties which do not require a complicated instrumentation or sample preparation. Many studies have reported wide uses and applications of such fluorescent sensor, for small ions or biomolecules detection, for example, cations or metal ions [40], anions [41], enzymes [42], amino acids [43] and neurotransmitters [44-45]. The design and development of highly efficient fluorescent sensor, providing a good fluorogenic properties and selectivity toward analyte, have become an important consideration.

Herein, the synthesis and development of the small-molecule-based metal ion sensors containing imine bond including dipicolylamine derivatives will be focused and reviewed of their sensing properties along with the quenching or enhancing mechanism under several conditions.

1.6.1 Metal ion fluorescent sensors

Metal ion can severely cause many serious health effects such as cancer organ damage nervous system damage and death in extreme cases. For instance, aluminum is the third most abundant metal in the earth's crust and naturally found in several environment, it is also one of most common heavy metal toxins which could directly affect to human's central nervous system (CNS) as well as seen in Alzheimer's and Parkinson's disease [46-47]. Magnesium is known well as an abundant mineral in human body and usually found not only in the sea water but also in the other natural sources of water. In human body, Mg^{2+} can induce the increase of neuromuscular excitability, muscle contraction along with hormone secretion [48-49]. However, the over recommended of Mg^{2+} intakes can cause some numerous symptoms and diseases including hypotension as well as gastrointestinal symptoms such as stomach upset, nausea, vomiting and abdominal cramping. Therefore, the design and development of fluorescent sensors for metal ions have become an increasingly important tool.

1.6.2 Imine-based fluorescent sensors

In 2012, Sinha and team [50] developed and synthesized a imine-based fluorescent sensor **BPS** by the condensation between 3,4-diaminobenzophenone and salicylaldehyde. Sensor **BPS** exhibited a strong fluorescence intensity towards Al^{3+} with a green light emission, and In^{3+} and Ga^{3+} with a yellow light emission (**Figure 1.13**). The fluorescence enhanced mechanism followed CHEF that the chelation between Al^{3+} and heteroatoms, phenolic OH, free NH_2 and lone-pair electrons of nitrogen atom at imine bond, suppressed the PET and ESIPT process. The fluorescence quantum yield and limit of detection of **JNH**-Al^{3+} were calculated to be 0.17 and 8.12 x 10^{-6} M, respectively.
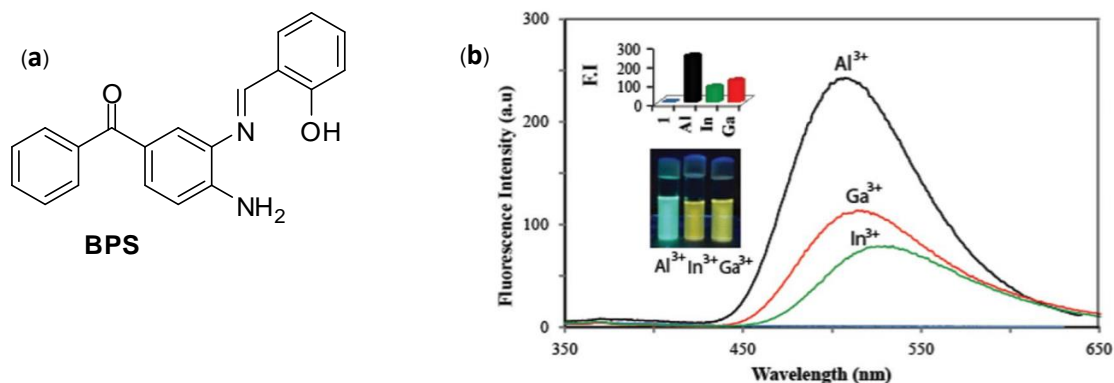
Figure 1.13 (a) Structure of fluorescent sensor **BPS** (b) its selectivity toward Al^{3+}, In^{3+} and Ga^{3+} in the same condition [50].

In 2015, Das and co-workers [51] developed the fluorescent sensor **HBTP**, which was synthesized from 2-aminothiophenol and 6-(hydroxymethyl)picolinohydrazide in three steps. After binding with Al^{3+}, the tautomerization process of **HBTP** between amido and iminol form would be inhibited leading to the suppression of the ESIPT and hence enhancement of the fluorescence signal in mixed solvent of CH_3OH/H_2O (1:9, v/v, pH = 7.3, 25 $^{\circ}$C). In addition, the X-ray diffraction experiment of crystal complex between **HBTP** and Al^{3+} confirmed that the phenolic oxygen atom, nitrogen at imine bond, oxygen and nitrogen atoms from 6-(hydroxymethyl)picolinohydrazide moiety were used to chelate Al^{3+} (**Figure 1.14a**). Moreover, **HBTP** was applied to investigate Al^{3+} in human's peripheral blood mononuclear cell (PBMCs) by using confocal fluorescence imaging technique (**Figure 1.14c**).
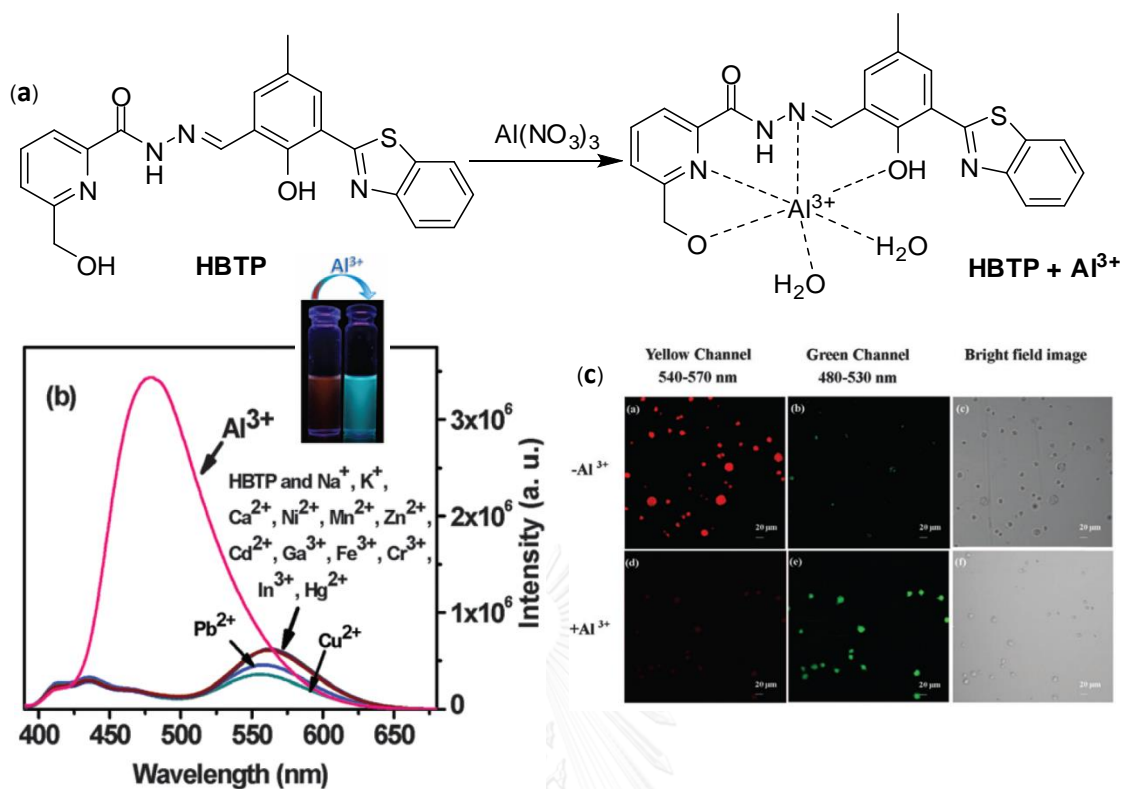
Figure 1.14 (a) Structure of **HBTP** fluorescent sensor and its complex structure, (b) the selectivity of **HBTP** in CH_3OH/H_2O and (c) confocal fluorescence images of PBMCs treated with **HBTP** [51].

In 2016, Guo and co-workers [52] designed and synthesized the fluorescent sensor **HPIN** by Schiff base coupling between 2-Hydroxy-1-naphthaldehyde and 2-aminophenol (**Figure 1.15a**). As the results, **HPIN** could enhance the fluorescence with aluminum giving yellow color (**Figure 1.15b**) under the solvent condition of $DMSO/H_2O$. Moreover, the ^1H NMR titration experiment showed that the lone-pair electrons on the imine nitrogen atom were used for the coordination between **HPIN** and aluminum. The detection limit of **HPIN** toward aluminum was calculated as 0.1 μM. HIPN was also applied in imaging applications of living SiHa cells (**Figure 1.15c**).
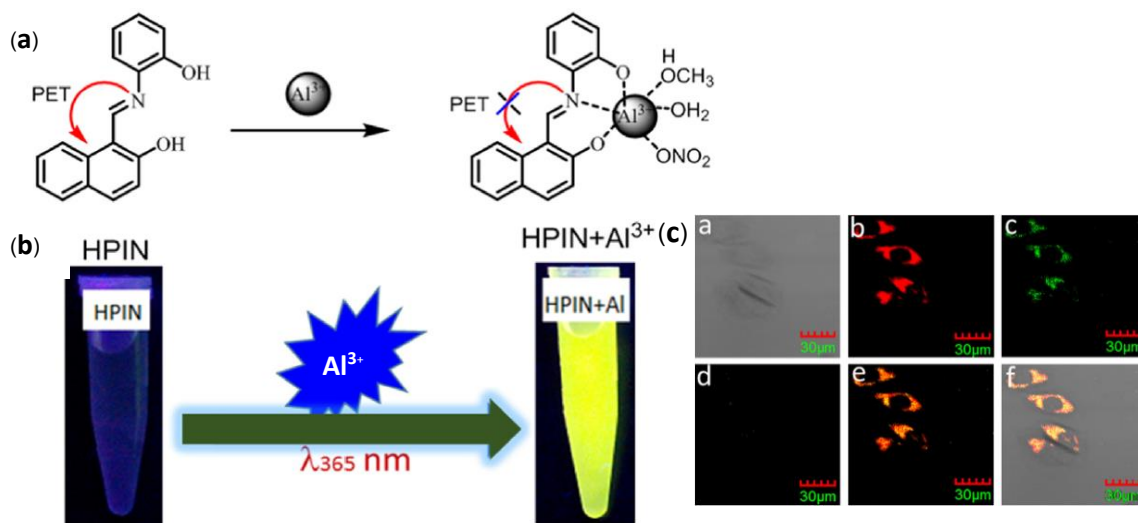
Figure 1.15 (a) Structure of **HPIN** fluorescent sensor and its complex structure (b) naked eye observation in the presence of Al^{3+} under black light and (c) fluorescence imaging of SiHa cells with **HPIN** [52].

In 2016, Boonkitpatarakul and colleagues [53] designed and synthesized *N*-salicylidenehydrazide based fluorescent probe **F1** and **F2** containing 1 and 2 groups of furan-2-carbohydrazide, respectively. Due to the PET as well as ESIPT process, **F1** and **F2** did not provide any fluorescence signal. In the presence of Al^{3+}, the strong fluorescence signals of both compounds were observed at 458 and 601 nm under the solvent condition of 0.1% DMSO/HEPES buffer solution (**Figure 1.16**). Moreover, the fluorescence enhancing phenomena demonstrated the inhibition of PET and ESIPT caused by CHEF effect. The association constant of **F1**-Al^{3+} and **F2**-Al^{3+} were reported as 1.6×10^{5} and 2.0×10^{10} M^{-1} corresponding the ratio of 1:1 and 1:2 stoichiometric complication of two complexes, respectively, due to compound **F2** containing two binding sites that could increase not only the conjugation of molecule but also the fluorescence intensity in the presence of Al^{3+}. Moreover, both fluorescent probes were applied to detect Al^{3+} on filter paper.
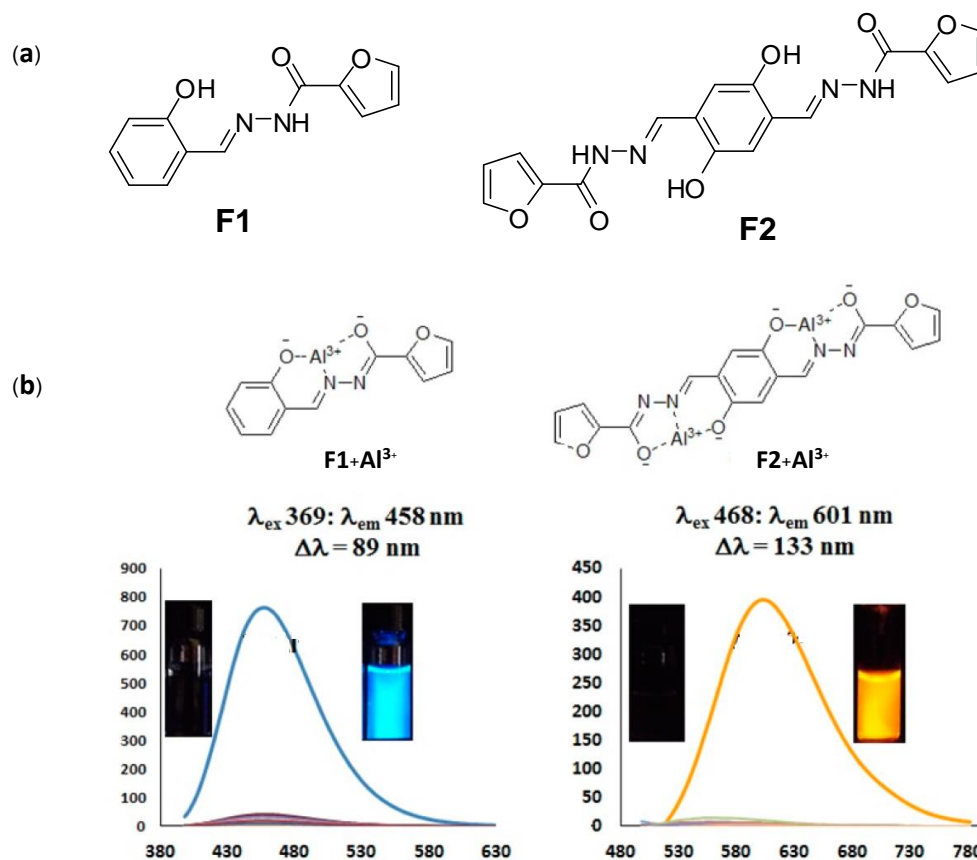
Figure 1.16 (a) Structure of fluorescent sensor **F1** and **F2** and (b) the selectivity and appearance under black light [53].

In 2016, Wang and co-workers [54] synthesized the fluorescent probe **HL** possessing Isatin-3-hydrazone linked with 3-formyl-7-methoxychromone unit by Schiff base reaction. In the presence of Mg^{2+}, the complexation with **HL** inhibited PET process and hence exhibited the strong fluorescence intensity at 547 nm using the excitation wavelength of 491 nm in ethanol (**Figure 1.17**). According to ^{1}H NMR titration, a lone pair electron at imine nitrogen atom as well as two carbonyl oxygen atoms were used in the coordination between **HL** and Mg^{2+}. The association constant of **HL**-Mg^{2+} complex and the detection limit were 3.33×10^4 M^{-1} and 5.16×10^{-7} M, respectively.
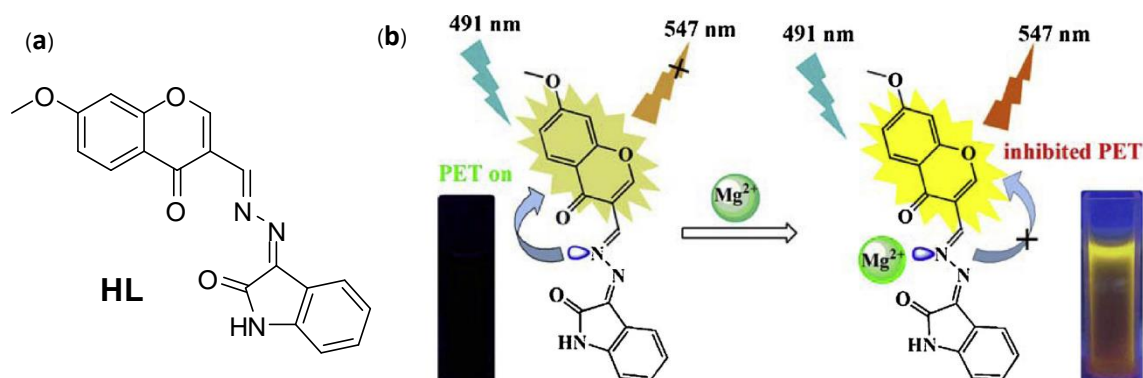
Figure 1.17 (a) The structure of fluorescent probe **HL** and (b) its fluorescence response in the presence of Mg^{2+} in ethanol [54].

In 2016, Kao and colleagues [55] successfully synthesized the quinoline-based sensor **AQH** by using the Schiff base reaction of 2-hydrazinopyridine with 8-hydroxy-2-quinolinecarboxaldehyde. The fluorescent probe **AQH** provided the good selectivity towards Mg^{2+} in CH$_3$CN. The emission band was observed at 487 nm as yellow fluorescence light when using the excitation wavelength at 353 nm. (**Figure 1.18**). The CHEF effect was proposed for the fluorescence enhancing mechanism of **AQH**. Moreover, sensor **AQH** was applied in qualitative detection of Mg^{2+} in water from some sources including lake, ground and also tap water.
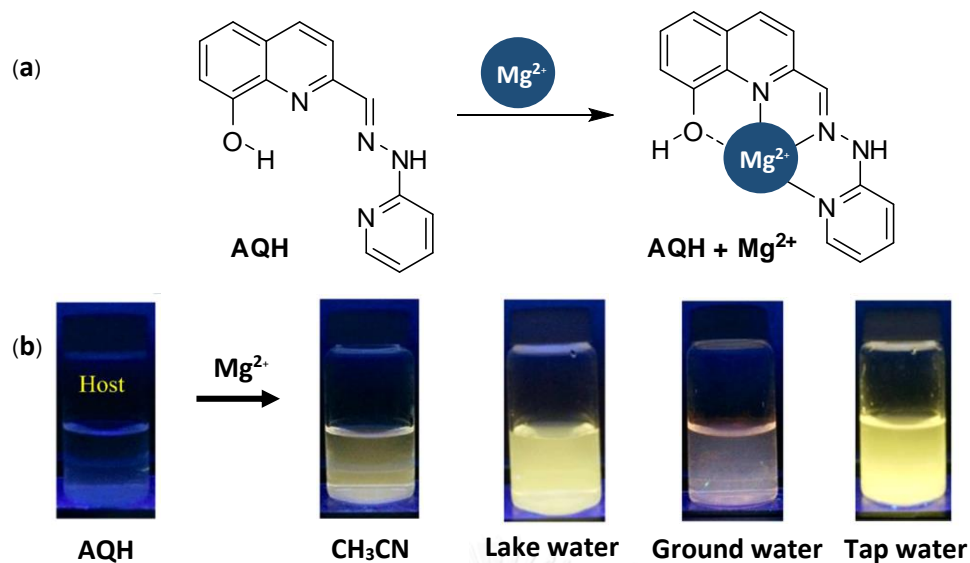
Figure 1.18 (a) The structure and binding position of **AQH** and (b) appearance under black light of **AQH** in the presence of Mg^{2+} in CH$_3$CN and different sources of water [55].

1.6.3 Fluorescent sensors containing iminyljulolidine derivatives

In 2013, Noh and colleages [56] reported a new fluorescent sensor *o*-phenyljulolidineimine (**PJI**) (**Figure 1.19a**), which could be synthesized from the imination reaction of 8-hydroxyjulolidine-9-carboxaldehyde and 2-aminophenol. **PJI** was found to be highly selective toward both Ga^{3+} and Al^{3+} in methanol (**Figure 1.19b**) as the fluorescence enhancements with both metal ions were observed under the same condition probably due to CHEF mechanism. In addition, **PJI** can be used to observe Al^{3+} in living HeLa cells (**Figure 1.19c**).
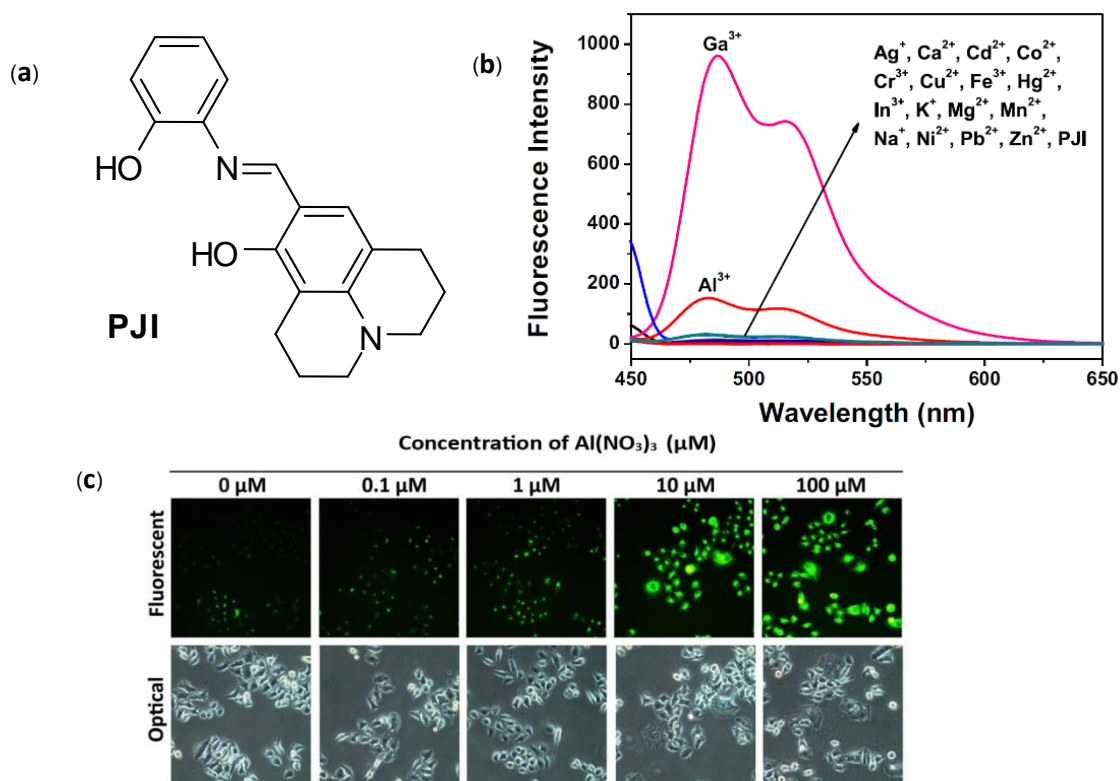
Figure 1.19 (a) Structure of fluorescent sensor **PJI**, (b) the selectivity results of **PJI** in methanol and (c) investigation of Al^{3+} in HeLa cells [56].

In 2014, Park and co-workers [57] developed the fluorescent sensor **JNH** containing julolidine derivative as fluorogenic moieties linked with 3-hydroxy-2-naphthoic hydrazide via Schiff base mechanism. The sensor **JNH** exhibited the strong fluorescence intensity toward Zn^{2+} (giving a yellow light) in DMF (**Figure 1.20**). Furthermore, CHEF principle was applied to describe the mechanism that an isomerization of C=N and ESIPT process were exhibited as sensor **JNH** coordinated with Zn^{2+} leading to the increase of fluorescence intensity.
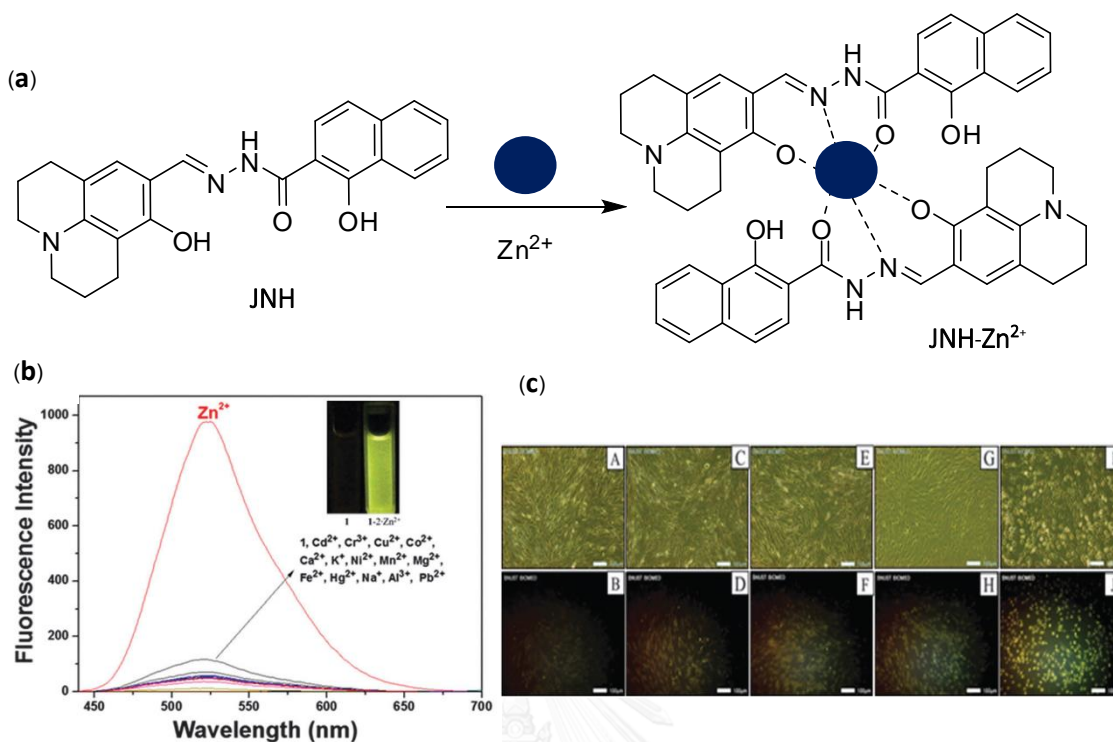
Figure 1.20 (a) Structure of fluorescent sensor **JNH** and its complex structure, (b) the selectivity of **JNH** in DMF and (c) Fluorescence images of fibroblasts cultured with Zn^{2+} [57].

1.6.4 Fluorescent sensor containing dipicolylamine derivatives

In 2009, Ballesteros and team [58] designed the new fluorescent sensor probe **5** containing dicyanomethylene indene equipped with quinoline as fluorophore and 2,2'-dipicolylamine moieties as signaling units. This fluorescent probe was synthesized and proved to have a selective fluorescence enhancement and colorimetric change (from purple to orange) with Cu^{2+} in mixed 1:1 MeCN/H$_2$O **(Figure 1.21)**. The results from ^{1}H NMR titration experiment showed that dipicolylamine moiety was directly involved in the coordination between the sensor probe and Cu^{2+}. Moreover, the red shift of fluorescence emission wavelength occurred upon increasing of water in the system.
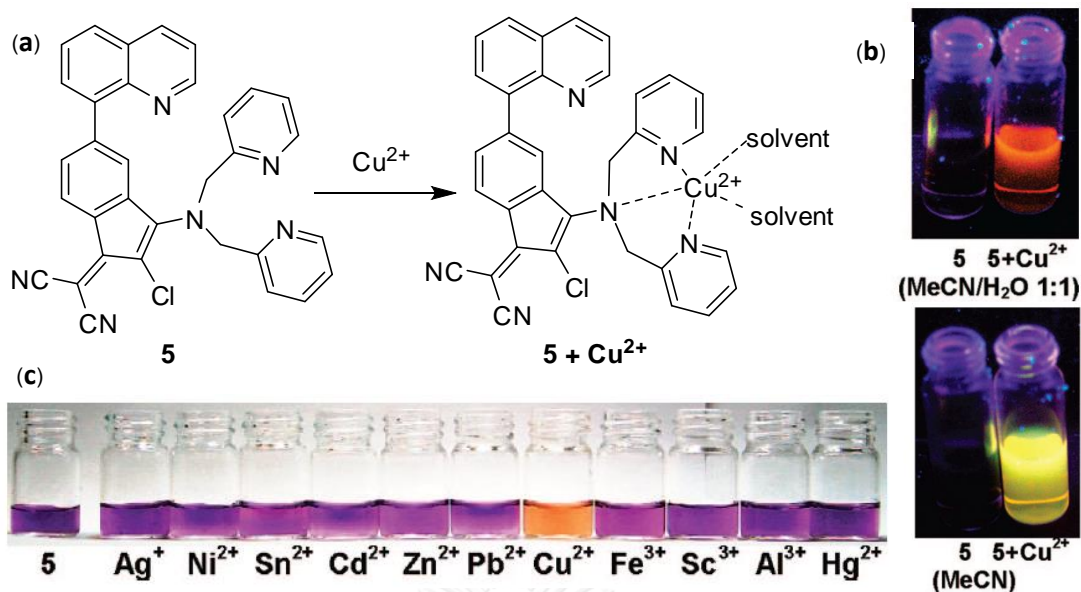
Figure 1.21 (a) Structure of fluorescent probe **5** and its complex structure (b) naked eye observation under black light in different solvent conditions and (c) color change of sensor **5** upon addition of metal ions [58].

In 2009, Xue and colleagues [59] successfully synthesized the new fluorescent sensor **QA** based on fluorogenic acetamidoquinoline with control part of DPA. **QA** showed a selectivity towards either Cd^{2+} or Zn^{2+} in DMSO and Tris-HCl buffer solution (10 mM, pH 7.4) (1:4, v/v) to form 1:1 complex **CdQA** and **ZnQA**, respectively **(Figure 1.22)**. According to ^{1}H NMR titration, three nitrogen atoms from DPA moiety cooperating with the heteroatoms from acetamide moiety were used to bind both Cd^{2+} and Zn^{2+} expressing the green and blue fluorescence light at the emission wavelength of 422 and 470 nm, respectively. The inhibition of PET process was also applied to describe the mechanism of this enhancement of fluorescence intensity.
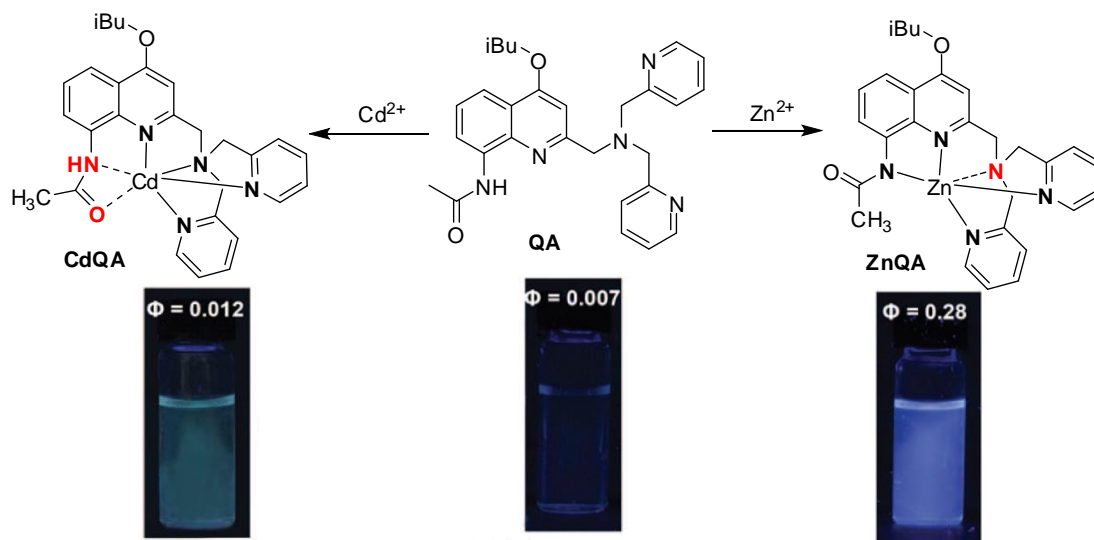
Figure 1.22 Structure of fluorescent sensor **QA** including its complex structures and naked eye observation under black light [59].

In 2010, Du and co-workers [60] reported the sensing properties of fluorescent sensor **ZRL1**, which composed of rhodamine B as a fluorogenic moiety and DPA derivative as a control part. According to the photophysical properties study, sensor **ZRL1** exhibits a high selectivity towards Zn^{2+} in a PIPES buffer solution (50 mM, pH 7.0). The fluorescence intensity increases around 220-fold upon the addition of Zn^{2+} (red light given) **(Figure 1.23)**. The enhancement of fluorescence intensity could be described occurring through the opening of the spirolactam ring resulting in the formation of longer conjugated system. In addition, **ZRL1** could be applied for quantitative analysis of Zn^{2+} in living HeLa cells.
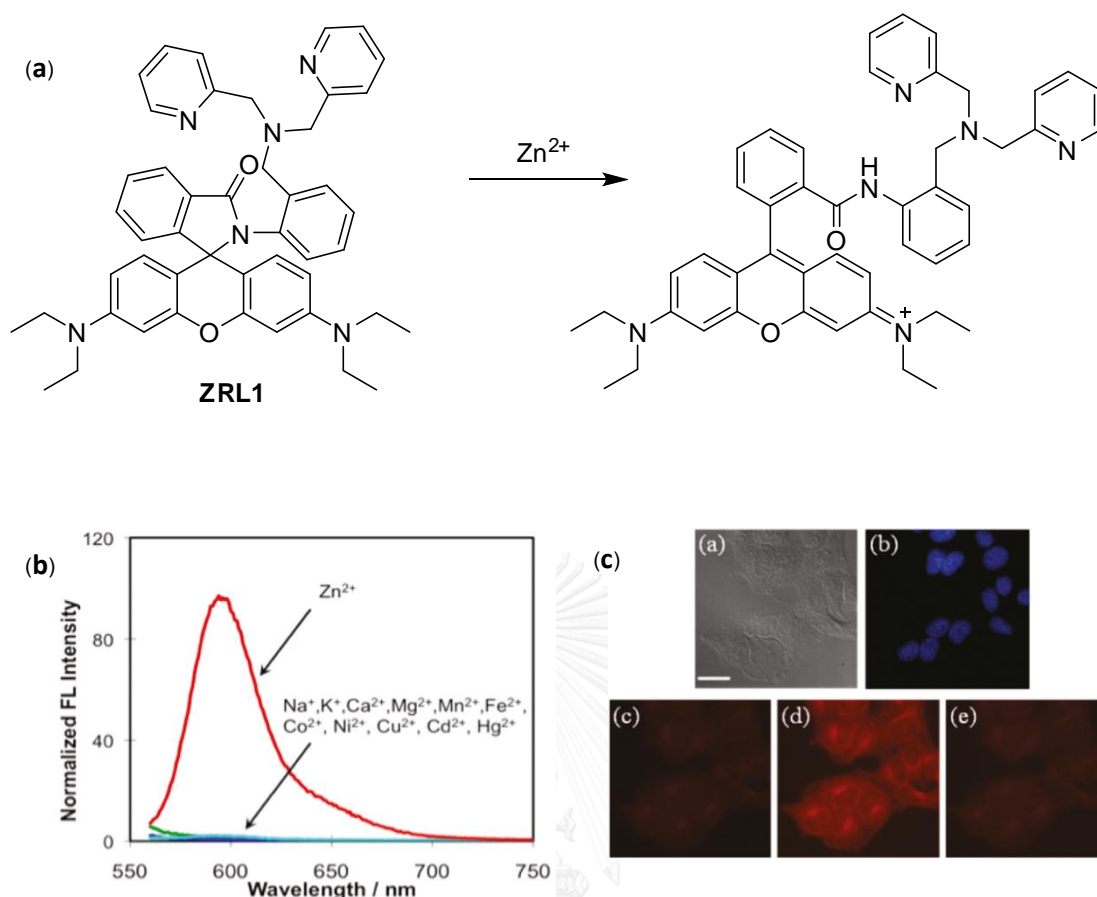
Figure 1.23 (a) Structure of fluorescent sensor **ZRL1** and (b) its selectivity toward Zn^{2+} in aqueous media (c) imaging of living HeLa cells after incubation with **ZRL1** [60].

1.7 Statement of problem

According to the literature reviews, the fluorescent sensors containing imine bond (C=N) and hydroxy group usually provided a high selectivity toward metal ions because the **π**-electron of nitrogen atom at imine bond could be used to coordinate with metal ions. Also hydroxy groups, hard base moiety, were found to increase not only a specificity of the fluorescent sensors toward hard acid metal ions, such as aluminum (Al^{3+}) [50-53] but also a solubility of sensor in aqueous media. Herein, julolidine, known to possess good fluorogenic and chromogenic properties [15,16], was applied for the development of the fluorescent sensor because it has a small structure, good solubility in aqueous media [18] and can be applied in bio-imaging applications

[56,57]. In addition, dipicolylamine derivatives were widely used to apply in the control part of fluorescent sensors due to their high selectivity toward metal ions including Zn^{2+}, Cu^{2+} and Cd^{2+} [58-60]. Nonetheless, there are no report found to be using a julolidine and dipicolylamine derivatives to develop a fluorescent sensor.

Considering the mentioned reasons, the development of novel target fluorescent sensor has been conceptually focused by linking julolidine building block with a selectivity enhancing unit, di-(2-picolyl)amine (DPA) moiety. Additionally, in order to see the effect of the position of the substituent, a series of fluorescent sensor was designed to hence the substitution of DPA on the *ortho-*, *meta-* and *para-* position of aniline ring. The coupling reaction between DPA derivatives and julolidine building block was performed via Schiff base reaction to generate the target imine molecules (**J2P**, **J3P** and **J4P**) **(Figure 1.24)**. The hypothesis of this work is that the fluorescent sensor containing hydroxy and imine group will exhibit a high selectivity toward metal ion leading to inhibit the isomerization of C=N and PET process causing the fluorescence enhancement via CHEF mechanism. Furthermore, the different positions of DPA on the aromatic aniline might provide some of interesting properties especially the sensing properties of the fluorescent sensor.

2-CH$_2$-DPA (J2P)
3-CH$_2$-DPA (J3P)
4-CH$_2$-DPA (J4P)
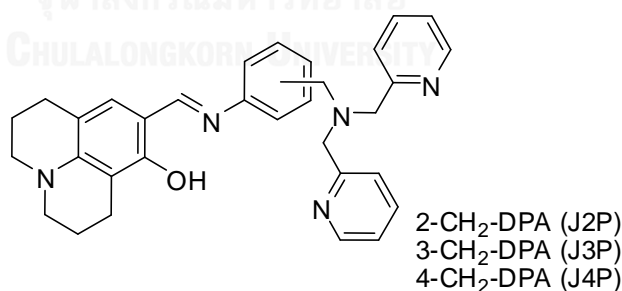
Figure 1.24 Target molecule **J2P**, **J3P** and **J4P**.

1.8 Objectives of this research

In this research, the fluorescent sensor containing julolidine derivative as a fluorogenic moiety and DPA derivatives as a control part are focused. The design and synthetic preparations of series of julolidine linked with various positions of DPA substituted on aniline ring as fluorescent sensors will be achieved (**Figure 1.24**). The study of photophysical and sensing properties of target molecules will be investigated in appropriate solvent(s) with the hope that the fluorescent sensor might exhibit the high selectivity towards metal ions or specific chemical species.

CHAPTER II

EXPERIMENTAL

2.1 Materials and chemicals

The solvents used in the synthesis procedure such as acetonitrile (ACN), ethanol (EtOH), dimethylformamide (DMF) and dichloroethane (DCE) were dried and distilled prior to use. Methanol (MeOH) and dimethyl sulfoxide (DMSO) in analytical applications were analytical grade purchased from RCI Labscan. 2-,4-nitrobenzyl bromide, dibenzylamine (DBA) and potassium hydroxide were purchased from Merck. 3-nitrobenzyl bromide and DPA were purchased from TCI. 3-methoxyaniline, 1-bromo-3-chloropropane were commercially available from Sigma-Aldrich. Thin layer chromatography (TLC) used Merck 60 F254 plates with a thickness of 0.25 mm. Column chromatography was performed using Merck silica gel 60 (70-230 mesh). MilliQ water was used in fluorescence and UV-Visible experiments including the preparations for stock solutions of metal ions and also fluorescent sensors. Julolidine derivatives were prepared by the literature reported procedure [13], Solvents used for column chromatography such as methanol, dichloromethane (DCM), ethyl acetate (EtOAc) and hexane were commercial grade and distilled before used.

2.2 Analytical instruments

Absorption spectra was collected from Varian Cary 50 UV-visible spectrophotometer using mixed solvent of MilliQ water, methanol and DMSO. Fluorescence spectra were carried out using Varian Cary Eclipse spectrofluorometer (Varian, USA) for the investigation of metal sensing applications and general photophysical property studies. ^{1}H NMR spectra were collected on a 400 MHz NMR spectrometer (Mercury 400, Varian) and ^{13}C NMR spectra were collected at 100 MHz on a Bruker NMR spectrometer. The high resolution mass spectrometer (HRMS) results were obtained using a Bruker micrOTOF-II mass spectrometer.

2.3 Synthesis procedure

2.3.1 Synthesis and characterization of 1,2,3,5,6,7-hexahydropyrido[3,2,1-ij]quinolin-8-ol (JD-OH)
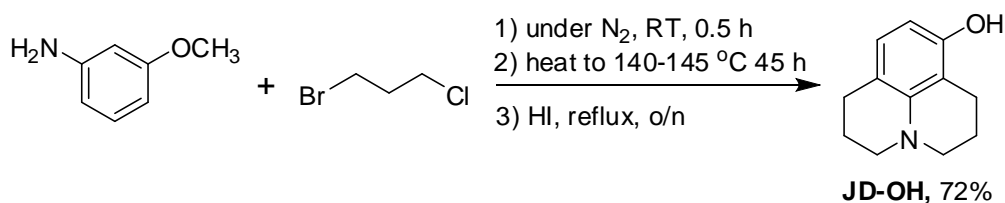
3-methoxyaniline (1.30 g, 10.0 mmol) was mixed with 1-bromo-3-chropropane (23.5 g, 150.0 mmol) under N_2 atmosphere in room temperature. After 30 minutes, the reaction mixture was heated to 95 $^{\circ}$C for 1 hour and 140 $^{\circ}$C for 24 hours, respectively. Then, the reaction was heated up to 145 $^{\circ}$C for further 21 hours and monitored by TLC. After that the reaction was cooled down to 80 $^{\circ}$C to get an orange solid. After 7 mL of HI was slowly added into the mixture, the reaction was again heated to 145 $^{\circ}$C for overnight. Finally, 20 mL of DI water was added to the reaction mixture and an organic phase was collected. The solvent was removed by a rotator evaporator and the residue was purified using column chromatography containing silica gel with 50% of EtOAc:DCM as the mobile phase to get the yellow powder of **JD-OH** (1.35 g, 72%); ^{1}H NMR (CDCl$_3$, 400 MHz) δ 6.66 (d, J = 8.0 Hz, 1H, H-e), 6.10 (d, J = 8.0 Hz, H-d), 3.18-3.00 (m, 4H, H-a), 2.76-2.59 (m, 4H, H-c), 2.10-1.88 (m, 4H, H-b).

JD-OH
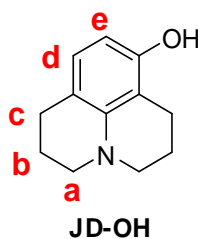
2.3.2 Synthesis and characterization of 8-hydroxy-1,2,3,5,6,7-hexahydro-pyrido[3,2,1-ij]quinoline-9-carbaldehyde (julolidine 1)

JD-OH → **1**, 52%

1) POCl$_3$, DMF, RT, 1 h
2) 60°C , 1 h
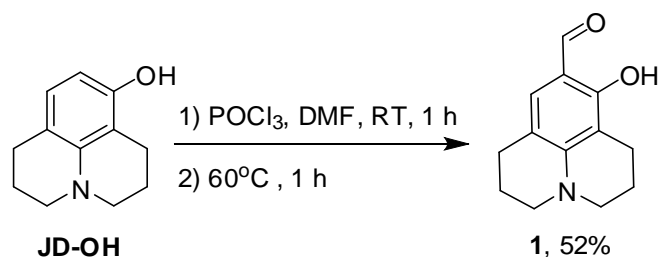
4.0 mL of POCl$_3$ was added dropwise into 4.0 ml of distilled DMF under N$_2$ atmosphere at room temperature and stirred for 1 hour to get a light yellow solution. Then the solution of **JD-OH** (1.0 g, 5.2 mmol) in 15 mL DMF was added to the reaction mixture and stirred at room temperature for 30 minutes then heated up to 60 °C for 1 hour The mixture was slowly added into 100 mL of ice water, stirred for 2 hours and filtered to yield a light green solid of julolidine **1** (0.58 g, 52%); ^{1}H NMR (CDCl$_3$, 400 MHz) δ 9.36 (s, 1H, *H*-f), 6.85 (s, 1H, *H*-d), 3.34-3.15 (m, 4H, *H*-a), 2.75-2.55 (m, 4H, *H*-c), 2.02-1.84 (m, 4H, *H*-b).

1
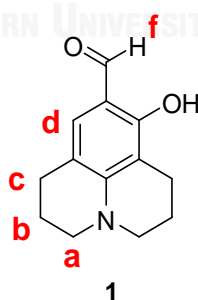
General synthesis of 1-methyl-2,2'dipicolylamine-nitrobenzene (2a-2c)

R = 2-CH$_2$Br
3-CH$_2$Br
4-CH$_2$Br

2a; R' = 2-CH$_2$DPA, 75%
2b; R' = 3-CH$_2$DPA, 79%
2c; R' = 4-CH$_2$DPA, 87%
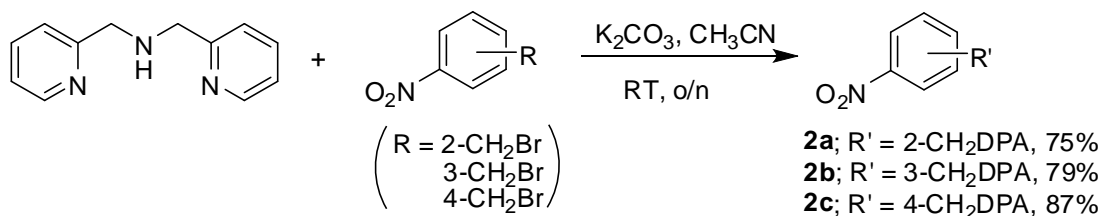
2.3.3 Preparation of 2-[bis(2-pyridylmethyl)aminomethyl]nitrobenzene (2a).

2-nitrobenzyl bromide (1.0 g, 4.6 mmol) and DPA (1.1 g, 5.5 mmol) were mixed with 2.0 g of K$_2$CO$_3$ in 10 mL CH$_3$CN under N$_2$ atmosphere at room temperature for overnight. The reaction progress was monitored by TLC. After the starting material DPA disappeared from the reaction mixture, the solvent was removed under reduced pressure to get a yellow oil crude. The residue was purified using column chromatography containing silica gel with CH$_2$Cl$_2$:CH$_3$OH = 95:5 as the mobile phase to yield an orange oil of **2a** (1.15 g, 75%). ^{1}H NMR (CDCl$_3$, 400 MHz) δ 8.40 (d, J = 3.7 H$_z$, 2H, H-j), 7.72-7.62 (m, 2H, H-a and H-d), 7.55 (t, J = 3.9 Hz, 2H, H-h), 7.41 (t, J = 3.7 Hz, 1H, H-c), 7.34 (d, J = 3.8 Hz, 2H, H-g), 7.25 (d, J =3.6 Hz, 1H, H-b), 7.04 (t, J = 3.7 Hz, 2H, H-i), 3.80 (s, 2H, H-e), 3.71 (s, 4H, H-f).

2a
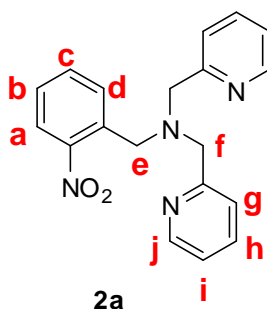
2.3.4 Preparation of 3-[bis(2-pyridylmethyl)aminomethyl]nitrobenzene (2b).

3-nitrobenzyl bromide (1.0 g, 4.6 mmol) was mixed with DPA (1.1 g, 5.5 mmol) according to the above general procedure to gain an orange oil of **2b** (1.21 g, 79%); ^{1}H NMR (CDCl$_3$, 400 MHz) δ 8.26 (d, J = 5.6 Hz, 2H, H-j), 8.03 (s, 1H, H-d), 7.77 (d, J = 7.8 Hz, 1H, H-a), 7.49 (d, J = 7.4 Hz, 1H, H-c), 7.41 (t, J =7.8 Hz, 2H, H-h), 7.30 (d, J = 7.6 Hz, 2H, H-g), 7.18 (t, J = 7.7 Hz, 1H, H-b), 6.87 (t, J = 5.0 Hz, 2H, H-i), 3.61 (s, 2H, H-e), 3.59 (s, 4H, H-f).

2b
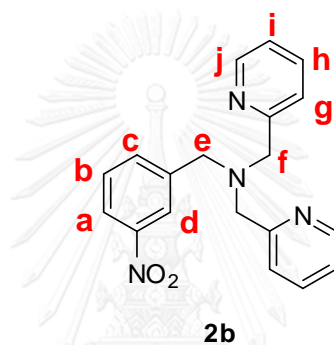
2.3.5 Preparation of 4-[bis(2-pyridylmethyl)aminomethyl]nitrobenzene (2c).

4-bitrobenzyl bromide (1.0 g, 4.6 mmol) was mixed with DPA (1.1 g, 5.5 mmol) according to the above general procedure to gain an orange oil of **2c** (1.33 g, 87%); ^{1}H NMR (CDCl$_3$, 400 MHz) δ 8.50 (d, J = 4.8 H$_z$, 2H, H-j), 8.12 (d, J = 8.7 Hz, 2H, H-a), 7.65 (t, J = 7.7 Hz, 2H, H-h), 7.56 (d, J = 8.7 Hz, 2H, H-b), 7.50 (d, J = 7.8 Hz, 2H, H-g), 7.14 (t, J = 6.3 Hz, 2H, H-i), 3.80 (s, 4H, H-f), 3.77 (s, 2H, H-e).

2c
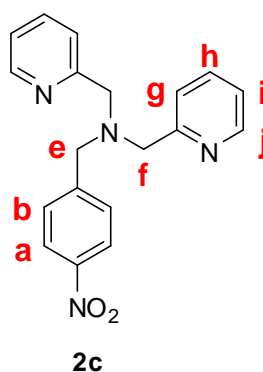
2.3.6 Preparation of *N,N*-dibenzyl-1-(2-nitrophenyl)methanamine (2d).
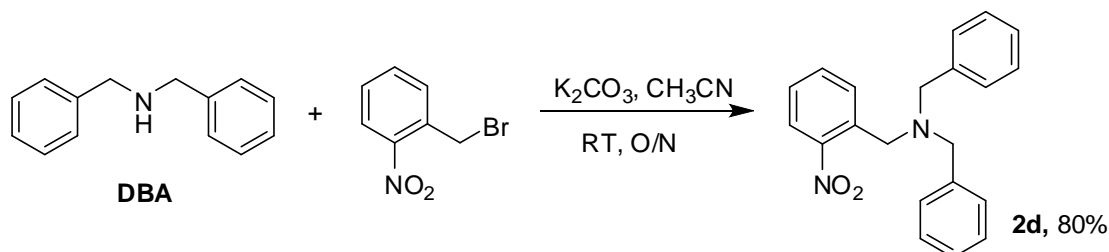
2-nitrobenzyl bromide (1.0 g, 4.6 mmol) was mixed with DBA (1.1 g, 5.6 mmol) according to the above general procedure. was purified using column chromatography containing silica gel using CH_2Cl_2:CH_3OH = 95:5 to gain a yellow oil of **2d** (1.22 g, 80%); ^{1}H NMR (CDCl$_3$, 400 MHz) δ 7.88 (d, *J* = 7.7 Hz, 1H, *H*-a), 7.81 (d, *J* = 8.1 Hz, 1H, *H*-d), 7.55 (t, *J* = 7.5 Hz, 1H, *H*-c), 7.39-7.33 (m, 8H, *H*-g, *H*-h and *H*-i), 7.26 (t, *J* = 5.6 Hz, 2H, *H*-b), 3.92 (s, 2H, *H*-e), 3.59 (s, 4H, *H*-f).

2d
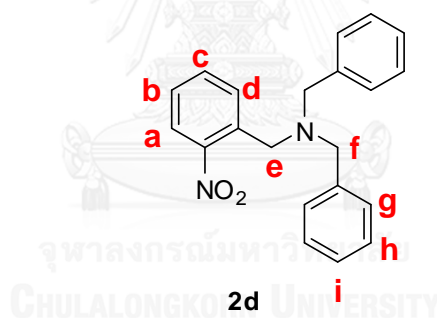
General synthesis of 1-methyl-2,2'dipicolylamine-aniline (3a-3c)

2a; R = 4-CH$_2$DPA
2b; R = 3-CH$_2$DPA
2c; R = 2-CH$_2$DPA

3a; R = 2-CH$_2$DPA, 90%
3b; R = 3-CH$_2$DPA, 93%
3c; R = 4-CH$_2$DPA, 95%
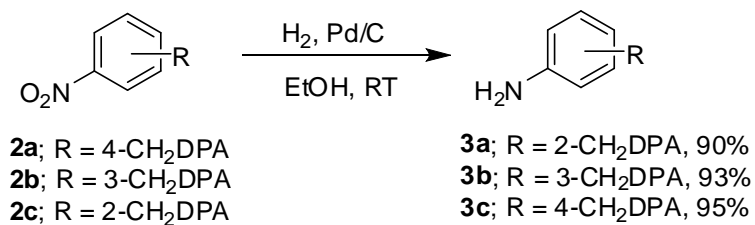
2.3.7 Preparation of 2-[bis(2-pyridylmethyl)aminomethyl]aniline (3a).

Compound **2a** (500 mg, 1.5 mmol) was dissolved in 10 mL of ethanol followed by addition of palladium on activated charcoal (Pd/C) (35 mg, 10% mol). The hydrogen gas was bubbled into the reaction mixture at room temperature and the reaction progress was monitored by TLC. After the starting compound **2a** disappeared, the solution was filtered to remove Pd/C powder and dried by a rotator evaporator to obtain a brown oil of **3a** (411 mg, 90%); ^{1}H NMR (CD$_3$OD, 400 MH$_z$) δ 8.44 (d, J = 4.1 Hz, 2H, H-j). 7.74 (t, J = 7.7 Hz, 2H, H-h), 7.48 (d, J = 7.9 Hz, 2H, H-g), **7**.25 (t, J = 6.3 Hz, 2H, H-i), 7.04 (d, J = 7.4 Hz, 1H, H-a), 7.00 (t, J = 7.4 Hz, 1H, H-b), 6.67 (d, J = 7.3 Hz, 1H, H-d), 6.58 (t, J = 7.4 Hz, 1H, H-c), 3.73 (s, 4H, H-f), 3.62 (s, 2H, H-e).

3a
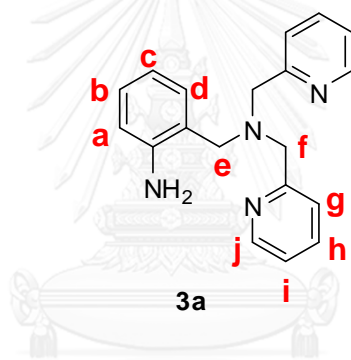
2.3.8 Preparation of 3-[bis(2-pyridylmethyl)aminomethyl]aniline (3b).

Compound **2b** (500 mg, 1.5 mmol) was dissolved in 10 mL of ethanol followed by addition of palladium on activated charcoal (Pd/C) (35 mg, 10% mol). The reaction was performed according to the above synthesis procedure to gain brown oil of **3b** (424 mg, 93%); ^{1}H NMR (CD$_3$OD, 400 MH$_z$) δ 8.37 (d, J = 4.9 Hz, 2H, H-j), 7.77 (t, J = 7.7 Hz, 2H, H-h), 7.67 (d, J = 7.8 Hz, 2H, H-g), 7.23 (t, J = 7.3 Hz, 2H, H-i), 7.01 (t, J = 7.7 Hz, 1H, H-b), 6.79 (s, 1H, H-d), 6.69 (d, J = 7.6 Hz, 1H, H-a), 6.57 (d, J = 7.2 Hz, 1H, H-c), 3.70 (s, 4H, H-f), 3.26 (s, 2H, H-e).
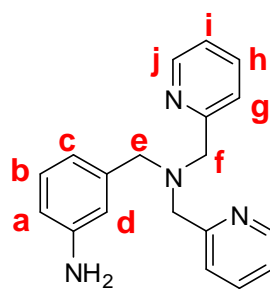
3b

2.3.9 Preparation of 4-[bis(2-pyridylmethyl)aminomethyl]aniline (3c).

Compound **2c** (500 mg, 1.5 mmol) was dissolved in 10 mL of ethanol followed by addition of palladium on activated charcoal (Pd/C) (35 mg, 10% mol). The reaction was performed according to the above synthesis procedure to obtain brown oil of **3c** (433 mg, 95%) ^{1}H NMR (CD$_3$OD, 400 MHz) **δ** 8.40 (d, J = 4.3 Hz, 2H, H-j), 7.80 (t, J = 6.8 Hz, 2H, H-h), 7.67 (d, J = 7.8 Hz, 2H, H-g), 7.26 (t, J = 6.3 H$_z$, 2H, H-i), 7.12 (d, J = 8.4 Hz, 2H, H-a), 6.69 (d, J = 8.4 Hz, 2H, H-b), 3.72 (s, 4H, H-f), 3.51 (s, 2H, H-e).
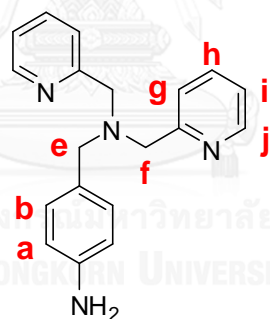
3c

2.3.10 Preparation of 2-((dibenzylamino)methyl)aniline (3d).

2d

H$_2$, Pd/C

EtOH, RT

3d, 97%
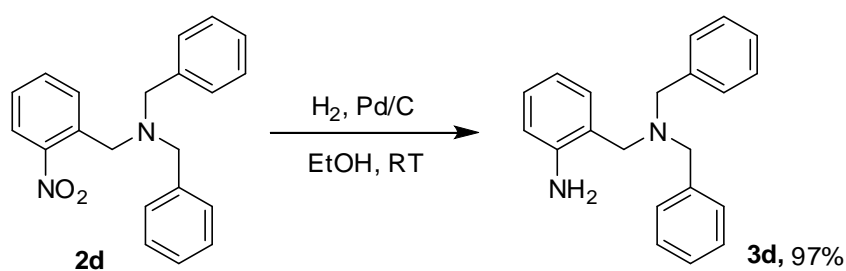
Compound **2d** (500 mg, 1.5 mmol) and Pd/C (10% mol) was dissolved in 10 mL of DCE followed by addition of palladium on activated charcoal (Pd/C) (10% mol). The reaction was operated according to above synthesis procedure. The residue was purified by column chromatography on silica gel using hexane:EtOAc = 5:1 as a mobile phase to obtain a white solid of **3d** (433 mg, 97%) ^{1}H NMR (DMSO-d_6, 400 MHz) **δ** 7.18-7.39 (10H, m, *H*-g, *H*-h and *H*-i), 7.02 (d, *J* = 7.1 Hz, 1H, *H*-a), 6.94 (t, *J* = 6.9 Hz, 1H, *H*-c), 6.57 (d, *J* = 7.9 Hz, 1H, *H*-d), 6.49 (t, *J* = 6.9 Hz, 1H, *H*-b), 3.41 (s, 4H, *H*-f), 3.39 (s, 2H, *H*-e).

3d
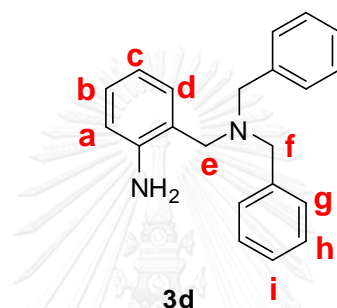
General synthesis of 8-hydroxy-9-iminyljulolidine derivatives (J2P, J3P and J4P)

3a; R = 4-CH₂DPA
3b; R = 3-CH₂DPA
3c; R = 2-CH₂DPA

J2P; R = 4-CH₂DPA, 71%
J3P; R = 3-CH₂DPA, 76%
J4P; R = 2-CH₂DPA, 81%
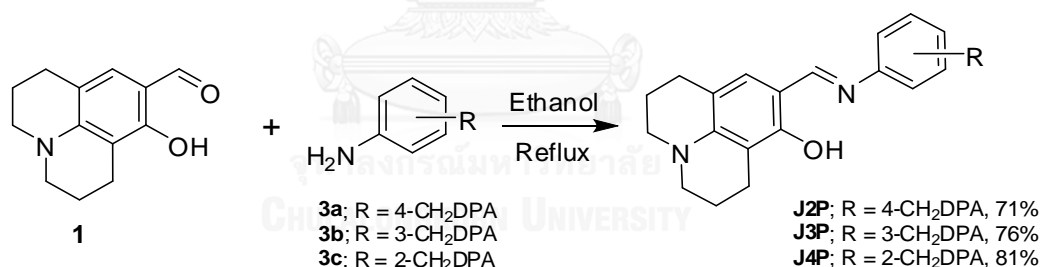
2.3.11 Preparation of (E)-9-((2-((bis(pyridin-2-ylmethyl)amino)methyl) phenylimino)methyl)-1,2,3,5,6,7-hexahydropyrido[3,2,1-ij]quinolin-8-ol (J2P).

Julolidine **1** (100 mg, 0.46 mmol) and compound **3a** (168 mg, 0.55 mmol) were combined in 10 mL of ethanol. The reaction mixture was stirred at room temperature under N₂ atmosphere for 10 minutes and heated up to the reflux temperature overnight. Then, the mixture was cooled down to room temperature and the solvent was removed under a reduced pressure to get a residue of yellow oil. The residue was purified by column chromatography on Sephadex (LH-20) using methanol as the

mobile phase to yield a bright yellow oil of **J2P** (164 mg, 71%); ^{1}H NMR (CD$_3$OD, 400 MHz) δ 8.28 (d, J = 4.8 Hz, 2H, H-o), 8.22 (s, 1H, H-e), 7.62-7.56 (m, 4H, H-l and H-m), 7.45 (d, J = 6.9 Hz, 1H, H-i), 7.22 (t, J = 7.0 Hz, 2H, H-n), 7.16-7.05 (m, 3H, H-g, H-f and H-h), 6.77 (s, 1H, H-d), 3.87 (s, 2H, H-j), 3.80 (s, 4H, H-k), 3.31-3.22 (m, 4H, H-a), 2.68-2.60 (m, 4H, H-c), 1.95-1.87 (m, 4H, H-b); ^{13}C NMR (100 MHz, CD$_3$OD) δ 160.6, 160.4, 149.6, 149.1, 138.4, 131.9, 131.8, 131.5, 129.8, 126.1, 124.9, 123.8, 123.5, 118.9, 115.1, 110.5, 107.5, 61.1, 56.8, 51.3, 50.9, 28.4, 23.3, 22.3, 21.5; HRMS (ESI) m/z 504.2758 (M+H$^+$, C$_{32}$H$_{34}$N$_5$O$^+$, requires 504.2758).

J2P
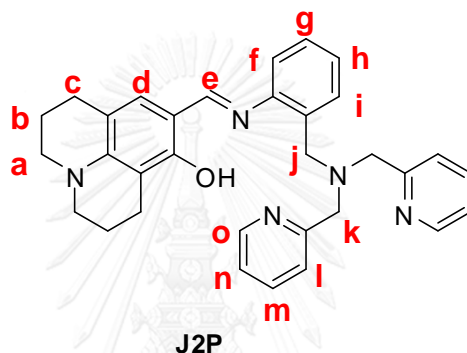
2.3.12 Preparation of (E)-9-((3-((bis(pyridin-2-ylmethyl)amino)methyl) phenylimino)methyl)-1,2,3,5,6,7-hexahydropyrido[3,2,1-ij]quinolin-8-ol (J3P).

Julolidine **1** (100 mg, 0.46 mmol) was mixed with compound **3b** (168 mg, 0.55 mmol). The reaction was operated under the above synthesis procedure to obtain a yellow oil of **J3P** (176 mg, 76%); ^{1}H NMR (CD$_3$OD, 400 MHz) δ 8.42 (d, J = 4.3 Hz, 2H, H-o), 8.29 (s, 1H, H-e), 7.81 (t, J = 7.9 Hz, 2H, H-m), 7.69 (d, J = 7.4 Hz, 2H, H-l), 7.24-7.35 (m, 3H, H-g and H-n), 7.21 (d, J = 8.0 Hz, 1H, H-h), 7.14 (d, J = 7.6 Hz, 1H, H-f), 6.82 (s, 1H, H-i), 6.75 (s, 1H, H-d), 3.80 (s, 4H, H-k), 3.69 (s, 2H, H-j), 3.25-3.33 (m, 4H, H-a), 2.68-2.62 (m, 4H, H-c), 1.95-1.87 (m, 4H, H-b); ^{13}C NMR (100 MHz, CD$_3$OD) δ 160.5, 156.4, 150.6, 149.5, 145.6, 141.8, 138.7, 131.6, 130.7, 126.8, 124.9, 124.7, 123.8, 120.4, 118.8, 110.3, 107.8, 61.0, 59.8, 51.4, 51.1, 28.5, 23.3, 22.2, 21.4; HRMS (ESI) m/z 504.2757 (M+H$^+$, C$_{32}$H$_{34}$N$_5$O$^+$, requires 504.2758).

J3P
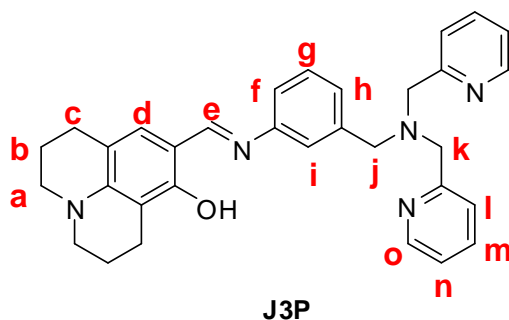
2.3.13 Preparation of (E)-9-((4-((bis(pyridin-2-ylmethyl)amino)methyl) phenylimino)methyl)-1,2,3,5,6,7-hexahydropyrido[3,2,1-ij]quinolin-8-ol (J4P).

Synthesized from julolidine **1** (100 mg, 0.46 mmol) was mixed with compound **3c** (168 mg, 0.55 mmol). The reaction was performed under the above synthesis procedure to obtain a yellow oil of **J3P** (188 mg, 81%); ^{1}H NMR (400 MHz, CD$_3$OD) δ 8.42 (d, J = 4.2 Hz, 2H, H-o), 8.28 (s, 1H, H-e), 7.81 (t, J = 7.6 Hz, 2H, H-m), 7.69 (d, J = 7.8 Hz, 2H, H-f), 7.43 (d, J = 8.3 Hz, 2H, H-l), 7.27 (t, J = 6.0 Hz, 2H, H-n), 7.23 (d, J = 8.4 Hz, 2H, H-g), 6.73 (s, 1H, H-d), 3.77 (s, 4H, H-k), 3.64 (s, 2H, H-j), 3.23-3.33 (m, 4H, H-a), 2.60-2.67 (m, 4H, H-c), 1.94-1.86 (m, 4H, H-b); ^{13}C NMR (100 MHz, CD$_3$OD) δ 160.0, 156.7, 150.5, 149.4, 144.7, 138.7, 136.9, 131.6, 131.4, 124.8, 123.8, 119.9, 115.8, 110.2, 107.8, 60.8, 59.4, 51.3, 51.0, 28.5, 23.3, 22.2, 21.4; HRMS (ESI) m/z 526.2589 (M+Na$^+$, C$_{32}$H$_{33}$N$_5$NaO$^+$, requires 526.2577).

J4P
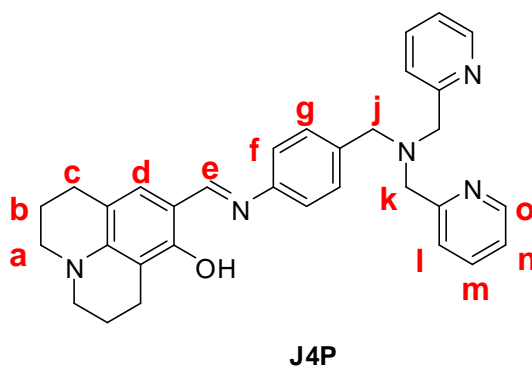
2.3.14 Preparation of (E)-9-((2-((dibenzylamino)methyl)phenylimino) methyl)-1,2,3,5,6,7-hexahydro-pyrido[3,2,1-ij]quinolin-8-ol (J2B).
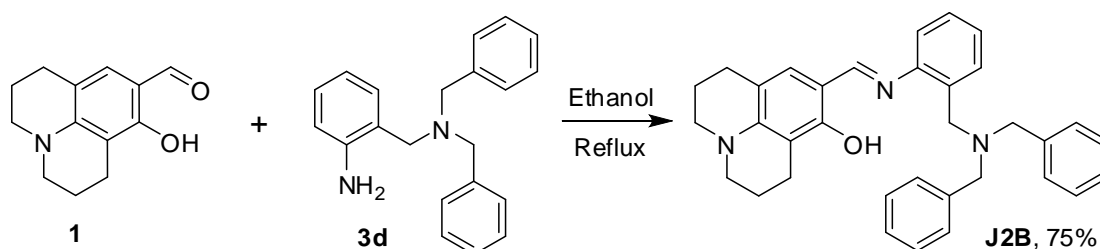
Julolidine **1** (100 mg, 0.46 mmol) was mixed with compound **3d** (166 mg, 0.55 mmol). The reaction was performed under the above synthesis procedure to obtain a yellow oil of **J2B** (230 mg, 75%); ^{1}H NMR (400 MHz, CD$_3$OD) δ 8.22 (s, 1H, *H*-e), 7.60 (d, *J* = 7.3 Hz, 1H, *H*-i), 7.35 (d, *J* = 7.4 Hz, 4H, *H*-l), 7.26-7.22 (m, 5H, *H*-g and *H*-m), 7.18-7.15 (m, 4H, *H*-f, *H*-h and *H*-n), 6.77 (s, 1H, *H*-d), 3.69 (s, 2H, *H*-j), 3.57 (s, 4H, *H*-k). 3.34-3.25, (m, 4H, *H*-a), 2.72-2.60 (m, 4H, *H*-c), 1.99-1.86 (m, 4H, *H*-b); ^{13}C NMR (100 MHz, CD$_3$OD) δ 159.3, 140.8, 132.7, 132.5, 131.5, 131.1, 130.0, 129.2, 127.9, 126.2, 118.5, 115.3, 110.5, 107.7, 59.1, 54.6, 51.3, 51.0, 28.4, 23.3, 22.3, 21.5; HRMS (ESI) *m/z* 502.2851 (M+H^{+}, C$_{34}$H$_{36}$N$_3$O$^+$, requires 502.2853).

J2B
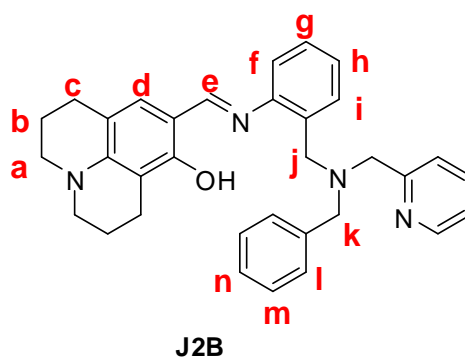
2.4 Analytical experiment

The metal sensing and photophysical property studies of all compounds were achieved in mixed solvent containing methanol and dimethylsulfoxide as an organic phase and using milliQ water as an aqueous media. UV-visible spectrophotometer and fluorescence spectrophotometer were applied to investigate the photophysical properties.

2.4.1 Photophysical property studies

The stock solutions of **J2P, J3P, J4P and J2B** were prepared in methanol and DMSO at the concentration of 100 μM. The photophysical property data of each compound was collected using UV-Visible spectrophotometer and fluorescence spectrophotometer at room temperature.

2.4.2 UV-Visible spectroscopy

The UV-Visible absorption spectra of the stock solutions of all samples were collected from 200 nm to 600 nm at ambient temperature.

2.4.3 Fluorescence spectroscopy

The concentration of each sample was diluted from 100 μM of the stock solution to 10 μM. According to their maximum absorption (λ_{max}), the excitation wavelength (λ_{ex}) of **J2P, J3P, J4P and J2B** was carried out at 380 nm, 415 nm, 420 nm and 368 nm, respectively. The fluorescence spectra were collected in visible region using their excitation wavelength at ambient temperature.

2.4.4 Molar extinction coefficient (ε)

Molar extinction coefficients (ε) of all target compounds were calculated by using an absorption value at various concentrations of analytical samples collected from the UV-Visible absorption spectra in methanol and DMSO. The absorbance at the maximum absorption wavelength (λ_{max}) of each compound was plotted against the

various concentrations of sample at the respective excitation wavelength (λ_{ex}). Each plot should be a linear relationship passing through the origin. Beer-Lambert law was applied to calculate the molar extinction coefficient (ε) where A is absorbance at λ_{max}, C is concentration and b represents the path length (1 cm).

$$A = \varepsilon bC$$

2.4.5 Fluorescence quantum yield

The fluorescence quantum yield of the complexes between fluorescent sensors and metal ions were performed by using quinine sulphate ($\Phi_F = 0.54$) in 0.1 M H_2SO_4 as a reference [61]. The UV-Visible absorption spectra of the reference of the analytical complexes were collected at various concentrations. The maximum absorbance of all samples should never exceed 0.1 so that the interaction among themselves at high concentration will be prevented. The fluorescence emission spectra of the same solution using appropriate excitation wavelengths selected were recorded based on the absorption maximum wavelength (λ_{max}) of each compound. The relative graphs of integrated fluorescence intensity were plotted against the absorbance at the respective excitation wavelengths. Each coordination should be a straight line with one interception and gradient *m* [62].

Furthermore, the fluorescence quantum yield (Φ_F) was obtained from plotting of integrated fluorescence intensity *vs* absorbance represented into the following equation:

$$\Phi_X = \Phi_{ST} \left(\frac{Grad_X}{Grad_{ST}} \right) \left(\frac{\eta_X^2}{\eta_{ST}^2} \right)$$

The symbol Φ_{ST} denotes the fluorescence quantum yield of the standard reference which was quinine sulphate in 0.1 M H_2SO_4 (Φ = 0.54) and Φ_X is the fluorescence quantum yield of sample and η is the refractive index of the solvent.

2.4.6 Metal ion sensor

The samples used in this experiment were prepared in the same manner to that of 2.4.1.

a) Selectivity study

To obtain the fluorescence enhancing profile, the stock solutions of all compounds were diluted to 10 µM and mixed with 100 µM metal ion solution at the molar ratio of 1:10. The experiments were performed under two solvent conditions including methanol/H_2O (9:1, v/v) and DMSO/H_2O (95:5, v/v). The selectivity results of each compound were collected at ambient temperature using fluorescence spectrophotometer. In order to gain the photograph of naked eye observation of fluorescence response under black light, the stock solution of **J2P** was diluted to 10 µM, then 100 µM metal ion solution was added. The photograph was collected by using Canon-60D DSLR camera with Sigma 17-70 mm F2.8-4 DC Macro.

b) Time-dependent fluorescence enhanced study

The stock solution of the fluorescent sensor **J2P** in methanol was diluted to 10 µM then the solvent condition was adjusted to ratio of methanol/H_2O (9:1, v/v) and mixed with aluminium nitrate solution 100 µM at the molar ratio of 1:10. Magnesium nitrate was also mixed with **J2P** at the same ratio under the solvent condition of DMSO/H_2O (95:5, v/v). The fluorescence signals were collected immediately using a fluorescence spectrophotometer upon addition of the metal solution and monitored continuously for 30 minutes at room temperature. The time-dependent fluorescence enhancement of **J2P** to Al^{3+} was reported by plotting I/I_o vs time.

c) Fluorescence and UV-Visible titration

To achieve the fluorescence titration spectra, **10** µM of **J2P** was prepared in methanol and DMSO for fluorescence titration experiment and 50 µM for UV-Visible titration experiment. This **J2P** was mixed with 0.2 equiv. to 5 equiv. of Al^{3+} and Mg^{2+}, respectively. The solvent condition was adjusted to the ratio of methanol/ H_2O (9:1, v/v) and DMSO/H_2O (95:5, v/v) for Al^{3+} and Mg^{2+} detection, respectively. UV-Visible titrations for metal binding of **J2P** toward both metal ions were operated similarly to the fluorescence titration experiment.

d) Job's Plot experiment

Job's Plot was generally used for determination of the coordination ratio between fluorescent sensor and analyte. In this experiment, the series of solutions were prepared by fixing the number of moles of **J2P** and Al^{3+} of Mg^{2+} whereas their mole fractions were varied (4:1 to 1:4). The experimental results were obtained from the relation between mole fraction of Al^{3+} or Mg^{2+} (X_B) and $(y-y_o)(1-X_B)$ where; y_o represents maximum fluorescence intensity of **J2P** after metal ions were added at X_B. The maximum coordination on the plot shows complex stoichiometry between two species. The excitation wavelength was used at 380 nm for Al^{3+} detection and 390 nm for Mg^{2+} detection, respectively.

e) ^1H NMR experiment

J2P (5.0 mg, 0.10 mmol) was dissolved in CD_3OD and DMSO-d_6 in an NMR tube. $Al(NO_3)_3$ and $Mg(NO_3)_3$ prepared in CD_3OD and DMSO-d_6 were added for equivalents of 0.5 and 1.0, respectively, to the solution of **J2P** and shaken thoroughly. The ^1H NMR spectra were collected at 15 minutes after the addition of the metal ions using a 400 MHz NMR spectrometer (Mercury 400, Varian) at ambient temperature.

f) Interference study

As **J2P** exhibits an interesting sensing properties toward Al^{3+} and Mg^{2+} in different solvent conditions, the interference from other cations was studied. The stock solution of **J2P** in methanol was diluted to 10 µM. The mixtures between Al^{3+} and other metal ions were prepared using milliQ water. The mixture of metal ions was added to the **J2P** solution in the **J2P**:Al^{3+}: interfering metal ions ratio of 1:1:1. Then the solvent was adjusted to the ratio of methanol/H_2O (9:1, v/v). The fluorescence spectra were collected at 15 minutes after the mixture of metal ions was added. In case of Mg^{2+} sensing, the interference study was performed in the similar operation of Al^{3+} in the mixed solvent of DMSO/H_2O (95:5, v/v).

g) Reversibility study

To achieve the experimental results, 10 µM of **J2P** in methanol was prepared and mixed with 1.0 equiv. of Al^{3+}. The fluorescence signal was observed at 15 minutes upon addition of Al^{3+} in the condition of methanol/H_2O (9:1, v/v). After that, 1 µL (1.0 equiv.) of EDTA, which was prepared at concentration of 10 mM, was added to the mixture and the fluorescence signal was repeatedly investigated again. The second time, 1 µL (1.0 equiv.) of Al^{3+} from 10 mM stock solution of $Al(NO_3)_3$ was added to the mixture then the fluorescence signal was collected over 15 minutes and followed by addition of EDTA. By the same method, the reversibility properties of **J2P**-Mg^{2+} were studied in the mixed solvent of DMSO/H_2O (95:5, v/v). The next experiment will be performed similarly in the same manner as that of the second time. The experimental results were reported by plotting of fluorescence intensity ration (I/I_o) and time of experiment.

h) The detection limit (LOD)

LOD is one of the important data to show the efficiency of the fluorescent sensor. The LOD illustrates the lowest quantity of the analyte in the system that can be detected. However, it may be not necessarily quantitated as an exact value. LOD can be approximated using the equation:

$$\text{Detection limit} = 3\,[\sigma\,/\,K_{sv}]$$

Where;

σ is the standard deviation of the response deriving from the maximum intensity of fluorophore at 1 µM of 9 samples.

K_{sv} is the slope of the calibration curve obtained from fluorescence titration spectra of sensor probe, plotting between I/I_o and molar concentration of considered analyte.

CHAPTER III

RESULTS AND DISCUSSION

3.1 Synthesis and characterization of julolidine precursor

The flurophore to be developed as the target fluorescent sensor was designed using julolidine building block containing hydroxy group and imine moiety. As these groups are expected to play an important role as a hard base unit in fluorescent sensor, the target molecules might have the specific interaction towards some hard acid metal ions. The julolidine **1** was synthesized in two important steps as shown in **Scheme 3.1.**
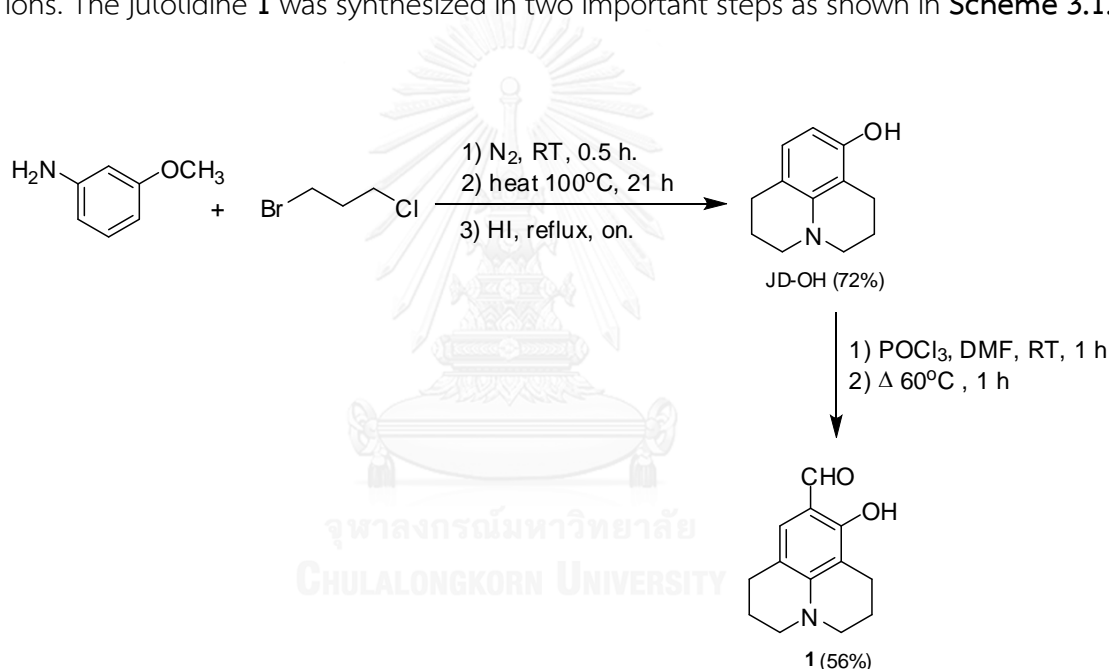
Scheme 3.1 The synthesis of julolidine **1**.

8-hydroxyjulolidine (**JD-OH**) was prepared from the coupling reaction between 2-methoxyaniline and 1-bromo-3-chloropropane under a high temperature condition, followed by an acid-induced demethylation. The reaction mechanism composed of two crucial steps (**Scheme 3.2**). First, a lone pair electron of nitrogen atom performed substitution reaction (S_N2) to carbon with bromide substituent of 1-bromo-3-chloropropane then two sets of electrophilic aromatic substitution (EArS) followed by rearomatization were repeated to obtain methoxy intermediate **1**. Finally, intermediate

1 was treated with hydroiodic acid for demethylation of a methyl group into a hydroxy group at the reflux temperature. In spite of the severe condition and longtime reaction with difficulty in controlling some parameters including temperature and moisture, the target product (**JD-OH**) was obtained in satisfactory yield.
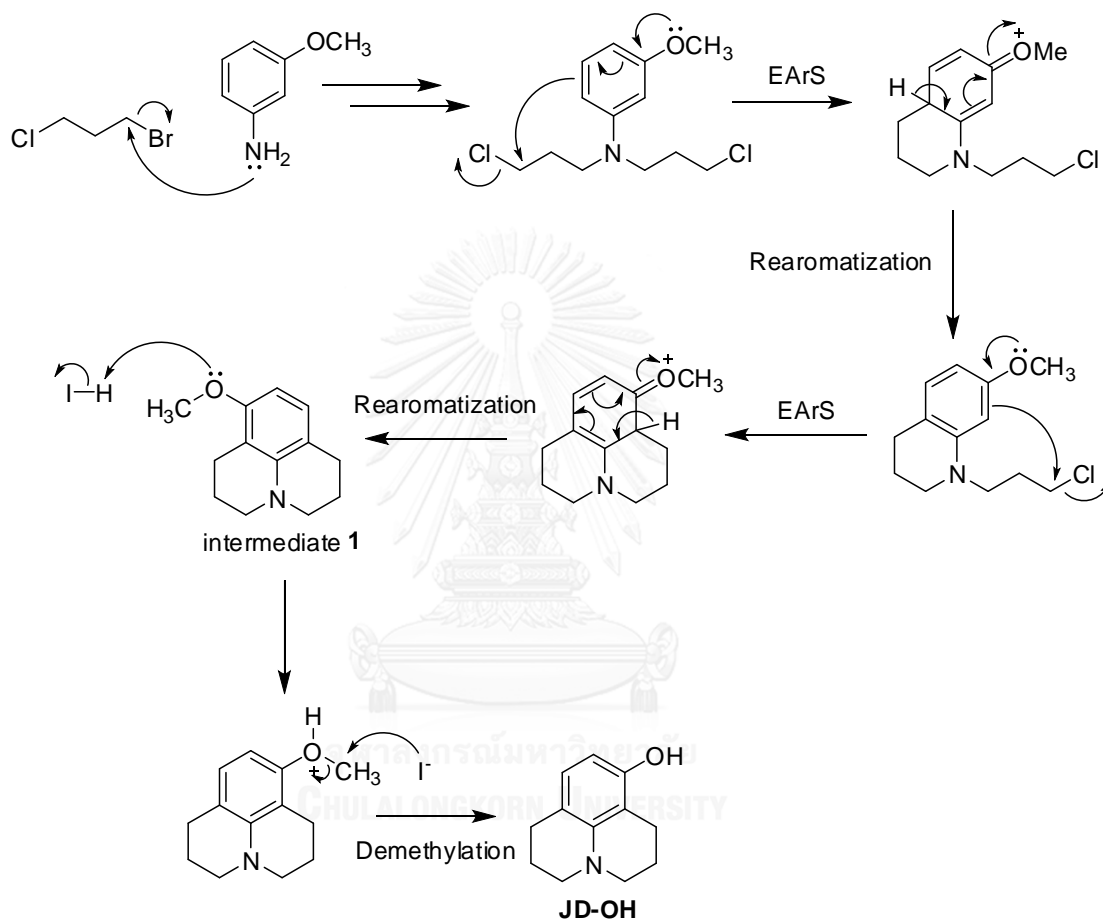
Scheme 3.2 The reaction mechanism of **JD-OH**.

To generate an aldehyde group in the molecule of **JD-OH**, the formylation reaction was performed using phosphorus oxychloride (POCl$_3$) in dimethylformamide (DMF) as a reagent (**Scheme 3.3**). Initially, POCl$_3$ and DMF was mixed at the room temperature followed by heating up to around 60 $^\circ$C after **JD-OH** was added. Vilsmeier–Haack reaction mechanism was used to describe the formylation reaction. The EArS was operated between **JD-OH** and iminium cation which was generated from

both reagents to attain an aromatic iminium ion intermediate followed by hydrolysis during work up to obtain julolidinyl aldehyde **1** in moderate yield.
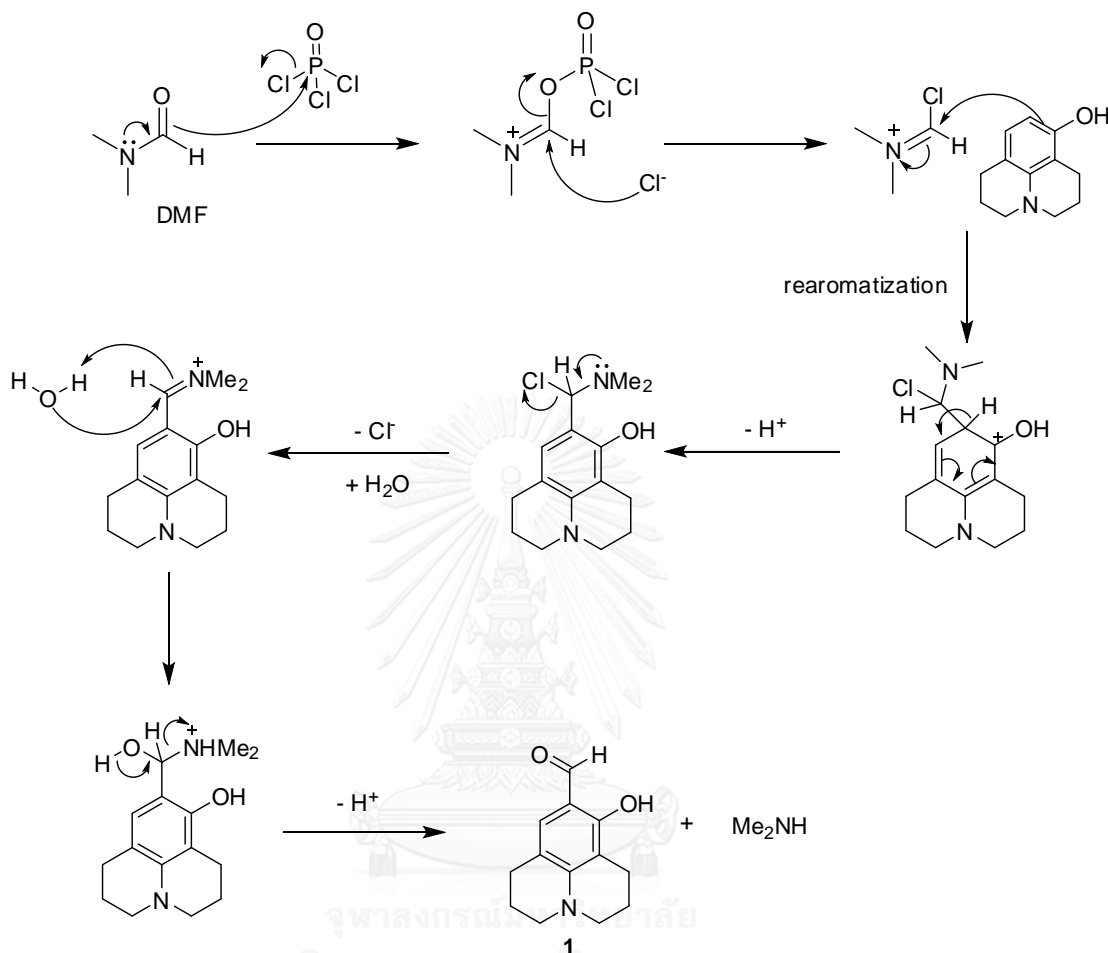
Scheme 3.3 The reaction mechanism of julolidine aldehyde **1**.

The ^{1}H NMR shows stacked chart the characteristic peaks which related to both molecules (**Figure 3.1**). The doublet peaks of the aromatic proton d and e in **JD-OH** were found at chemical shift of 6.10 and 6.70 ppm, respectively. After the formulation reaction was proceeded to gain julolidine **1**, the aromatic proton e disappeared and proton d changed from doublet peak to singlet peak at downfield region due to the substitution of an electron withdrawing group to aromatic ring. Moreover, the single peak of aldehyde proton f at around 9.40 ppm appeared to confirm the production of julolidine **1**.
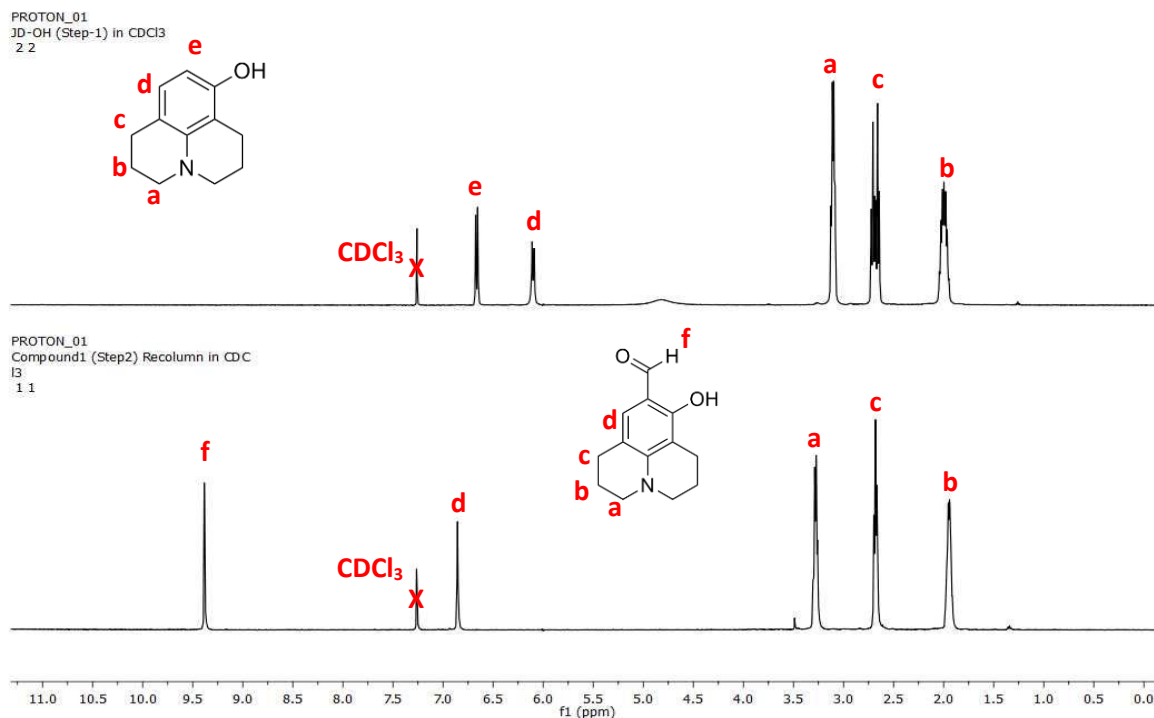
Figure 3.1 ^{1}H NMR spectra (400 MHz) of **JD-OH** and julolidine **1**.

According to the ^{1}H NMR of **JD-OH**, the proton signals were investigated at the chemical shift (δ) of 6.66 (d, J = 8.0 Hz, 1H, H-e), 6.10 (d, J = 8.0 Hz, H-d), 3.18-3.00 (m, 4H, H-a), 2.76-2.59 (m, 4H, H-c) and 2.10-1.88 (m, 4H, H-b). After the formylation reaction was performed to obtain julolidinyl aldehyde **1**, the target product was characterized also using ^{1}H NMR. The proton signals of julolidine **1** were observed at the chemical shift (δ) of 9.36 (s, 1H, H-f), 6.85 (s, 1H, H-d), 3.34-3.15 (m, 4H, H-a), 2.75-2.55 (m, 4H, H-c) and 2.02-1.84 (m, 4H, H-b).

3.2 Synthesis and characterization of control part precursors

According to the design of imine-based fluorescent sensor, dipicolylamine (DPA) derivative was used to develop and synthesize as a control part (**Scheme 3.4**). Compounds **2a**-**2c** were collected from the coupling reaction between the corresponding nitrobenzyl bromide and di-(2-picolyl)amine using K_2CO_3 as catalytic

base. The reduction reaction of **2a**-**2c** were performed using hydrogen gas bubbling through the solution containing palladium on activated charcoal (Pd/C) as a catalyst to gain compounds **3a**-**3c** in excellent yields.
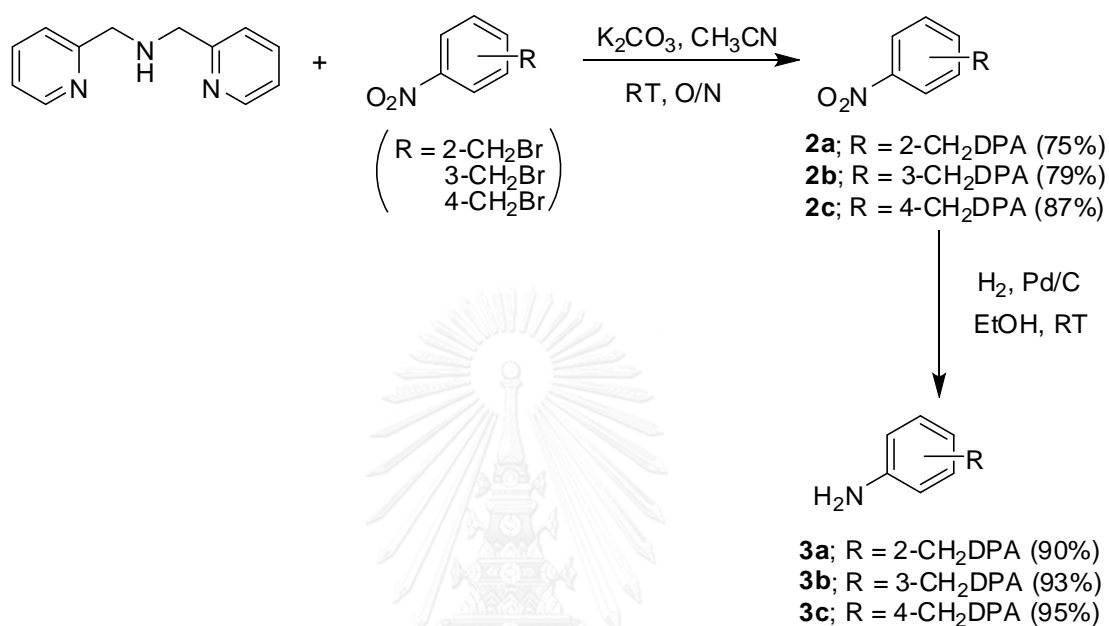
Scheme 3.4 The synthesis of compound **3a**-**3c**.

The couplings of 2-, 3-, and 4-nitrobenzyl bromide with DPA by nucleophilic substitution (S_N2) attain 75%, 79% and 87% yields of **2a**, **2b** and **2c**, respectively. Based on the steric effect of the substituent group that caused the difficulty of the substitution of DPA to the *ortho*-position of 2-nitrobenzyl bromide resulted in lower yield of compound **2a** than those of **2b** and **2c**. Then, the reductions of the three nitroaromatic compounds to get the aniline derivatives (**3a**-**3c**) were performed. According to ^{1}H NMR comparison between compounds **2** (**2a**-**2c**) containing nitro groups and compounds **3** (**3a**-**3c**) containing amine groups (**Figure 3.2**-**3.4**), the results showed that after a nitro group, electron withdrawing group (EWG), was reduced to an amine group, electron donating group (EDG), the proton signals at the benzene ring (red label) were drastically shifted to the upfield region. On the other hand, the chemical shifts of protons in pyridine ring (blue label) were not changed significantly.
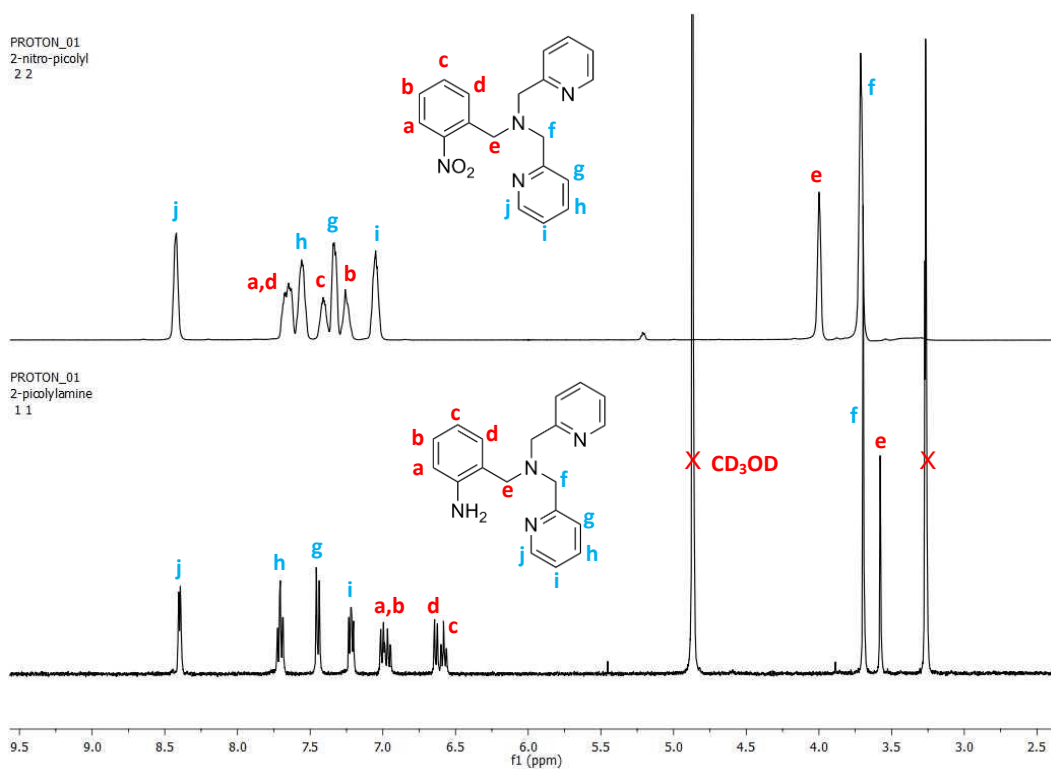
Figure 3.2 ^{1}H NMR spectra (400 MHz) of **2a** and **3a**.

According to the ^{1}H NMR of compound **2a** found the proton signals were found at the corresponding chemical shift (δ) as follows: 8.40 (d, J = 3.7 H$_z$, 2H, H-j), 7.72-7.62 (m, 2H, H-a and H-d), 7.55 (t, J = 3.9 Hz, 2H, H-h), 7.41 (t, J = 3.7 Hz, 1H, H-c), 7.34 (d, J = 3.8 Hz, 2H, H-g), 7.25 (d, J =3.6 Hz, 1H, H-b), 7.04 (t, J = 3.7 Hz, 2H, H-i), 3.80 (s, 2H, H-e) and 3.71 (s, 4H, H-f). In case of compound **3a**, the proton signals appeared in the chemical shifts (δ) of 8.44 (d, J = 4.1 Hz, 2H, H-j). 7.74 (t, J = 7.7 Hz, 2H, H-h), 7.48 (d, J = 7.9 Hz, 2H, H-g), **7**.25 (t, J = 6.3 Hz, 2H, H-i), 7.04 (d, J = 7.4 Hz, 1H, H-a), 7.00 (t, J = 7.4 Hz, 1H, H-b), 6.67 (d, J = 7.3 Hz, 1H, H-d), 6.58 (t, J = 7.4 Hz, 1H, H-c), 3.73 (s, 4H,H-f) and 3.62 (s, 2H, H-e)
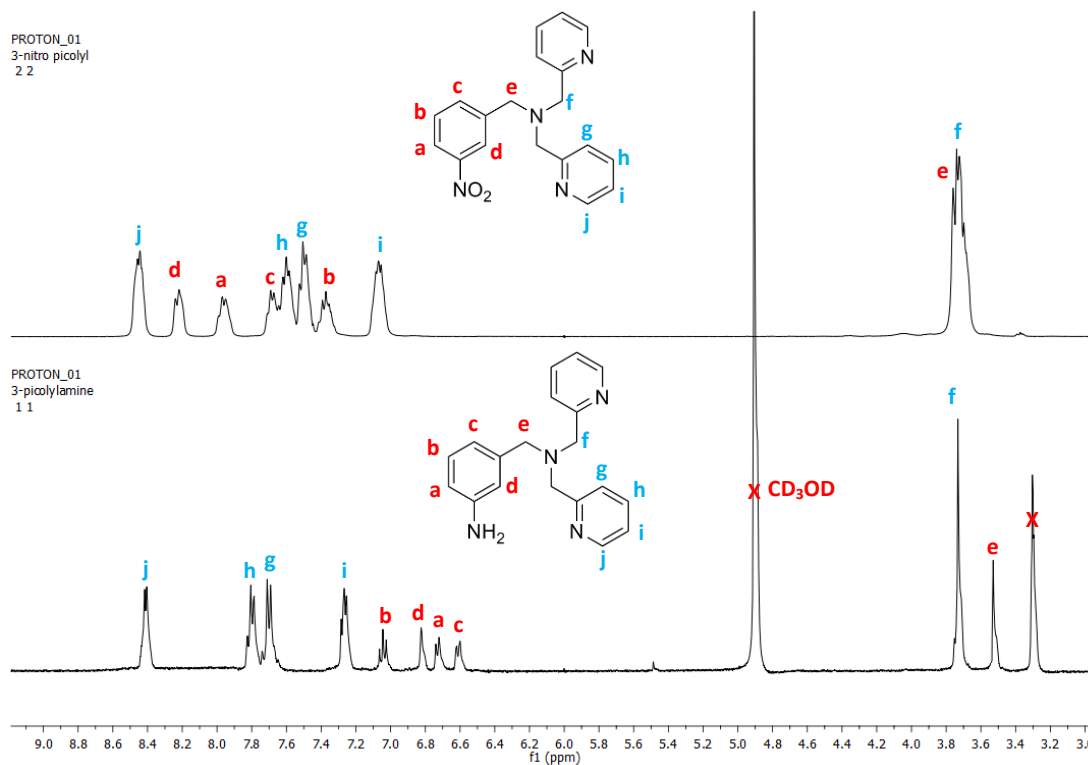
Figure 3.3 ^{1}H NMR spectra (400 MHz) of **2b** and **3b**.

According to the characterization of compound **2b** using ^{1}H NMR as depicted in **Figure 3.3**, the result showed that the proton signals were observed at the chemical shifts (δ) of 8.26 (d, J = 5.6 Hz, 2H, H-j), 8.03 (s, 1H, H-d), 7.77 (d, J = 7.8 Hz, 1H, H-a), 7.49 (d, J = 7.4 Hz, 1H, H-c), 7.41 (t, J =7.8 Hz, 2H, H-h), 7.30 (d, J = 7.6 Hz, 2H, H-g), 7.18 (t, J = 7.7 Hz, 1H, H-b), 6.87 (t, J = 5.0 Hz, 2H, H-i), 3.61 (s, 2H, H-e) and 3.59 (s, 4H, H-f). And the proton signals of compound **3b** were found at the chemical shifts (δ) of 8.37 (d, J = 4.9 Hz, 2H, H-j), 7.77 (t, J = 7.7 Hz, 2H, H-h), 7.67 (d, J = 7.8 Hz, 2H, H-g), 7.23 (t, J = 7.3 Hz, 2H, H-i), 7.01 (t, J = 7.7 Hz, 1H, H-b), 6.79 (s, 1H, H-d), 6.69 (d, J = 7.6 Hz, 1H, H-a), 6.57 (d, J = 7.2 Hz, 1H, H-c), 3.70 (s, 4H, H-f) and 3.26 (s, 2H, H-e).
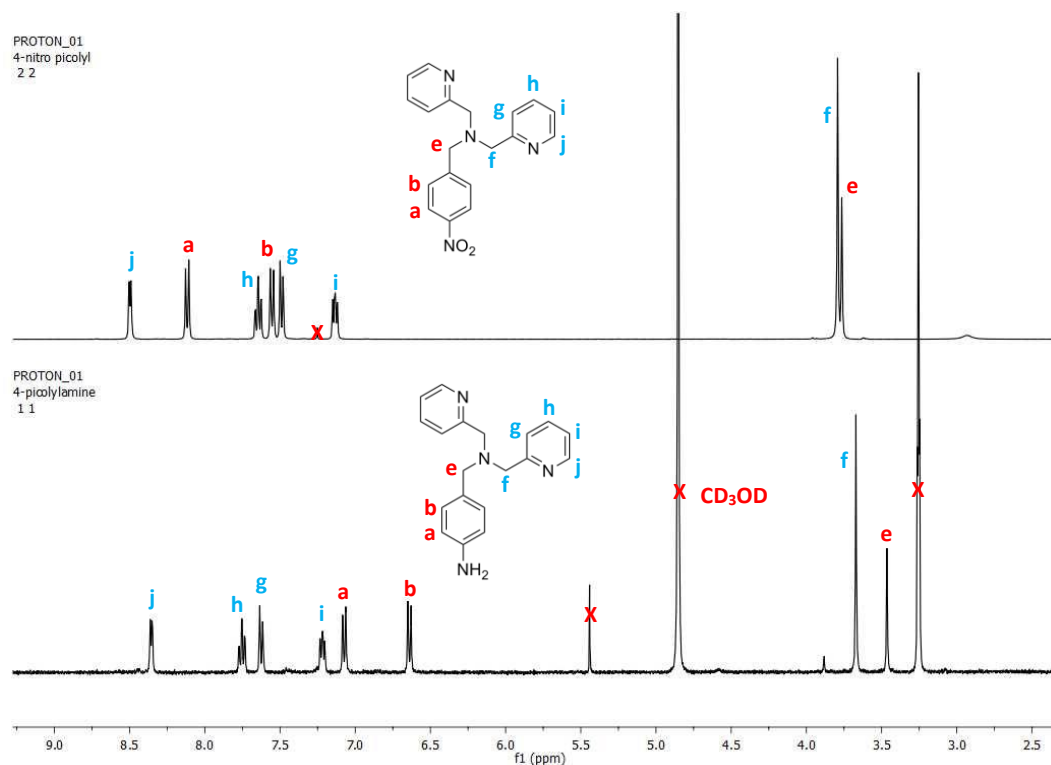
Figure 3.4 ^{1}H NMR spectra (400 MHz) of **2c** and **3c**.

The characterization of these two compounds was performed by ^{1}H NMR, the proton signals of compound **2c** were observed at the chemical shifts (δ) as follows: 8.50 (d, J = 4.8 H$_z$, 2H, H-j), 8.12 (d, J = 8.7 Hz, 2H, H-a), 7.65 (t, J = 7.7 Hz, 2H, H-h), 7.56 (d, J = 8.7 Hz, 2H, H-b), 7.50 (d, J = 7.8 Hz, 2H, H-g), 7.14 (t, J = 6.3 Hz, 2H, H-i), 3.80 (s, 4H, H-f) and 3.77 (s, 2H, H-e). Meanwhile, the proton signals of **3c** were found at the chemical shifts (δ) of 8.40 (d, J = 4.3 Hz, 2H, H-j), 7.80 (t, J = 6.8 Hz, 2H, H-h), 7.67 (d, J = 7.8 Hz, 2H, H-g), 7.26 (t, J = 6.3 H$_z$, 2H, H-i), 7.12 (d, J = 8.4 Hz, 2H, H-a), 6.69 (d, J = 8.4 Hz, 2H, H-b), 3.72 (s, 4H, H-f) and 3.51 (s, 2H, H-e).

3.3 Synthesis and characterization of target compounds (J2P, J3P and J4P)

The target molecules were synthesized by the imine formation coupling between aldehyde **1** and the corresponding amine derivatives **3a**-**3c** (**Scheme 3.5**). In this step, the reaction was proceeded under reflux temperature using ethanol as a

solvent to gain the target **J2P**, **J3P** or **J4P** in 71%, 76% and 81% yields, respectively that supposingly related to a steric effect of each molecule.
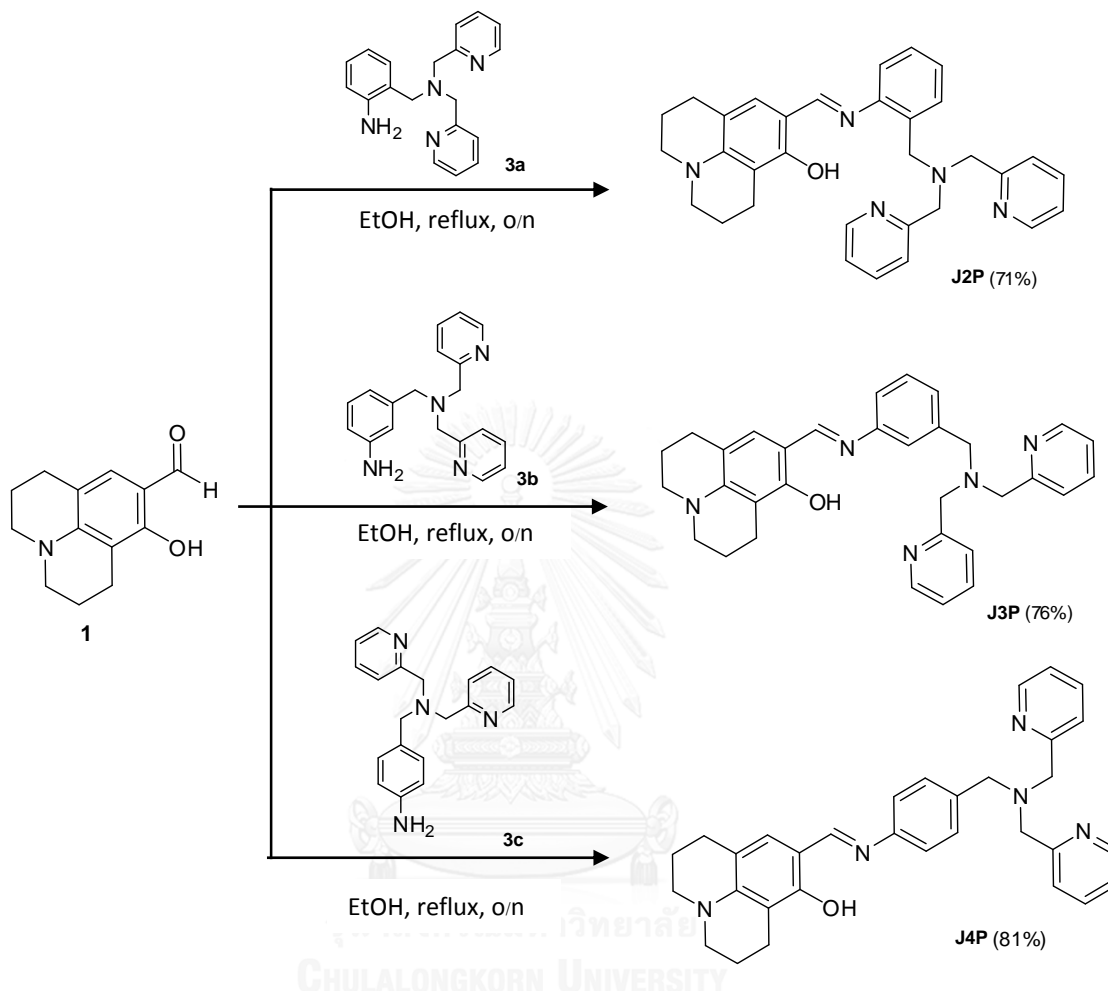
Scheme 3.5 The synthesis of **J2P**, **J3P** and **J4P**.

The reaction mechanism of the imime formation step, the Schiff base reaction (**Scheme 3.6**), involved two important steps including the addition reaction followed by elimination step. In the nucleophilic addition steps, carbonyl carbon at aldehyde was attacked by nucleophilic lone-pair electrons of the amine nitrogen atom to give an unstable intermediate known as carbinolamine. The intermediate eliminates water molecule by acid-catalyzed dehydration to yield the imine compound.
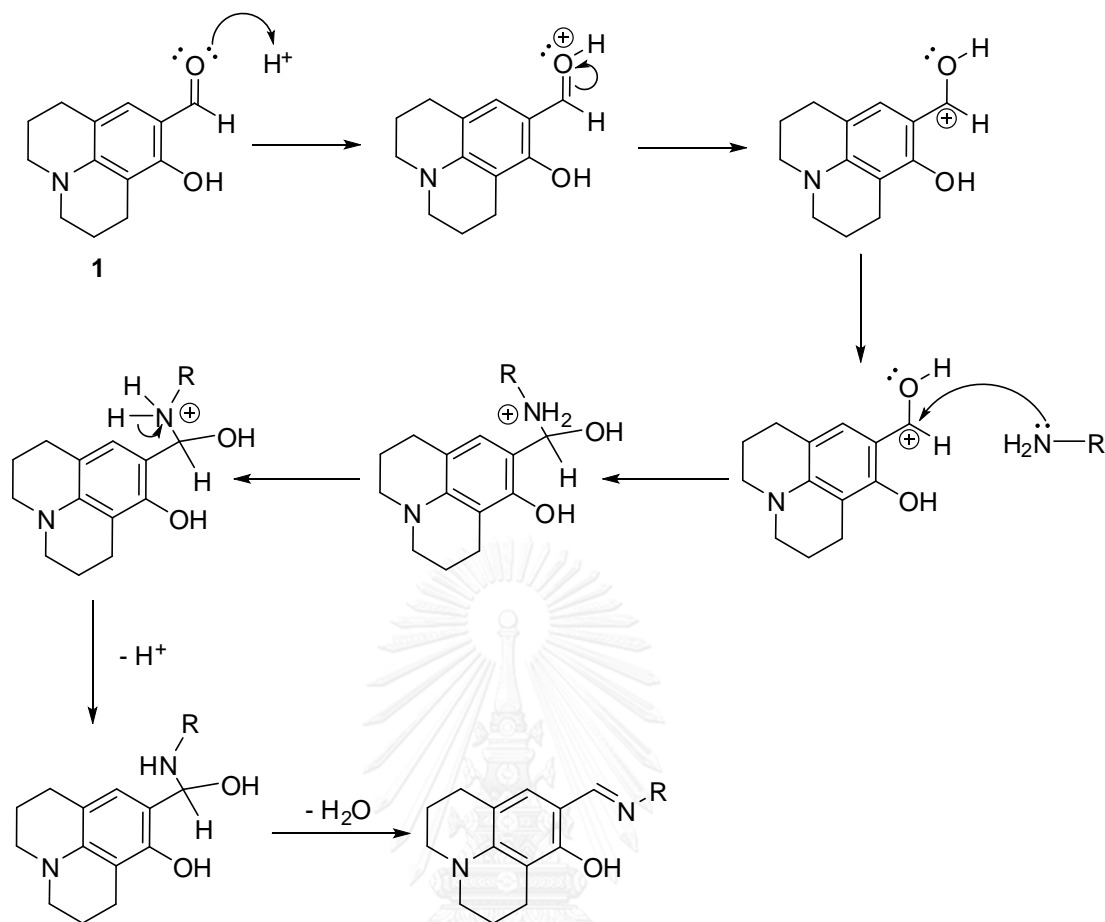
Scheme 3.6 The imination mechanism.

The target products were characterized by using ^{1}H NMR (**Figure 3.5**). The imine proton (blue label) of all target compounds were observed as a singlet peak at about 8.25 ppm confirming the successful imination reaction. The proton signals of a, b and c from julolidine moiety appeared at 1.90, 2.70 and 3.75 ppm the same area as those of the starting material (julolidine **1**) but the observed chemical shift of proton d of three compounds at around 6.75 ppm, slightly shifted to upfield region compared to that of julolidine **1**, due to the disappearance of the EWG of aldehyde group. In addition, HRMS was applied to complete the structural characterizations of all novel products. The HRMS results showed the molecular ion peaks of the positive charges of [**J2P**+H], [**J3P**+H] and [**J4P**+Na] at *m/z* = 504.2758, 504.2757 and 526.2589, respectively, (**Figure 3.6**) which agree with their calculated molecular weights.
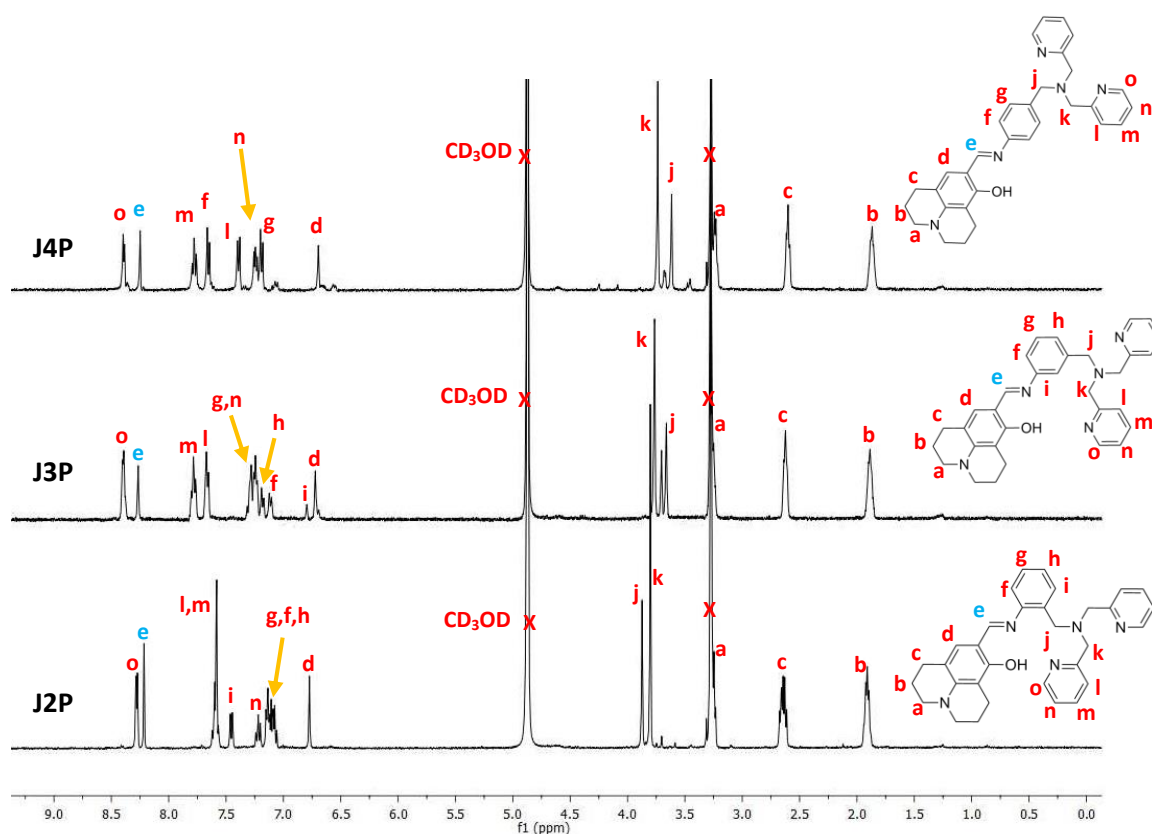
Figure 3.5 ^{1}H NMR spectra (400 MHz) of **J2P**, **J3P** and **J4P**.

According to the characterization of these target products using ^{1}H NMR, the proton signals of **J2P** were observed at the chemical shifts (δ) of 8.28 (d, J = 4.8 Hz, 2H, H-o), 8.22 (s, 1H, H-e), 7.62-7.56 (m, 4H, H-l and H-m), 7.45 (d, J = 6.9 Hz, 1H, H-i), 7.22 (t, J = 7.0 Hz, 2H, H-n), 7.16-7.05 (m, 3H, H-g, H-f and H-h), 6.77 (s, 1H, H-d), 3.87 (s, 2H, H-j), 3.80 (s, 4H, H-k), 3.31-3.22 (m, 4H, H-a), 2.68-2.60 (m, 4H, H-c) and 1.95-1.87 (m, 4H, H-b). In care of compound **J3P**, the proton signals in ^{1}H NMR spectrum were found at the chemical shifts (δ) of 8.42 (d, J = 4.3 Hz, 2H, H-o), 8.29 (s, 1H, H-e), 7.81 (t, J = 7.9 Hz, 2H, H-m), 7.69 (d, J = 7.4 Hz, 2H, H-l), 7.24-7.35 (m, 3H, H-g and H-n), 7.21 (d, J = 8.0 Hz, 1H, H-h), 7.14 (d, J = 7.6 Hz, 1H, H-f), 6.82 (s, 1H, H-i), 6.75 (s, 1H, H-d), 3.80 (s, 4H, H-k), 3.69 (s, 2H, H-j), 3.25-3.33 (m, 4H, H-a), 2.68-2.62 (m, 4H, H-c) and 1.95-1.87 (m, 4H, H-b). And the proton signals of **J4P** were observed at the chemical shifts (δ) of 8.42 (d, J = 4.2 Hz, 2H, H-o), 8.28 (s, 1H, H-e), 7.81 (t, J = 7.6 Hz, 2H, H-m), 7.69 (d, J = 7.8 Hz, 2H, H-f), 7.43 (d, J = 8.3 Hz, 2H, H-l), 7.27 (t, J = 6.0 Hz, 2H, H-n), 7.23 (d,

J = 8.4 Hz, 2H, *H*-g), 6.73 (s, 1H, *H*-d), 3.77 (s, 4H, *H*-k), 3.64 (s, 2H, *H*-j), 3.23-3.33 (m, 4H, *H*-a), 2.60-2.67 (m, 4H, *H*-c) and 1.94-1.86 (m, 4H, *H*-b).
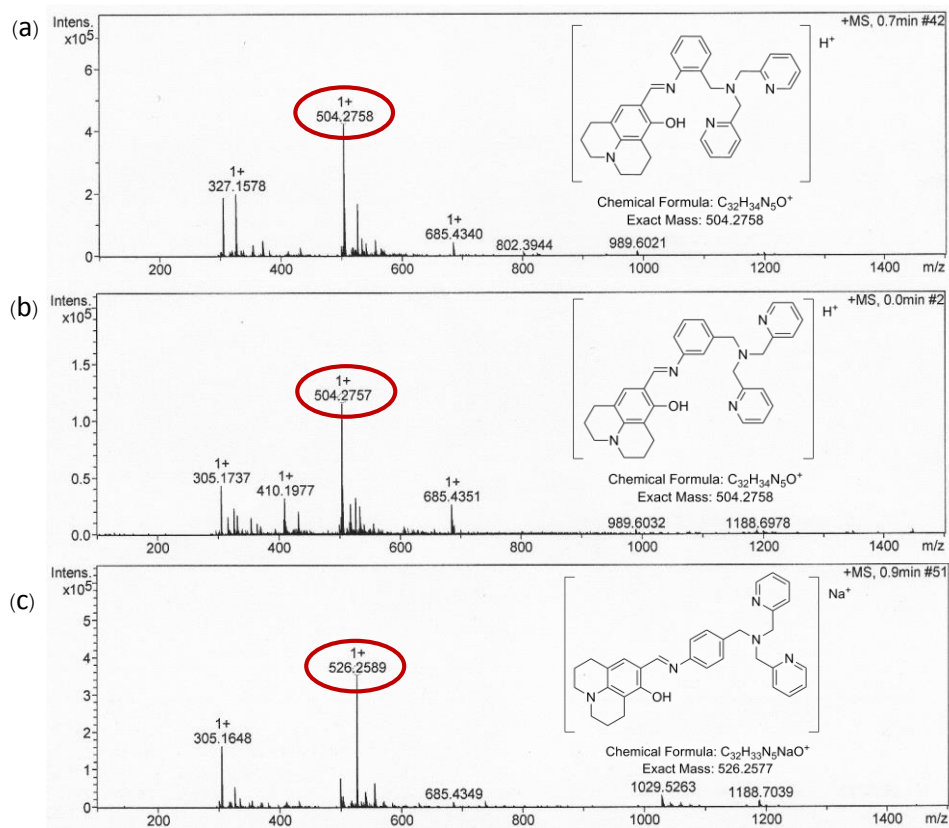
Figure 3.6 HR mass spectra of (a) **J2P**, (b) **J3P** and (c) **J4P**.

3.4 Photophysical property study

According to the absorption and the fluorescence information/data of all products as depicted in **Table 3.1**, the maximum absorption in mixed solvent (10% H_2O/methanol) of **J2P**, **J3P** and **J4P** were observed at 380, 415 and 420 nm, respectively. The molar absorption coefficient ($\mathcal{E}$) of **J2P** was determined as 1.45×10^4 $M^{-1}cm^{-1}$ while those of **J3P** and **J4P** were calculated as 2.06×10^4 and 2.68×10^4 $M^{-1}cm^{-1}$, respectively. In 5% H_2O/DMSO, the maximum absorption of these three sensors were investigated at 390, 397 and 398 nm along with the molar extinction coefficients ($\mathcal{E}$) of 1.37×10^4, 2.50×10^4 and 3.42×10^4, respectively. The difference of the absorption band and the molar extinction coefficient of the three compounds might be based on an electron delocalization in molecule which related to the planarity of each compound. This is due to the steric effect of the bulky substituent that cause the twisting of the planarity, especially in the case of *ortho-* positioned substituent of **J2P**. However, as shown in the **Table 3.1**, the fluorescence properties of these three compounds could not be observed due to the ESIPT and PET processes (**Figure 3.7**). In case of ESIPT, the phenolic proton from julolidine moiety can transfer to imine nitrogen atom that acts as a proton acceptor. The transferring of electrons from the imine nitrogen atom to julolidine moiety also allowed the PET process in the molecule.

Table 3.1 Photophysical properties of **J2P**, **J3P** and **J4P**.

Sensor	Absorption		Emission		Appearance (50 µM) under day light	Appearance (50 µM) under black light
	λ_{ab} (nm)	ε ($M^{-1}cm^{-1}$)	λ_{em} (nm)	Φ_F [*]		
J2P	380[a] 390[b]	1.45 x 10^{4a} 1.37 x 10^{4b}	N/A	N/A		
J3P	415[a] 397[b]	2.06 x 10^{4a} 2.50 x 10^{4b}	N/A	N/A		
J3P	420[a] 398[b]	2.68 x 10^{4a} 3.42 x 10^{4b}	N/A	N/A		
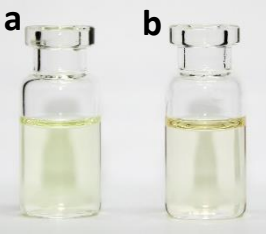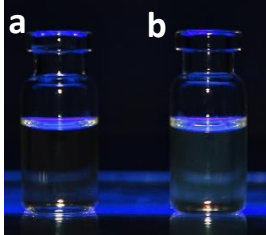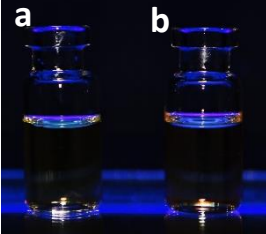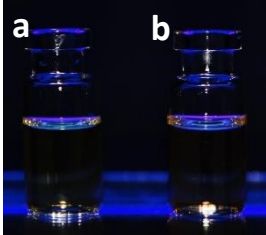
[*] Quinine sulfate in 0.1 M H_2SO_4 (Φ = 0.54) was used as the reference.

[a] Experiment data achieved in mixed solvent of 10% H_2O/MeOH.

[b] Experiment data achieved in mixed solvent of 5% H_2O/DMSO.

N/A = not available
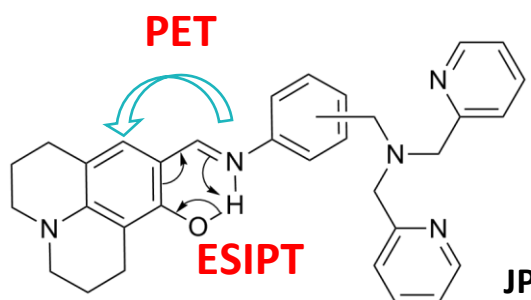
Figure 3.7 Fluorescence quenching mechanism of **JP** compounds.

3.5 Metal ion sensors of JP

3.5.1 Selectivity study of JP towards metal ions

According to the results of the photophysical property study of all target products including **J2P**, **J3P** and **J4P**, all compounds did not exhibit any fluorescence signal due to PET and ESIPT process as previously mentioned. This has provided in the expectation that the fluorescence signal may appear after selective binding with a specific metal ion. The fluorescence signals of **J2P** (10 μM in 10% H_2O/methanol) were observed at 15 minutes after addition of 10 equiv. of metal ions including Li^+, Na^+, K^+, Ag^+, Hg^+, Mg^{2+}, Ca^{2+}, Mn^{2+}, Fe^{2+}, Co^{2+}, Ni^{2+}, Cu^{2+}, Zn^{2+}, Sr^{2+}, Cd^{2+}, Ba^{2+}, Hg^{2+}, Pb^{2+}, Al^{3+}, Cr^{3+}, Fe^{3+}, Ga^{3+} and Bi^{3+}.

Expectedly, the strong fluorescence enhancement that exhibited the maximum emission wavelength (λ_{em}) of 490 nm around 60-folds of I/I_o ($\Phi_F = 0.156$) occurs after 10 equiv. of Al^{3+} was added to 10 μM of **J2P** in H_2O/methanol (1:9, v/v) (**Figure 3.8**) with stokes shift ($\Delta\lambda_{ex-em}$) of 110 nm. In contrast, the fluorescence signal did not show any response upon addition 10 equiv. of other metal ions in the similar condition (**Figure 3.9**). In cases of **J3P** and **J4P**, no significant responses of the fluorescence signal towards any metal ion including Al^{3+} was observed (**Figure 3.10**).
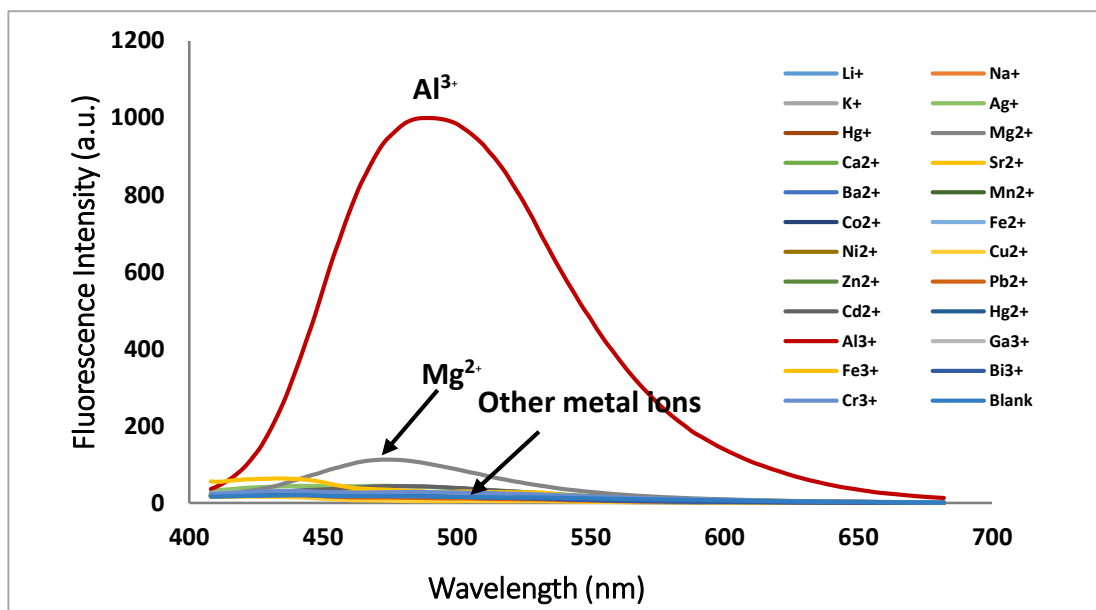
Figure 3.8 Fluorescence spectra of **J2P** (10 μM in 10% H_2O/methanol) after the addition of 10 equiv. of Li^+, Na^+, K^+, Ag^+, Hg^+, Mg^{2+}, Ca^{2+}, Mn^{2+}, Fe^{2+}, Co^{2+}, Ni^{2+}, Cu^{2+}, Zn^{2+}, Sr^{2+}, Cd^{2+}, Ba^{2+}, Hg^{2+}, Pb^{2+}, Al^{3+}, Cr^{3+}, Fe^{3+}, Ga^{3+} and Bi^{3+}. The fluorescence spectra were investigated at 15 minutes after the addition of metal ion with λ_{ex} = 380 nm.

Figure 3.9 (a) Fluorescence signal ratio (I/I_o)-1 of **J2P** (10 μM in 10% H_2O/methanol) after addition of each metal ion with λ_{ex} = 380 nm and λ_{em} = 490 nm. (b) The photograph under black light of **J2P** upon addition of each metal ion.
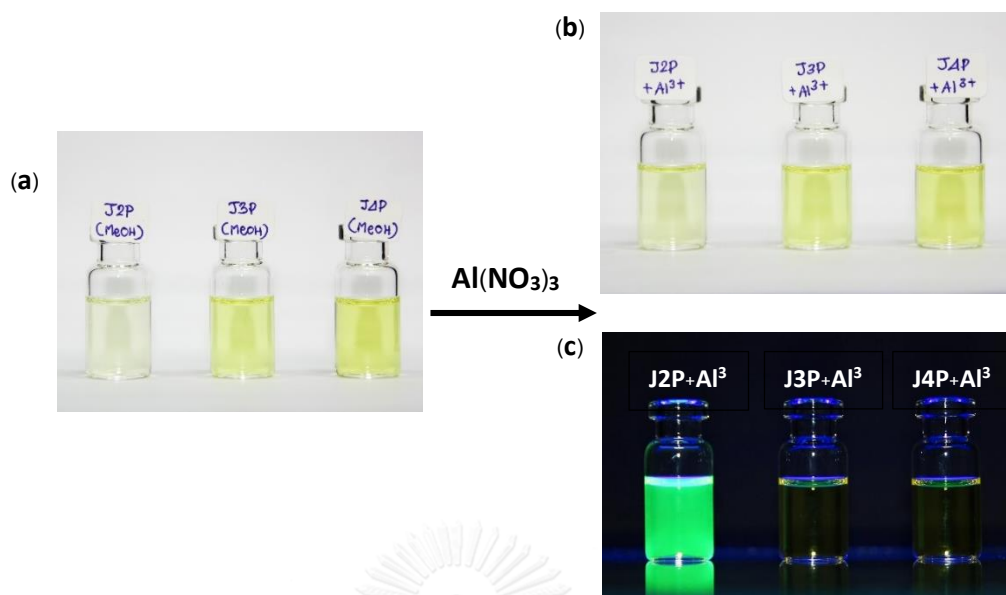
Figure 3.10 Appearance of **JP** compounds (10 µM) (a) before addition of Al^{3+} and (b) upon the addition of Al^{3+} (10 equiv.) in 10% H_2O/methanol under day light and (c) under black light.

Furthermore, fluorescent sensor **J2P** demonstrated not only significant selectivity towards Al^{3+} in 10% H_2O/methanol but also a good one towards Mg^{2+} when the solvent mixture was changed to 5% H_2O/DMSO (**Figure 3.11**). The fluorescence intensity increased around 14-folds (Φ_F = 0.096) (**Figure 3.12**) upon the addition 10 equiv. of Mg^{2+} to **J2P** (10 µM in 5% H_2O/DMSO). On the contrary, other metal ions could not significantly change the fluorescence signal under this condition. The maximum fluorescence emission signal (λ_{em}) of the complex **J2P**-Mg^{2+} was observed at 478 nm using λ_{ex} = 390 nm (Stoke shift ($\Delta\lambda_{ex-em}$) = 88 nm). In contrast, **J3P** and **J4P** did not show any response in the presence of Mg^{2+} under this condition (**Figure 3.13**)
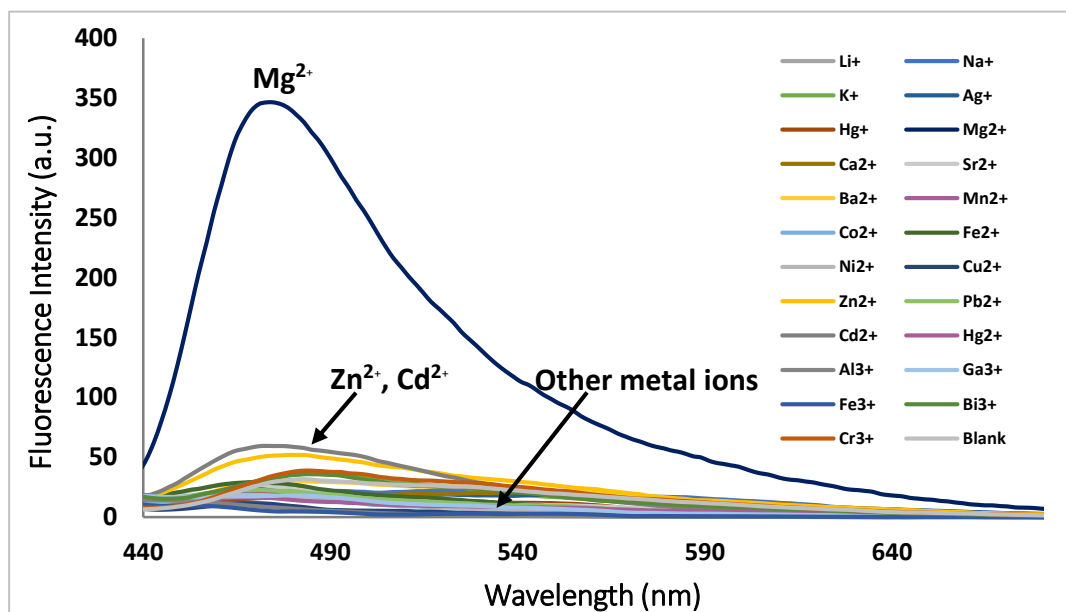
Figure 3.11 Fluorescence spectra of **J2P** (10 µM in 5% H_2O/DMSO) after the addition of 10 equiv. of Li^+, Na^+, K^+, Ag^+, Hg^+, Mg^{2+}, Ca^{2+}, Mn^{2+}, Fe^{2+}, Co^{2+}, Ni^{2+}, Cu^{2+}, Zn^{2+}, Sr^{2+}, Cd^{2+}, Ba^{2+}, Hg^{2+}, Pb^{2+}, Al^{3+}, Cr^{3+}, Fe^{3+}, Ga^{3+} and Bi^{3+}. The fluorescence spectra were investigated upon the addition of metal ion with λ_{ex} = 390 nm.
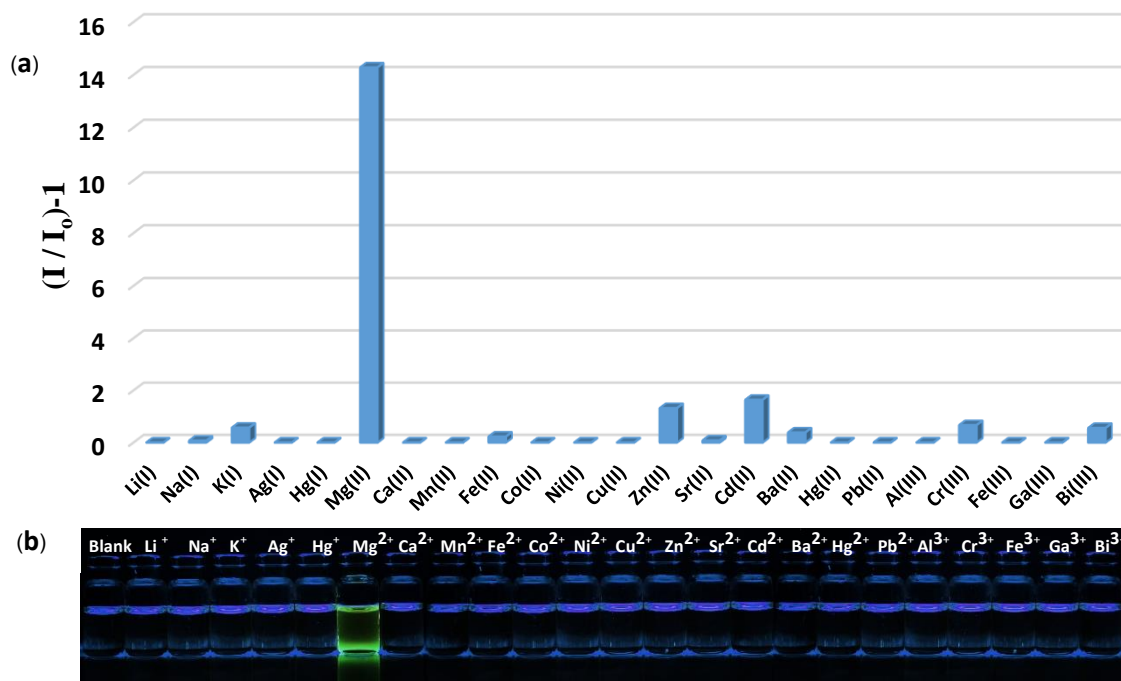
Figure 3.12 (a) Fluorescence signal ratio (I/I_o)-1 of **J2P** (10 µM in 5% H_2O/DMSO) after the addition of each metal ion with λ_{ex} = 390 nm and λ_{em} = 478 nm. (b) The photograph under black light of **J2P** upon the addition of each metal ion.
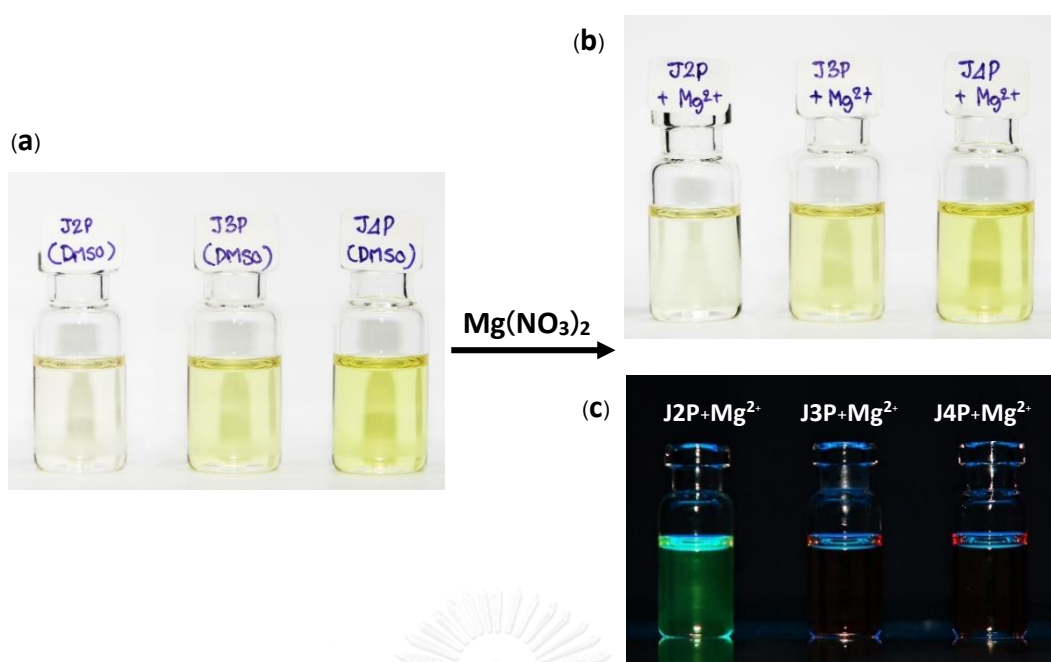
Figure 3.13 Appearance of **JP** compounds (10 μM) (a) before addition of Mg^{2+} and upon the addition of Mg^{2+} (10 equiv.) in 5% H_2O/DMSO (b) under day light and (c) under black light.

By the change of solvent condition, **J2P** can be selective towards not only Al^{3+} in 10% H_2O/methanol but also Mg^{2+} in 5% H_2O/DMSO. In 10% H_2O/methanol, phenolic hydroxy group is deprotonated to phenoxide (Ar-O⁻) which acts as the hard-base donor site that prefer to chelate with the hard-acid Al^{3+}. On the other hand, in the aprotic solvent such as DMSO, acidic proton from phenolic moiety might not be deprotonated remaining in the neutral form (ArOH) as soft-base binding site and can be specify towards soft-acid Mg^{2+}.

The selectivity of **J2P** was also studied using UV-Visible spectroscopy. As shown in **Figure 3.14**, the maximum absorption of **J2P** in H_2O/methanol (1:9, v/v) (**Figure 3.14a**) and H_2O/DMSO (5:95, v/v) (**Figure 3.14b**) were observed at 380 and 390 nm, respectively. The absorption spectra were further investigated at 15 minutes upon addition of 10 equiv. of metal ions. The results showed that the absorption band of **J2P** in H_2O/methanol (1:9, v/v) significantly bathochromic shifted in the presence of Al^{3+} and Zn^{2+}. And in H_2O/DMSO (5:95, v/v), the bathochromic shift of **J2P** was observed only in the presence of Zn^{2+}.
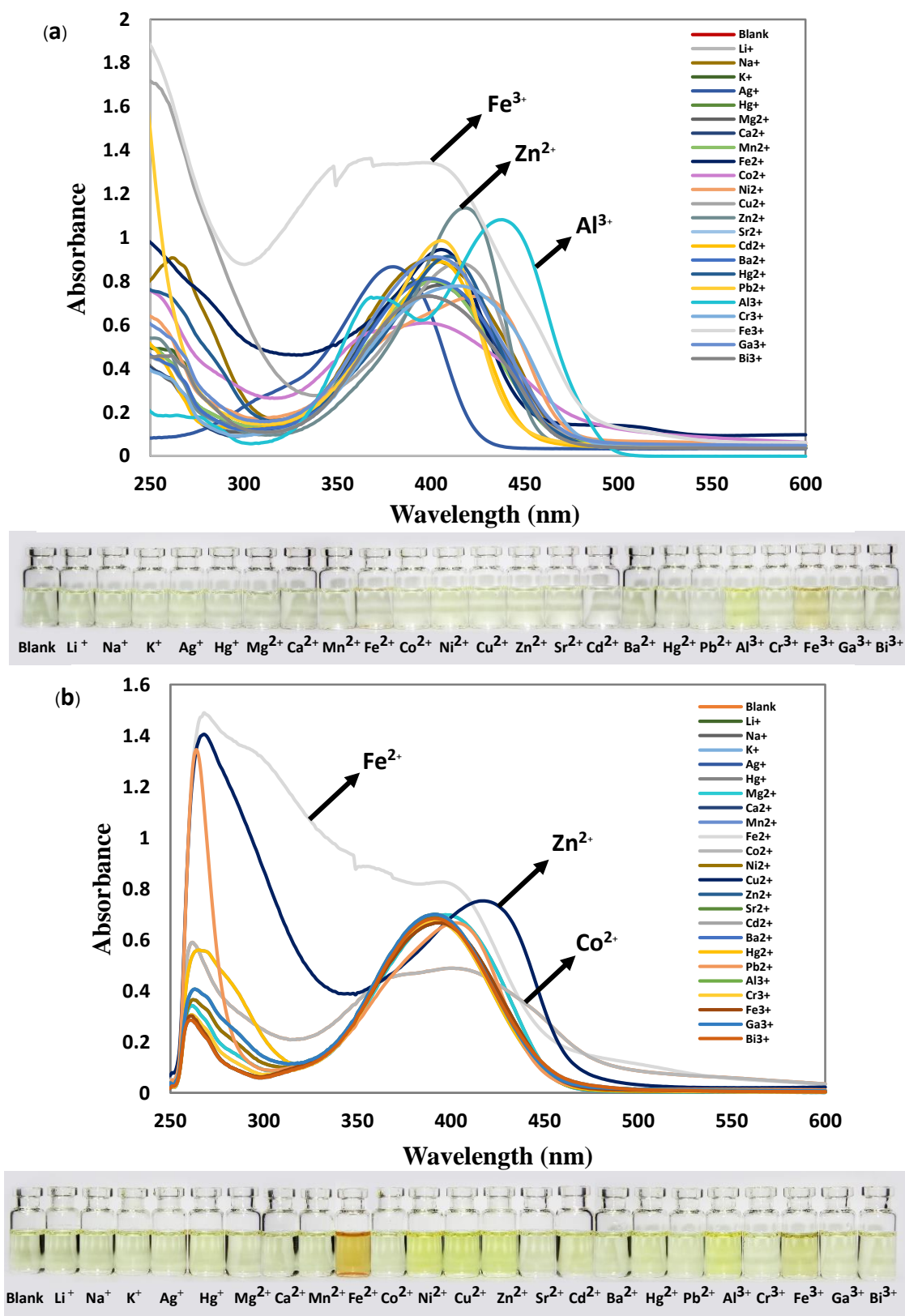
Figure 3.14 Absorption spectra and appearances under day light of **J2P** (50 µM) after addition of metal ions (10 equiv.) in (a) H_2O/methanol (1:9, v/v) and (b) H_2O/DMSO (5:95, v/v).

3.5.2 Time-dependent fluorescence enhancement of J2P to Al³⁺

According to the preliminary results of sensing property, **J2P** was selective towards Al³⁺ generating the fluorescence enhancement of **J2P**. The fluorescence intensity was monitored for 50 minutes (**Figure 3.15**). The results showed that the fluorescence intensity increased continuously during 15 minutes then remain stable until 50 minutes. Due to the steric effect from the bulky group of dipicolylamine which composed of two pyridine rings might affect the kinetic binding between **J2P** and metal ion. Meanwhile, the fluorescence signal of **J2P** in H_2O/DMSO (5:95, v/v) completely enhanced within 5 minutes after addition of Mg^{2+} as shown in **Figure 3.16.**
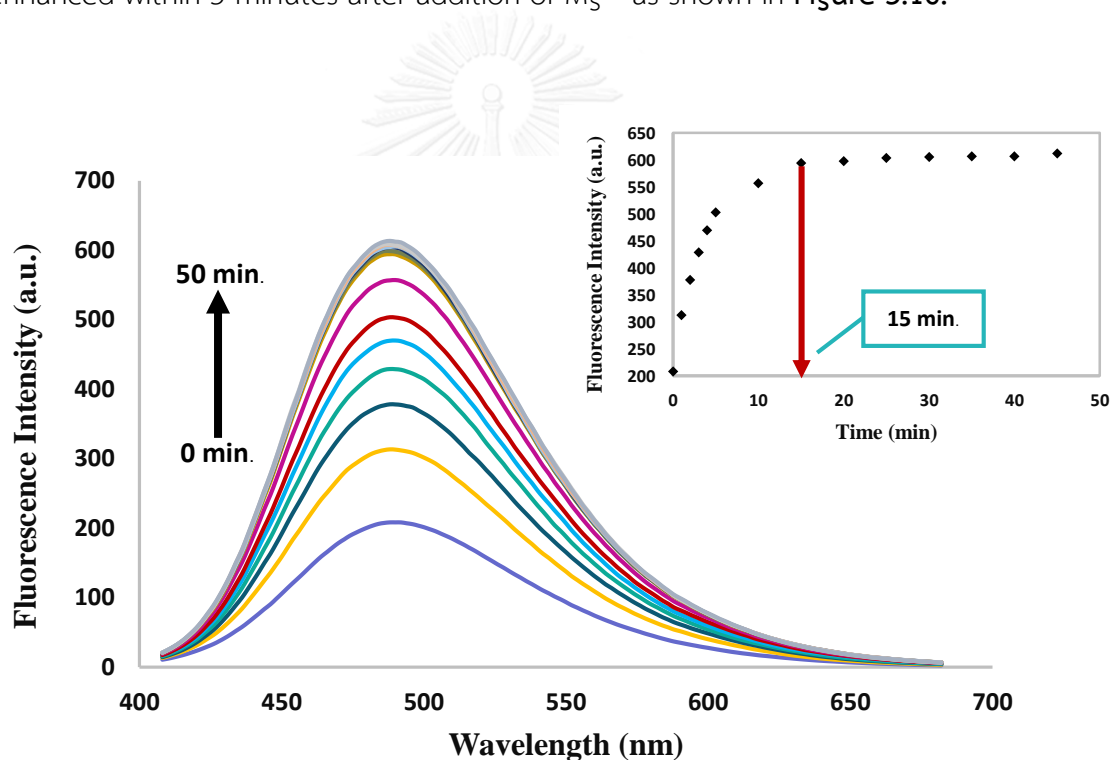
Figure 3.15 Time-dependent fluorescence enhancing profile of **J2P** (10 μM in 10% H_2O/methanol) towards Al³⁺.
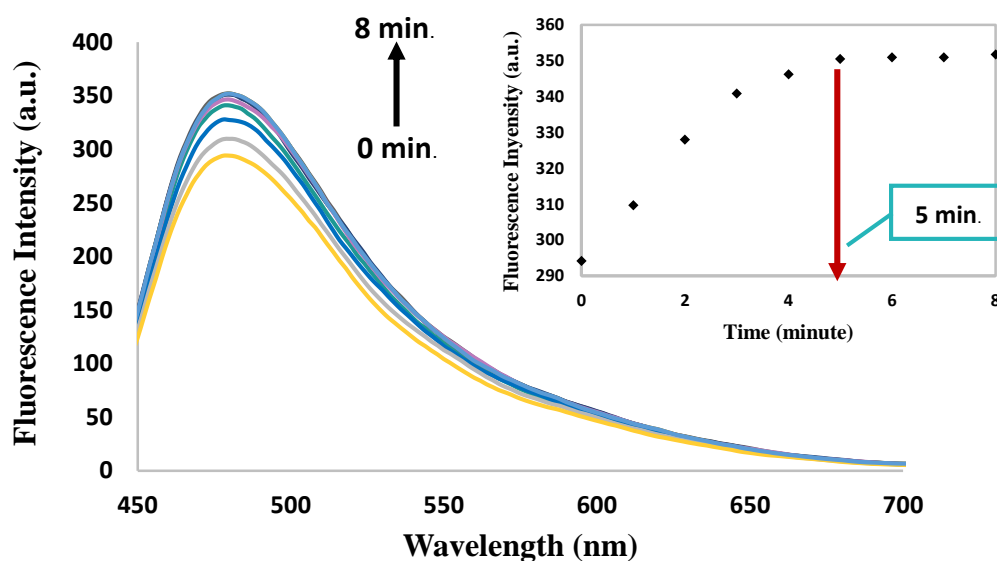
Figure 3.16 Time-dependent fluorescence enhancing profile of **J2P** (10 µM in 5% H₂O/DMSO) towards Mg^{2+}.

3.5.3 Solubility effect to fluorescence enhancement

The solubility effect was achieved by titration between **J2P** (10 µM) and Al^{3+} (10 equiv.) in series of mixed solvent containing H₂O/methanol. The proportion of water was varied from 5% to 90% using the excitation wavelength (λ_{ex}) at 380 nm. The fluorescence intensity of each fraction was observed at 15 minutes after the metal was added (**Figure 3.17**). According to the experimental results, the fluorescence intensity of **J2P**-Al^{3+} decreased when the water fraction was increased. At 10% of water, **J2P**-Al^{3+} exhibited the strongest fluorescence intensity. The decrease of fluorescence signal might be based on its solubility that **J2P** is completely dissolved in methanol but cannot be dissolved in water. Therefore, when the proportion of water is increased **J2P** will precipitate as shown in **Figure 3.18**. On the other hand, at 5% H₂O/methanol showed the drop of fluorescence intensity probably due to water might assist the deprotonation of hydroxy proton in **J2P** and might enhance the chelation between the fluorophore (**J2P**) and Al^{3+} causing the low fluorescence signal in too small aqueous proportion. Thereby, 10% H₂O/methanol, the proper proportion of water in mixed solvent of H₂O/methanol was used.
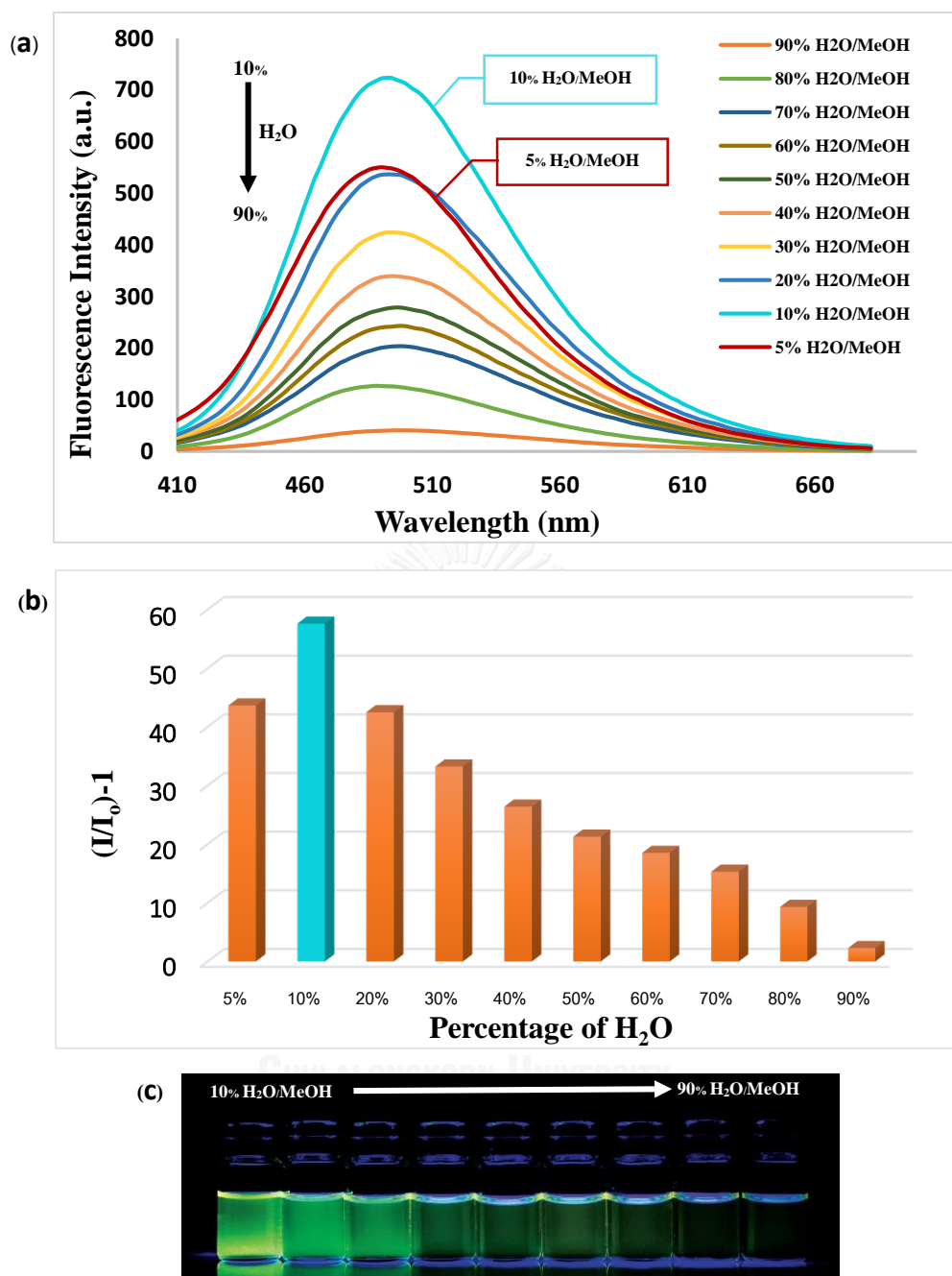
Figure 3.17 (a) Fluorescence spectra of **J2P** (10 μM) upon the addition of Al^{3+} (10 equiv.), (b) the relative fluorescence intensity in various solvent conditions and (c) appearance of each fraction under black light.
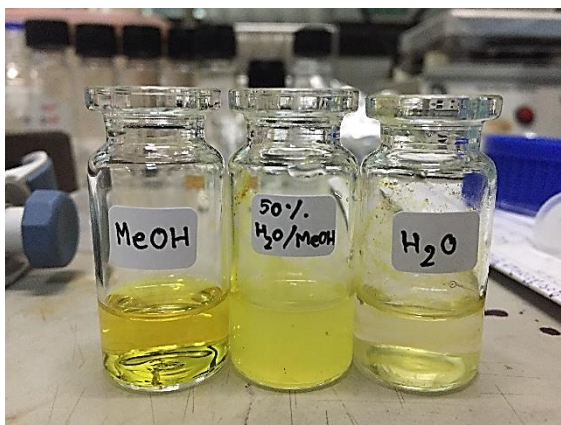
Figure 3.18 Solubility appearance of **J2P** (1.5 mg, 1 mM) in total 3 mL of solvent.

In case of mixed H_2O/DMSO solution, the significant fluorescence signal of **J2P** was observed after addition of Mg^{2+} and the solvent effect to fluorescence intensity was studied. As shown in **Figure 3.19**, the strongest fluorescence intensity was observed at H_2O/DMSO (5:95, v/v) solution, while the water proportion was increased, the fluorescence intensity was dropped. Likewise, these effects might be based on the solubility of **J2P**.
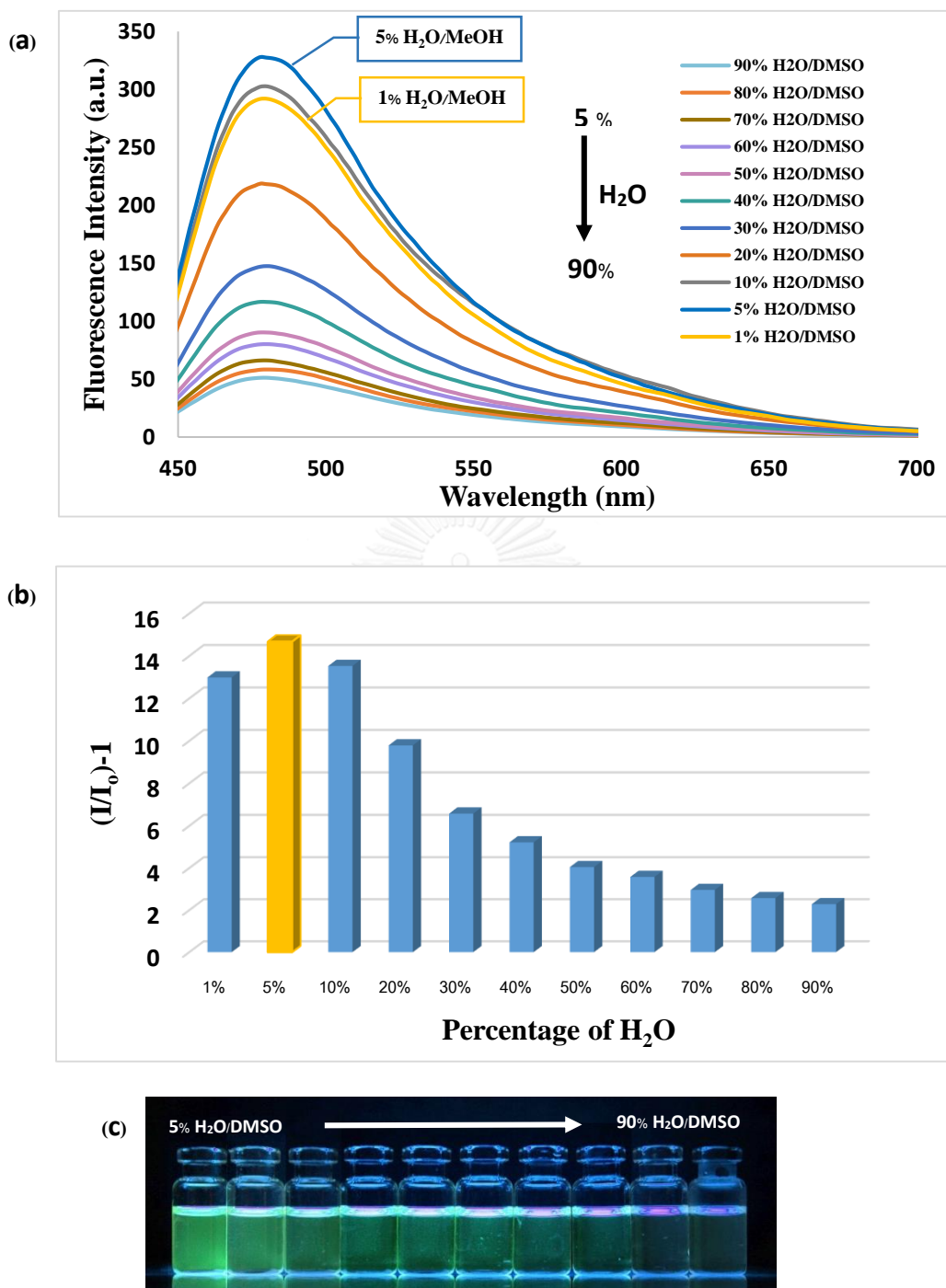
Figure 3.19 (a) Fluorescence spectra of **J2P** (10 μM) upon the addition of Mg^{2+} (10 equiv.) (b) the relative fluorescence intensity in various solvent conditions and (c) appearance of each fraction under black light.

3.5.4 Fluorescence and UV-Visible titration

In order to gain the clear understanding about the emission mechanism, the fluorescence titration was further carried out by addition of Al^{3+} (0.2-5.0 equiv.) to 10 µM of **J2P** in H_2O/methanol (1:9, v/v). As shown in **Figure 3.20**, the fluorescence spectra were obtained at 15 minutes after the addition of Al^{3+} using excitation wavelength of 380 nm. The fluorescence intensities at maximum emission (λ_{em} = 490 nm) were used to plot against the equivalent of Al^{3+}. The results demonstrated that the fluorescence intensity was increased along with the increase of the concentration of Al^{3+} and completely enhanced at 1.0 equiv. of Al^{3+}. In case of magnesium sensing (**Figure 3.21**), the fluorescence titration was investigated using excitation wavelength of 390 nm and the maximum enhancing signal at 478 nm was observed upon the amount of Mg^{2+} increased to be 1.0 equiv.
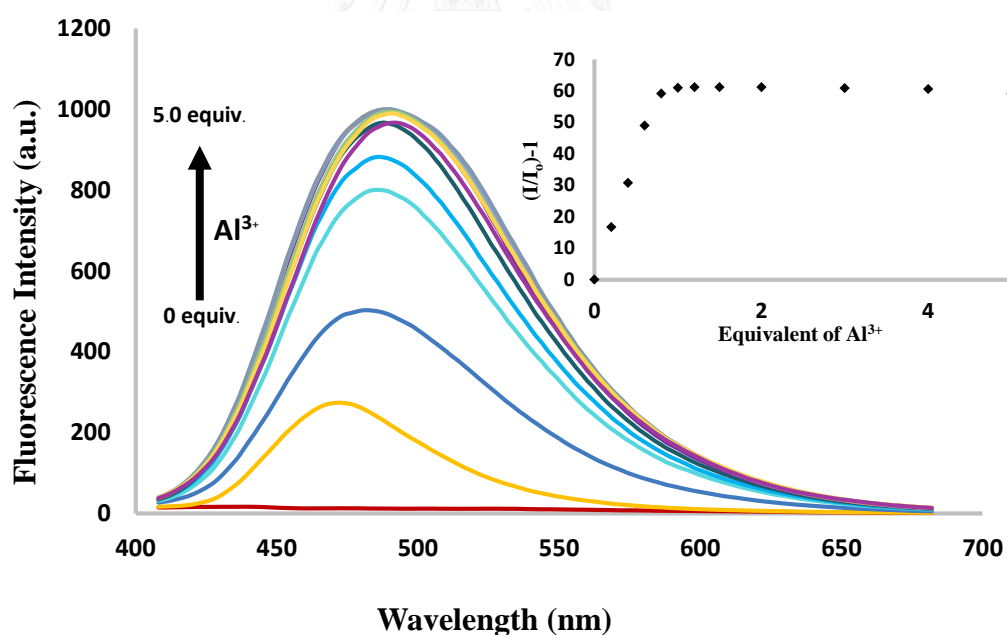
Figure 3.20 Fluorescence change of **J2P** (10 µM) with the addition of Al^{3+} (0 to 5.0 equiv.) in 10% H_2O/methanol using excitation wavelength (λ_{ex}) at 380 nm.
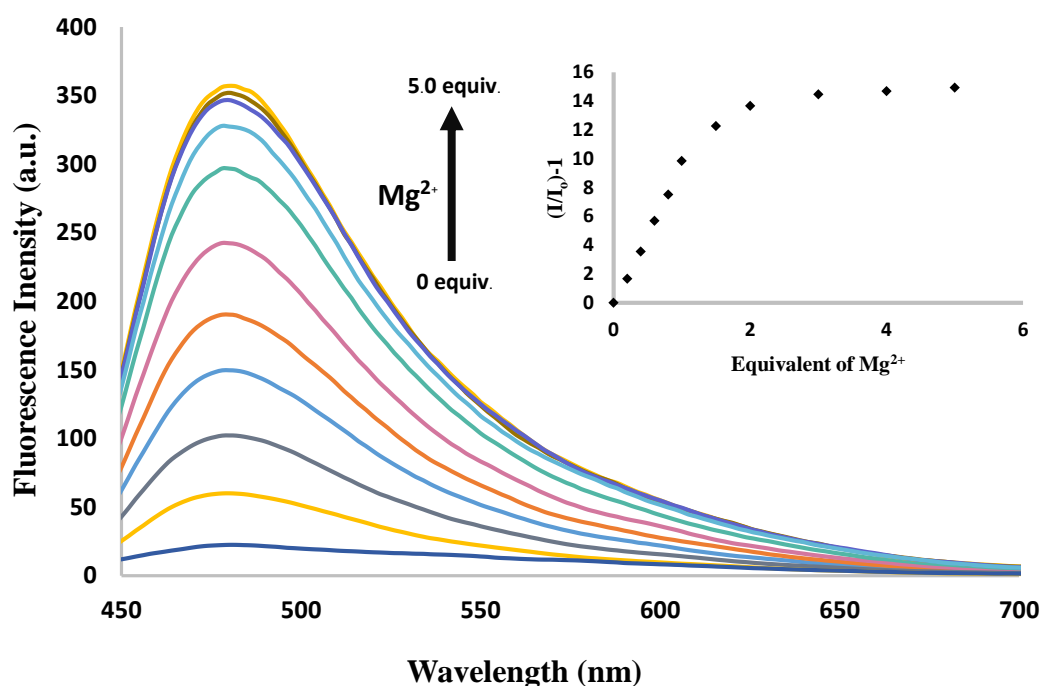
Figure 3.21 Fluorescence change of **J2P** (10 μM) with the addition of Mg^{2+} (0 to 5.0 equiv.) in 5% H_2O/DMSO using excitation wavelength (λ_{ex}) at 390 nm.

According to the UV-Visible titration experiments, the maximum absorption wavelength in 10% H_2O/methanol solution of **J2P** was observed at 380 nm (**Figure 3.22a**). Upon addition of Al^{3+} ions to a solution of **J2P**, the absorption bands at 380 nm slightly decreased, and the new absorption band at 435 nm appeared. Furthermore, a clear isosbestic point was observed at 395 nm, indicating that only one product was generated from **J2P** upon binding to Al^{3+}. The fact that 1.0 equiv. of aluminium ion was used for the full spectral conversion of **J2P** indicated the formation of a 1:1 stoichiometric complex between **J2P** and Al^{3+}. In addition, the bathochromic shift ($\Delta\lambda_{ab} = 55$ nm) as well as an appearance of the new absorption band at 435 nm demonstrated that the hydrogen atom at hydroxy group of **J2P** was deprotonated during the coordination of **J2P** with Al^{3+}.

On the other hand, **J2P** showed the maximum absorption band in 5% H_2O/DMSO at 390 nm (**Figure 3.22b**) after the addition of Mg^{2+} slightly decreased. Meanwhile, the slight bathochromic shifted ($\Delta\lambda_{ab} = 15$ nm) illustrated that the proton

at hydroxyl group of **J2P** might not be deprotonated in the polar aprotic solvent like DMSO. Moreover, only one isosbestic point was found at 401 nm referring also to the 1:1 stoichiometric complex towards Mg^{2+}.
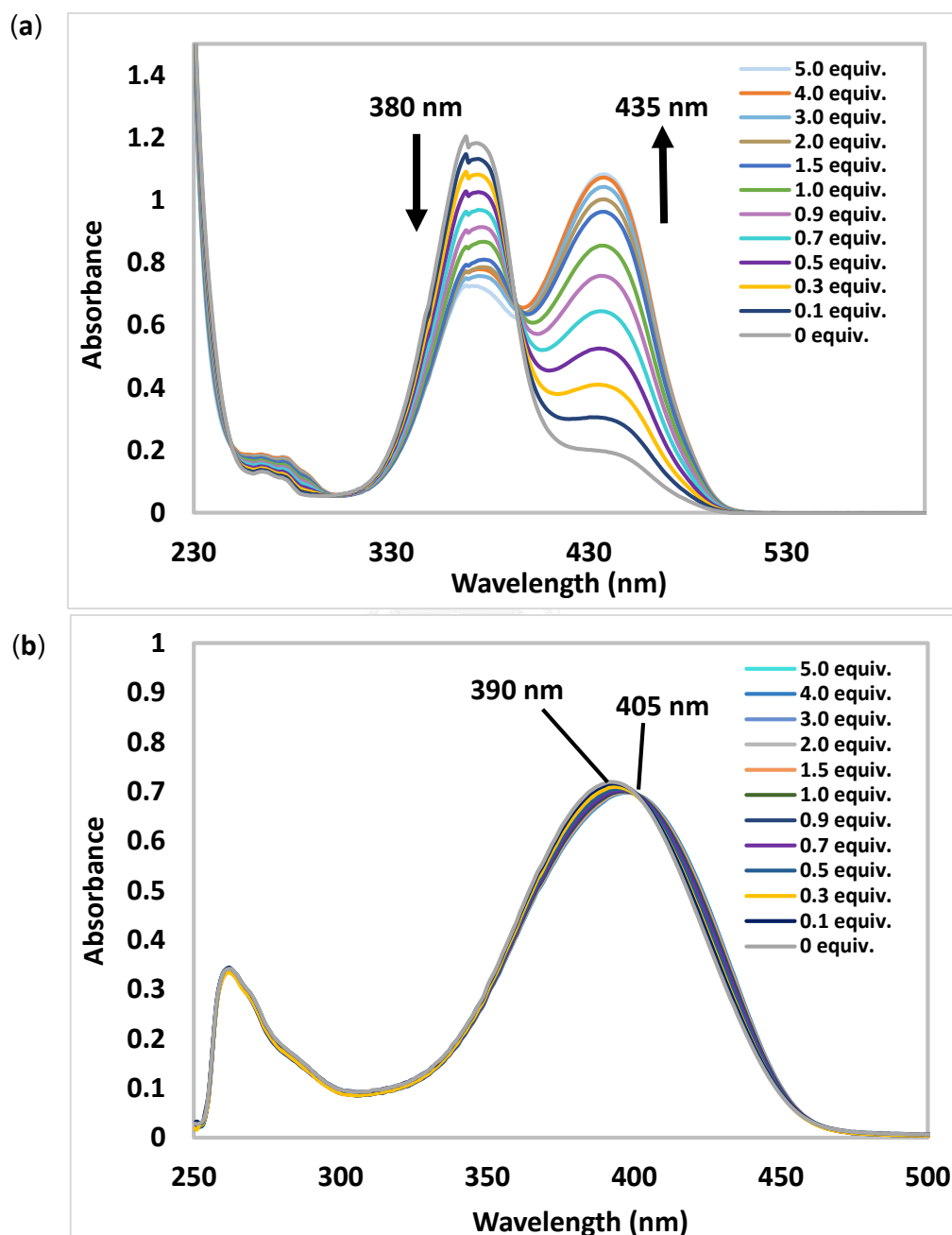
Figure 3.22 Absorption spectra of **J2P** (50 µM) at 15 minutes (a) after mixed with Al^{3+} (0-5.0 equiv.) in 10% H_2O/methanol and (b) after addition of Mg^{2+} (0-5.0 equiv.) in 5% H_2O/DMSO.

3.5.5 Benesi–Hildebrand method

Benesi-Hildebrand plot was used to determine the binding constant or association constant (K_a) of non-bonded interactions between fluorophore probe with metal ion based on fluorescence change. As the fluorescence intensities in the linear range were used to plot of $1/(I-I_o)$ against $1/[Metal]$ in the unit of M^{-1}. The data are fitted to the corresponding linear. Using computer simulation the calculation of the association constant from the slope of linear range (B) and y-intercept (A) by represented into the following equation: $K_a = A/B$. According to Benesi-Hildebrand plot of **J2P**-Al^{3+} (**Figure 3.23**) and **J2P**-Mg^{2+} **(Figure 3.24)**, the association constants (K_a) were calculated as 2.25×10^5 and 4.00×10^4, respectively. The results showed that the binding between **J2P** and Al^{3+} is stronger than that between **J2P** and Mg^{2+}. The different of binding constant is probably resulted from its acidity of metal ion (Mg^{2+} is lower than Al^{3+}) which is selective to hard base of binding site. Moreover, they both exhibited the similar stoichiometric complexation of **J2P**:metal ion as 1:1.
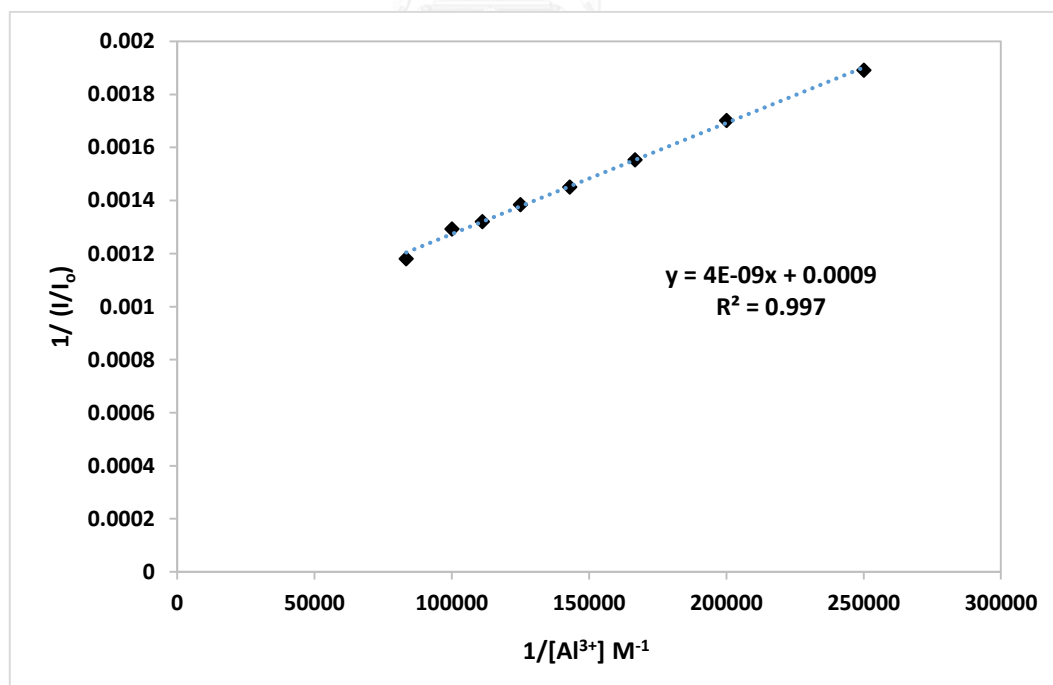
Figure 3.23 Benesi–Hildebrand plot of **J2P**-Al^{3+}.
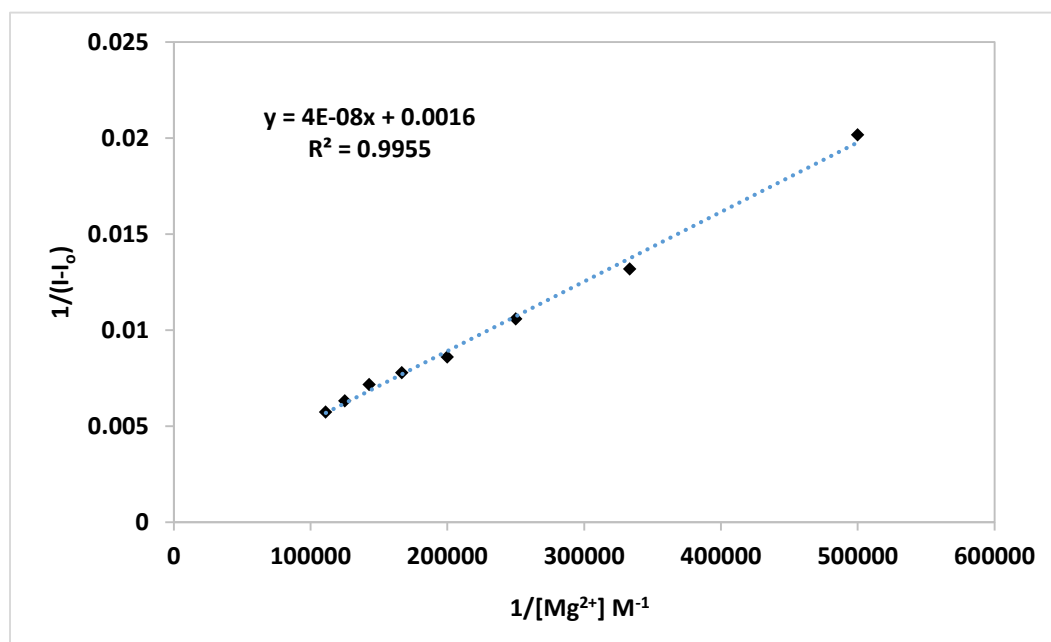
Figure 3.24 Benesi–Hildebrand plot of **J2P**-Mg^{2+}.

3.5.6 Job's method

The stoichiometric coordination between **J2P** and Al^{3+} was also determined by using Job's method experiment. To give an experimental data, the series of mixed solutions in 10% H_2O/methanol containing a fixed total number of moles of **J2P** and Al^{3+} were prepared by varying their mole fractions (**J2P**:Al^{3+}) of 1:4, 1:3, 1:2, 1:1, 2:1, 3:1 and 4:1, respectively. The maximum fluorescence emission intensity at 490 nm of each fraction was used to plot against the mole fractions of these two species. The results showed the maximum coordination at 0.5 mole fraction of Al^{3+} indicating that complex of **J2P**-Al^{3+} was generated as the stoichiometric ratio of 1:1 (**Figure 3.25**). Likewise, a maximum coordination point in case of **J2P**-Mg^{2+} was observed when the molar fraction of Mg^{2+} reached 0.5 (**Figure 3.26**), which is also indicating a 1:1 stoichiometry complexation between **J2P** and Mg^{2+}.
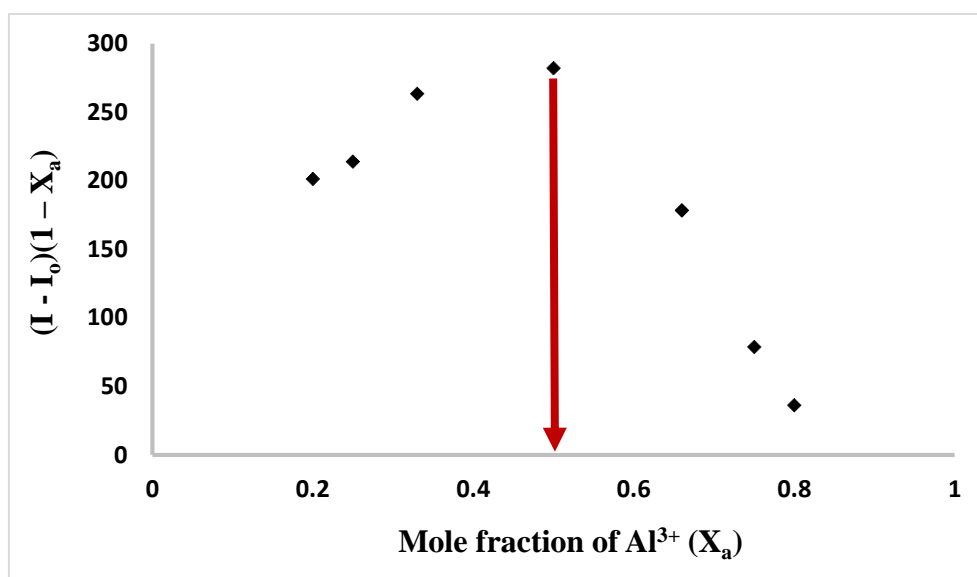
Figure 3.25 Job's plot examined between **J2P** and Al^{3+} by fluorescence responses.
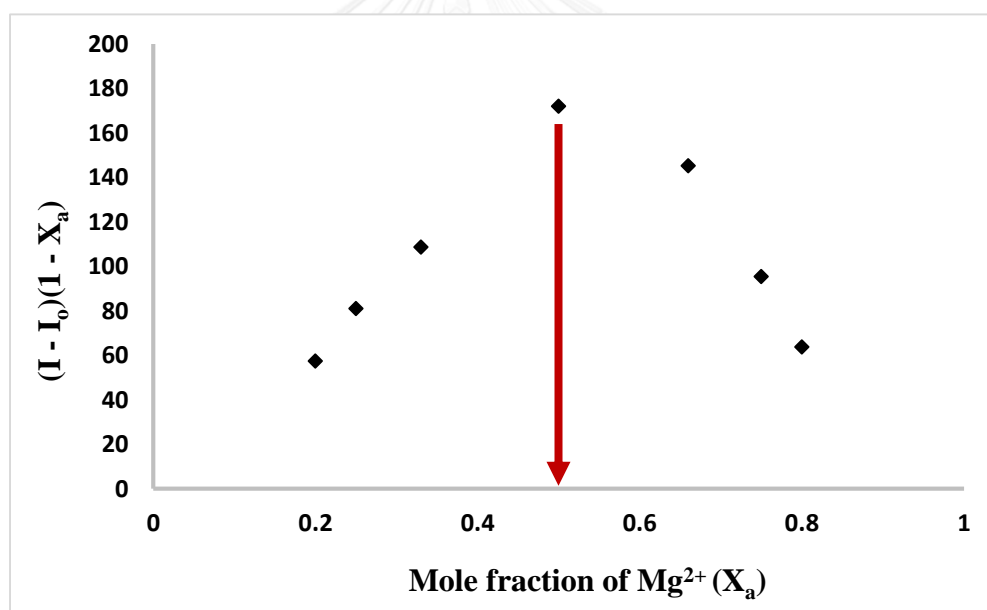
Figure 3.26 Job's plot examined between **J2P** and Mg^{2+} by fluorescence responses.

In addition, the complexation between **J2P** and Al^{3+} was investigated by using mass spectrometry. The ESI-MS spectrum (**Figure 3.27**) showed ion peak of 1:1 stoichiometric coordination between **J2P** and Al^{3+} at 624.7 related to the complexation

structure of $[(AlNO_3)\bullet(\mathbf{J2P}+H)\bullet CH_3OH]^+$ in which the calculated exact mass requires 624.26.
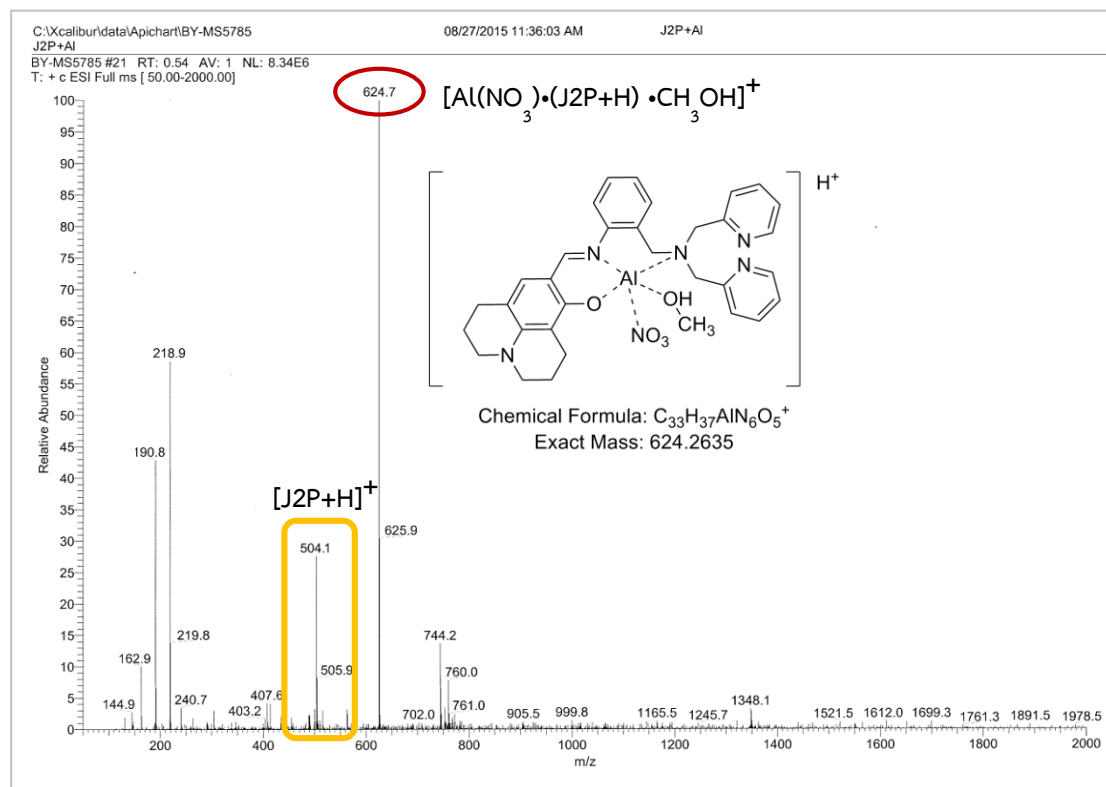
Figure 3.27 ESI-MS of **J2P**-Al$^{3+.}$

3.5.7 ^{1}H NMR experiment

To determine the complex formation of two species, the ^{1}H NMR titration was used to support the evidence of the bonding position of **J2P** with Al^{3+}. The ^{1}H NMR experiment was performed using CD$_3$OD as NMR solvent. Aluminium nitrate was dissolved in CD$_3$OD then added to **J2P**. The ^{1}H NMR spectra were investigated at 15 minutes after the addition of 0.5 and 1.0 equivalent of Al^{3+}, respectively (**Figure 3.28**). As the results, the chemical shifts (δ) of some protons in **J2P** had significantly changed upon the increasing in amount of Al^{3+} (**Figure 3.29**). The signals of methylene protons (-CH$_2$-) of j and k at dipicolylamine moiety were shifted to downfield region around $\Delta\delta$ = 0.22 and 0.26 ppm while proton d at the fluorophore (julolidine moiety)

significantly downfield shifted about $\Delta\delta$ = 0.27 ppm. These results might be become of an electronic effect due to the loss of electron using in the chelation of two species. The imine proton showed the downfield shifted around $\Delta\delta$ = 0.16 ppm. Nevertheless, the signal of other protons from julolidine and DPA had not significantly changed. According to the ^{1}H NMR results, the binding position between **J2P** and Al^{3+} illustrated that nitrogen atom at dipicolylamine moiety, nitrogen atom at imine bond (C=N) and phenolic oxygen atom at julolidine group might involve in the coordination toward Al^{3+}. However, the two nitrogen atoms at pyridine rings in DPA did not involve in the chelation of two species.
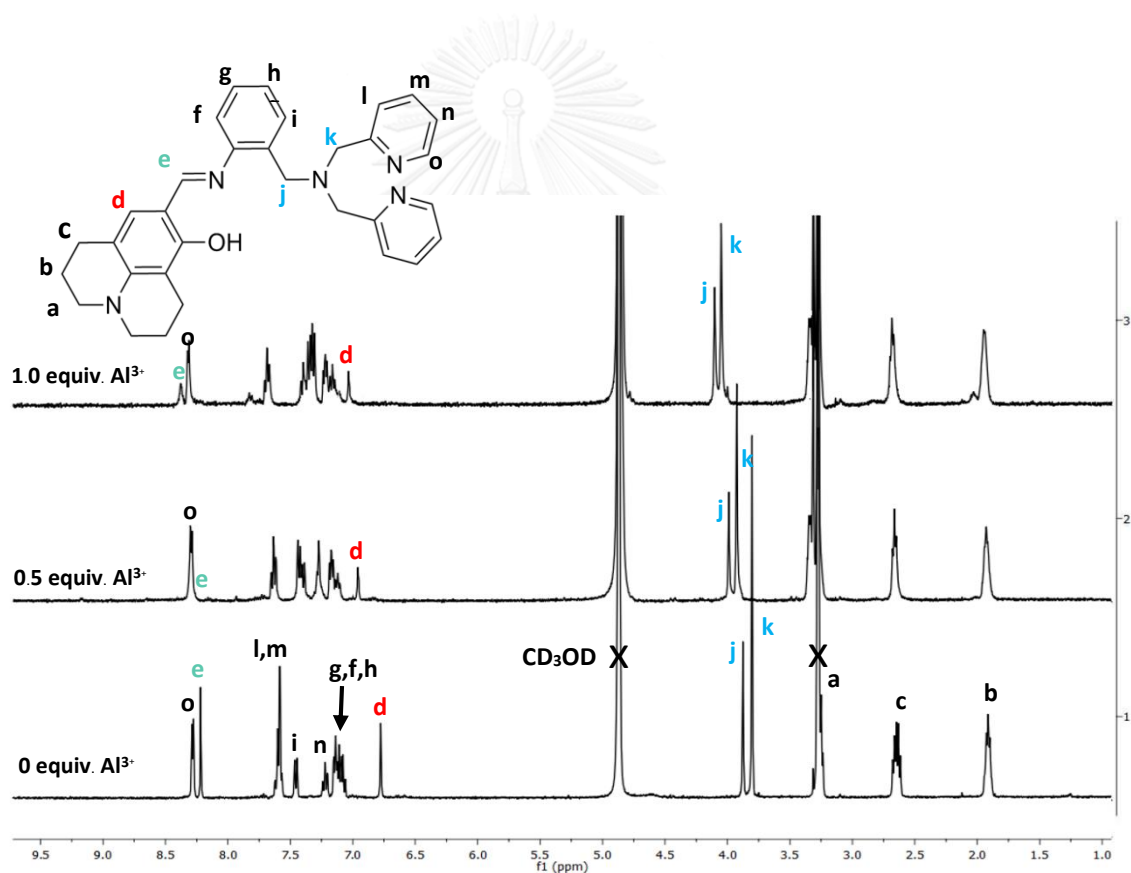
Figure 3.28 ^{1}H NMR spectra of **J2P** in CD_3OD upon the addition of 0, 0.5 and 1.0 equiv. of Al^{3+}.
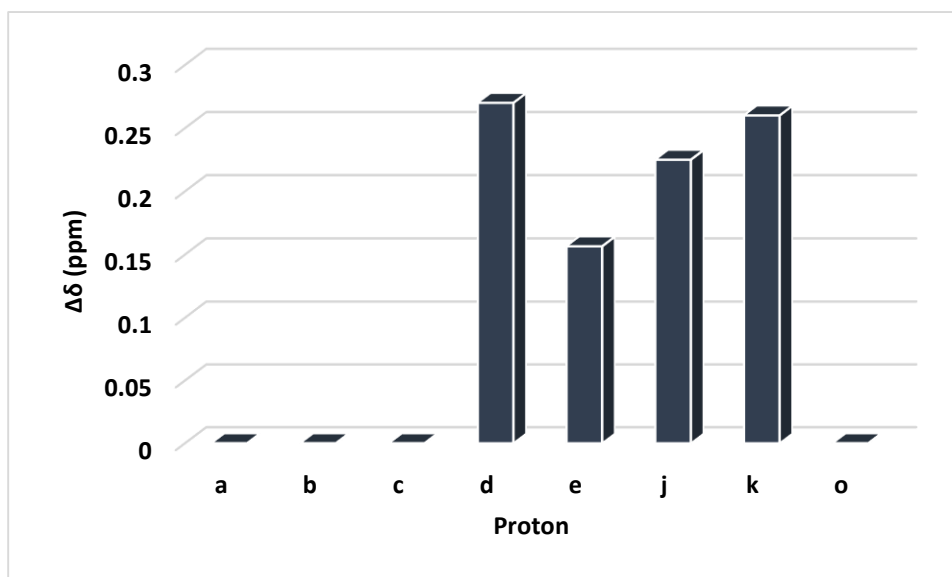
Figure 3.29 Graph of the change in chemical shifts ($\Delta\delta$) of **J2P**-Al^{3+} titration.

The dertermination of binding position of **J2P**-Mg^{2+} was further studied by using ^{1}H NMR titration technique (**Figure 3.30**). The results showed that upon the amount of Mg^{2+} increased from 0 equiv to 1.0 equiv., the imine proton e including two methylene proton j and k significantly downfiled shifted with $\Delta\delta$ = 0.33, 0.25 and 0.24 ppm, respectively (**Figure 3.31**), inferring that the two nitrogen atoms at imine bond (C=N) and the middle of DPA moiety were used to bind Mg^{2+}. Additionally, there was no involvement of picolyl moieties observed in binding Mg^{2+}, as proton signals such as pyridine proton l, m, n and o had not significantly shifted. Moreover, the appearance of singlet peak at δ = 13.6 ppm inferred that the phenolic proton of **J2P** was not deprotonated during the coordination under this polar aprotic solvent.
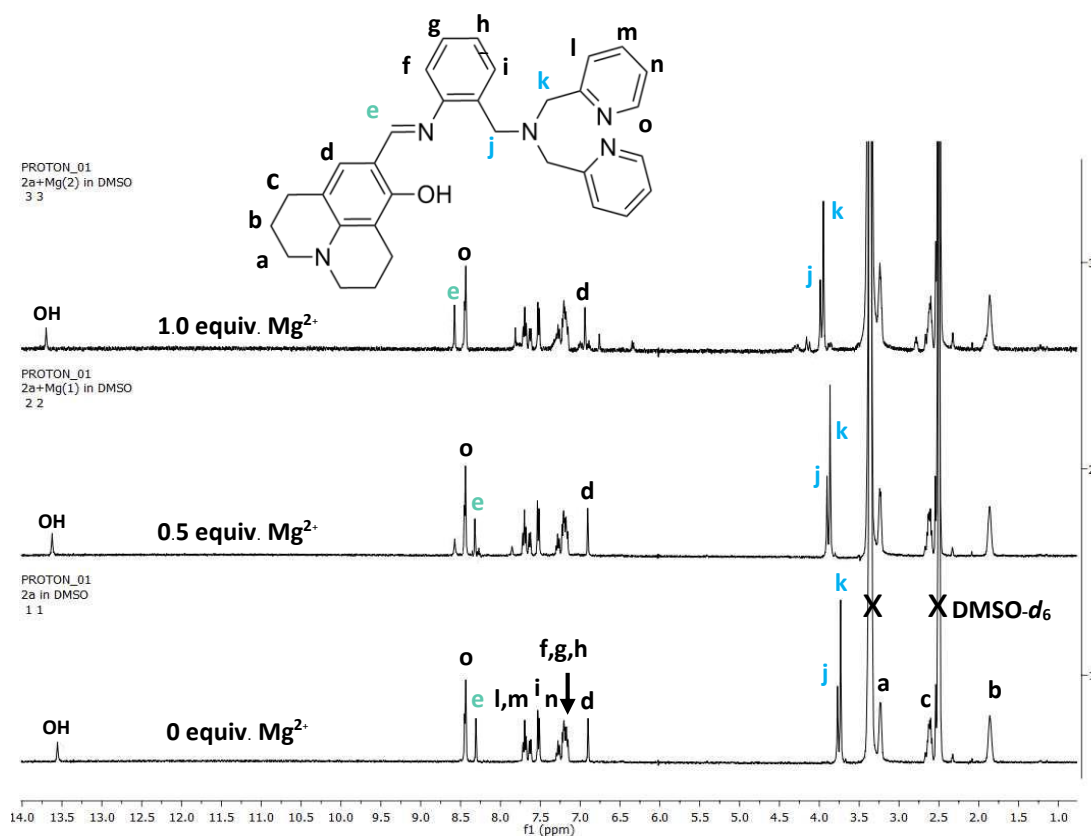
Figure 3.30 ^{1}H NMR spectra of **J2P** in DMSO-d_6 upon the addition of 0, 0.5 and 1.0 equiv. of Mg^{2+}.
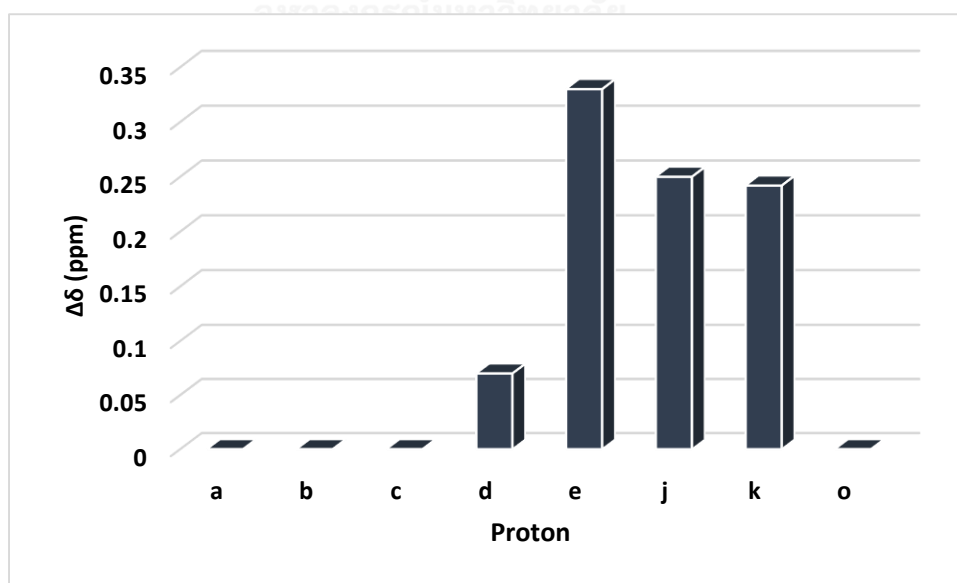
Figure 3.31 Graph of the change in chemical shifts ($\Delta\delta$) of **J2P**-Mg^{2+} titration.

3.5.8 Sensing mechanism of J2P-M^{n+} complexation

According to the Job's plot, the 1:1 stoichiometric complexation of **J2P**-Al^{3+} (**Figure 3.25**) and **J2P**-Mg^{2+} (**Figure 3.26**) were revealed. In the case of **J2P**-Al^{3+}, this 1:1 complexation was also confirmed by the ESI-MS result of the complex [(AlNO$_3$)•(**J2P**+H)•CH$_3$OH]$^+$ (**Figure 3.27**). As one more important evidence, the ^{1}H NMR titration experiment between **J2P** and Al^{3+} under deuterated methanol had demonstrated that the chemical shift of the related protons are significantly low-field-shifted especially aromatic proton d (**Figure 3.28**) probably due to the deprotonation of hydroxy group (Ar-OH) to be a phenolate anion (Ar-O$^-$) causing the change of electron density in aromatic ring. As a result, the phenolate moiety including imine nitrogen atom might act as hard base to bind with hard acid metal ion like Al^{3+}. On the other hand, when the mixed solvent condition was changed to H$_2$O:DMSO, the polar aprotic solvent for Mg^{2+} sensing application, the ^{1}H NMR titration between **J2P** and Mg^{2+} showed that the proton at hydroxyl group was not deprotonated, as hydroxyl proton in the ^{1}H NMR spectrum did not disappear (**Figure 3.30**). Generally, hydroxyl group can act as soft base moiety to specify with the soft base metal ion, Mg^{2+} in this case. On top of that, the assumption that the binding cavity of **J2P** might be providing a high specificity to the size of both metal ions as the ionic radii of both Al^{3+} and Mg^{2+} are also closed to each other, which are 1.25 Å and 1.50 Å, respectively [63]. Therefore, the cavity size of **J2P** could possibly matched with both metal ions and as a consequence, the complex, which was sketched by using Chem3D Ultra 10.0, can be illustrated as shown in **Figure 3.32**.
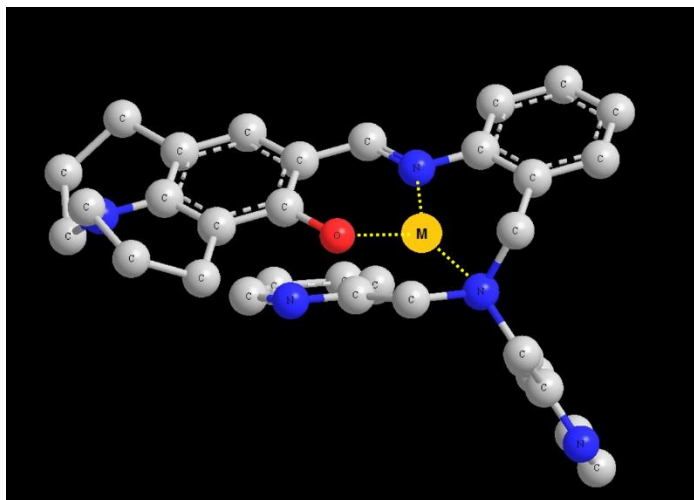
Figure 3.32 The complex structure of **J2P**-M^{n+} from Chem3D Ultra 10.0.

The keto-enol tautomerization type of ESIPT could be assumed in the structure of **J2P**, resulting in the energy loss during the excitation decay process, and hence the loss of fluorescent. PET process might also be occurring but without any affirmative evidence. Three main reasons for the non-fluorescence property of **J2P** are possible C=N isomerization, ESIPT and PET. According to the proposed structural coordination of **J2P**-M^{n+}, the isomerization of imine bond (C=N) was conceivably obstructed, therefore, CHEF effect could be considered as the fluorescence enhancing mechanism ESIPT and PET process were consequently inhibited resulting in the fluorescence enhancement as depicted in **Figure 3.33**.
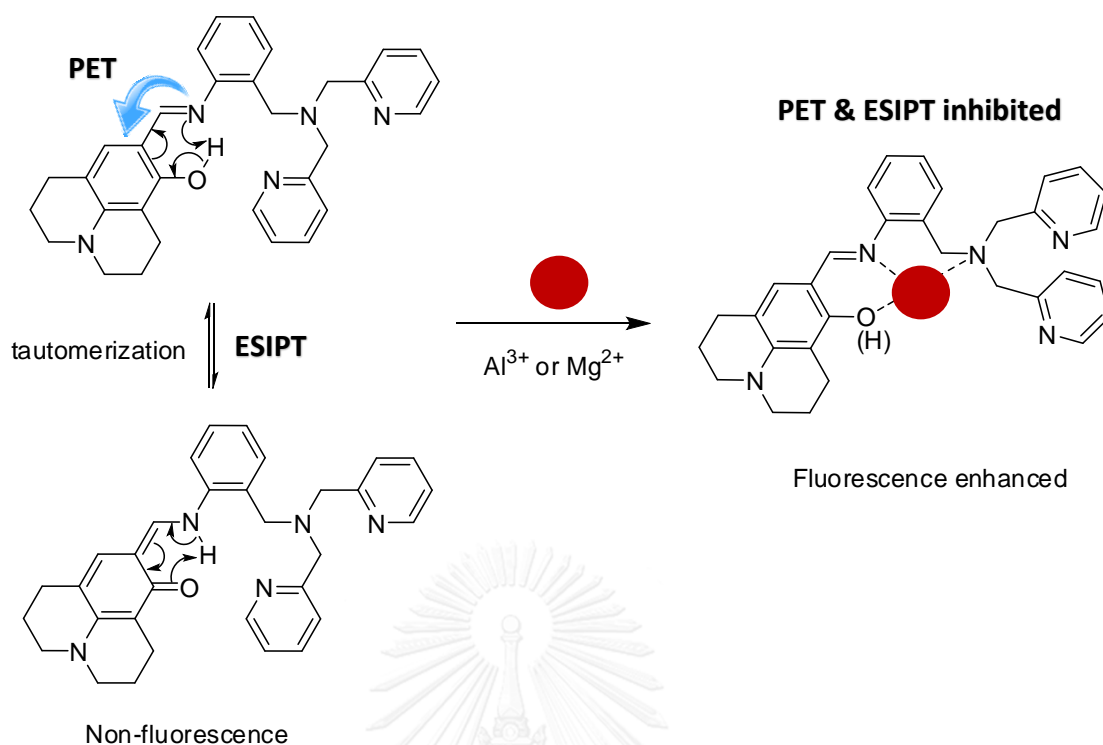
Figure 3.33 Complex structure of **J2P**-(Al^{3+} or Mg^{2+}) and fluorescence enhancing mechanism.

3.5.9 Competitive experiments over other metal ions

In order to seek the practical use of the fluorescent sensor, the competitive experiment of **J2P** was carried out. For aluminum sensing, the mixtures of Al^{3+} (1.0 equiv.) and interfering metal ions (1.0 equiv.) were added to **J2P** under 10% H_2O/ methanol condition. At the same concentration, the mixtures of Mg^{2+} and another metal ion was added to 5% H_2O/DMSO solution of **J2P**. The fluorescence response was measured and plotted of relation intensity (I/I_o) where I = maximum fluorescence intensity of **J2P**-Al^{3+}or Mg^{2+} and competitive metal ion] mixtures and I_o = maximum fluorescence intensity of **J2P**. As shown in **Figure 3.34**, the fluorescence signal was not significantly interfered by other metal ions but in the presence of Fe^{3+}, the fluorescence signal was partially reduced around 10-folds. In case of magnesium sensing (**Figure 3.35**), most of metal ion did not interfere the fluorescence signal of **J2P** and Mg^{2+}. Nonetheless, the fluorescence intensities were reduced partially in the

presence of Fe^{2+} and Cu^{2+} and almost completely reduced in the presence of Fe^{3+}. According to the results, **J2P** exhibited outstanding turn-on fluorescent sensor especially in Al^{3+} detection and be suitable for quantitative analysis of both metal ions.
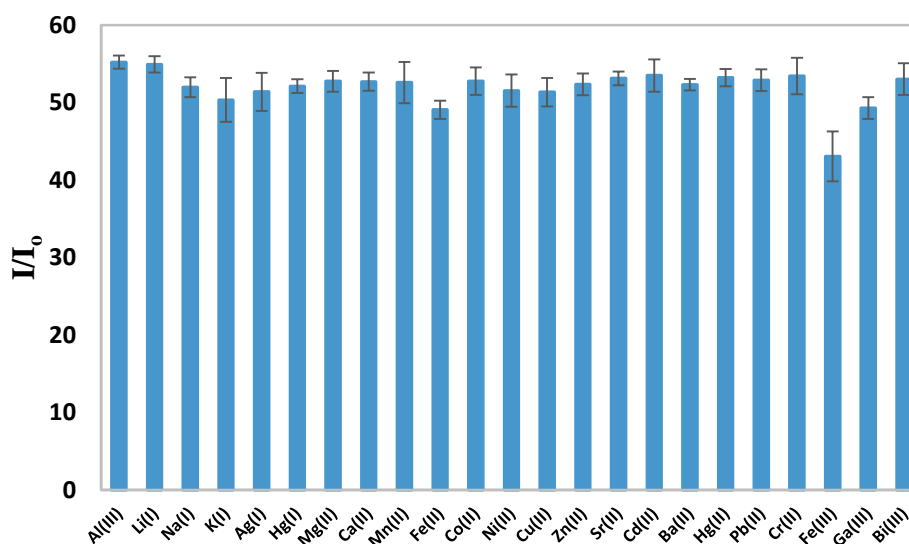
Figure 3.34 Relative fluorescence (I/I_o) of **J2P** (10 µM) in 10% H_2O/methanol in the presence of Al^{3+} (1.0 equiv.) and interfering metal ion (1.0 equiv.)
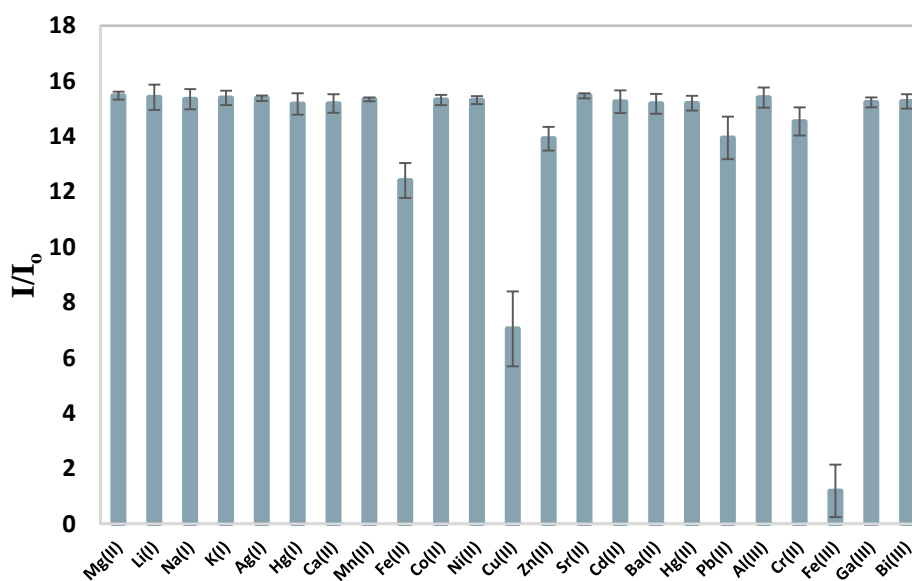
Figure 3.35 Relative fluorescence (I/I_o) of **J2P** (10 µM) in 5% H_2O/DMSO in the presence of Mg^{2+} (1.0 equiv.) and interfering metal ion (1.0 equiv.).

3.5.10 The detection limit

The detection limit (LOD) of **J2P** to Al^{3+} was determined by the fluorescence response to nanomolar range of Al^{3+} concentration in 10% H_2O/methanol solution. The calibration curve (**Figure 3.36**) showed a good straight line in aluminum concentration between 90 and 300 nM with $R^2 = 0.9880$. In case of magnesium detection, the linear range ($R^2 = 0.9927$) of the relative fluorescence signal was observed at Mg^{2+} concentration of 2.0 to 9.0 µM in mixed 5% H_2O/DMSO solution (**Figure 3.37**). According to the plot of relative fluorescence intensity against concentration of metal ion, the detection limit of Al^{3+} and Mg^{2+} was calculated as 0.17 and 1.32 µM, respectively. Based on the maximum value of World Health Organization (WHO) in drinking water, the maximum level of Al^{3+} and Mg^{2+} are not allowed to exceed 7.41 µM or 200 µg/l [64-66] and 2.06 mM or 50 mg/l [67], respectively.
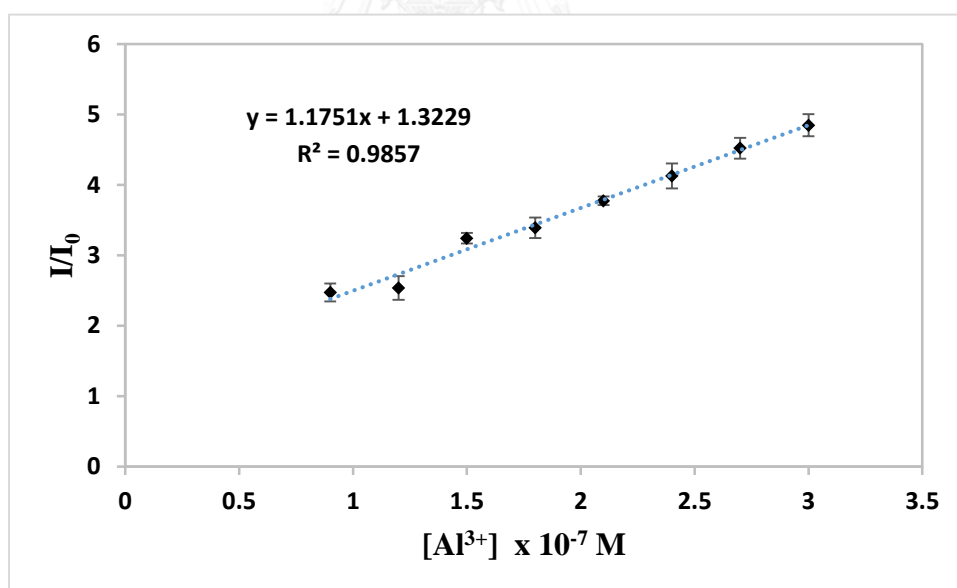
Figure 3.36 Calibration curves of fluorescence intensity ratio of **J2P** to Al^{3+} concentration.
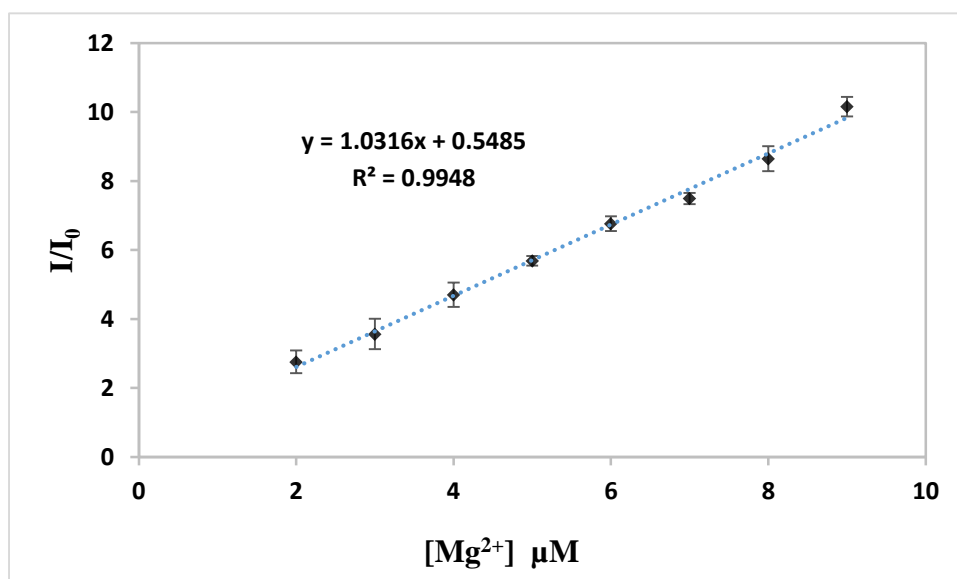
Figure 3.37 Calibration curves of fluorescence intensity ratio of **J2P** to Mg^{2+} concentration.

3.5.11 Reversibility study

To confirm the reusability, the complex regeneration of both **J2P**-Al^{3+} and **J2P**-Mg^{2+} was studied using EDTA, a chelating agent that sequesters a variety of polyvalent cations including aluminum and magnesium providing the 1:1 stociometric complex (**Figure 3.38**). The stability constants (Log K_a) of EDTA-Al^{3+} and EDTA-Mg^{2+} were reported as 16.13 (K_a = 1.35 x 10^{16} M^{-1}) and 8.69 (K_a = 4.90 x 10^8 M^{-1}), respectively [68], which are much higher than those of **J2P**-Al^{3+} and **J2P**-Mg^{2+}, which are 2.25 x 10^5 M^{-1} and 4.00 x 10^4 M^{-1}, respectively. The fluorescence profiles were repeated by recorded in the sequence of after addition of EDTA and metal ion, for 3 cycles. The results demonstrated that **J2P**-Al^{3+} complex can be regenerated as three times (**Figure 3.39**) by using 1.0 equiv. of EDTA and Al^{3+} for each cycle. In contrast, the fluorescence intensity of **J2P**-Mg^{2+} decreased upon addition of EDTA (1.0 equiv.) and then the fluorescence signal could not be regenerated even after Mg^{2+} was added to the solution mixture (**Figure 3.40**).
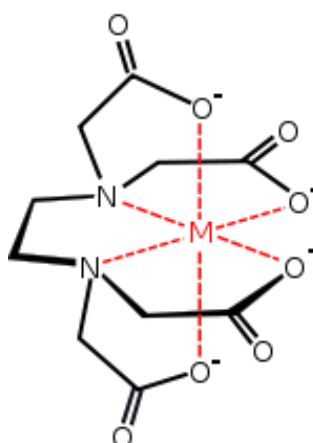
Figure 3.38 Coordination structure of EDTA with metal ion.
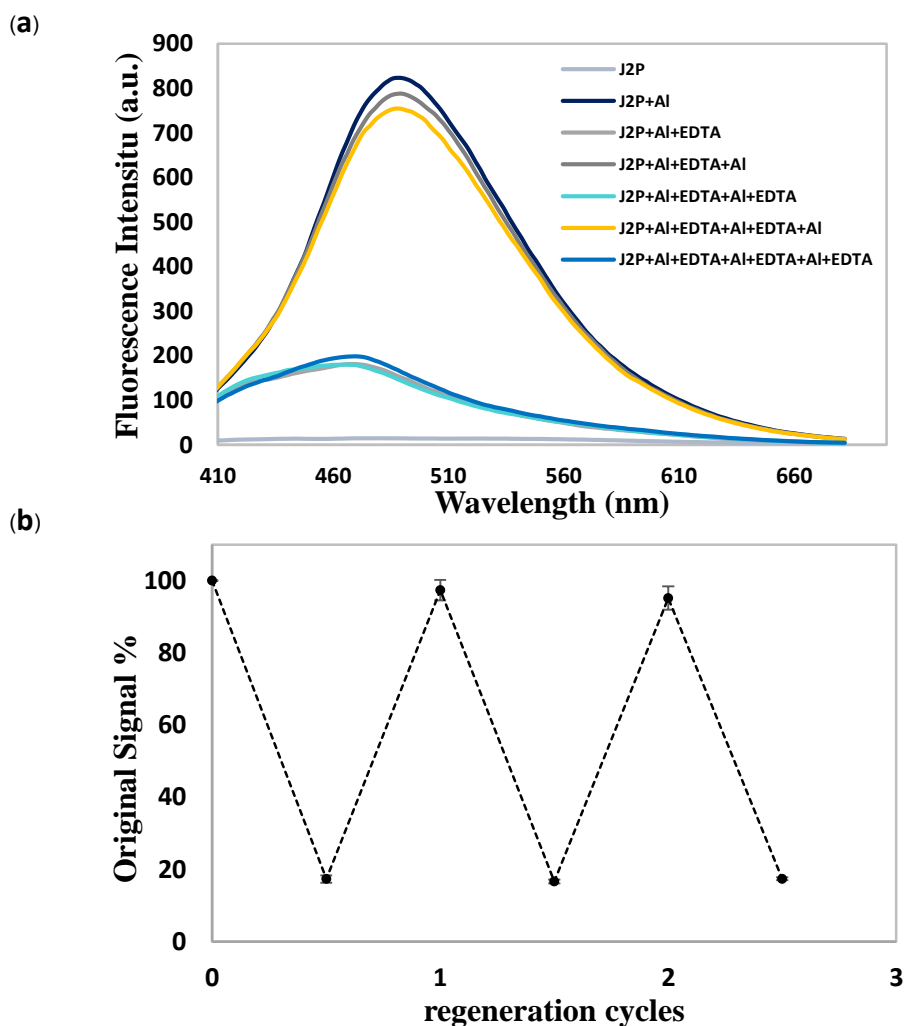
Figure 3.39 (a) Fluorescence emission spectra of **J2P** in present of Al^{3+} (1.0 equiv.) and its signal regeneration by EDTA and (b) Regeneration cycle and recovery percentage of **J2P**.
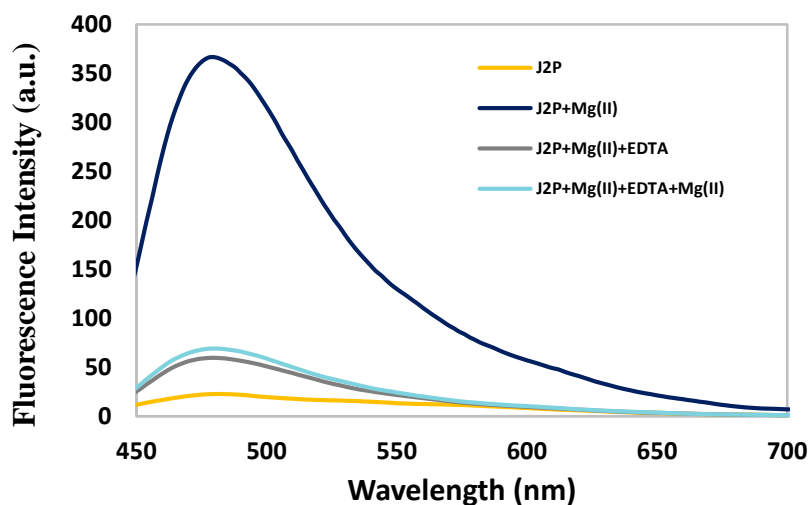
Figure 3.40 Fluorescence emission spectra of **J2P** in the presence of Mg^{2+} (1.0 equiv.) and its signal regeneration by EDTA.

3.5.12 Synthesis and characterization of J2B

In order to confirm whether there is any involvement of two nitrogen atoms on DPA moiety of **J2P** in the chelation between **J2P** and matal ions, compound **3d** containing dibezylamine (DBA) group instead of DPA was designed and synthesized. The fluorescent sensor **J2B** was synthesized by coupling of julolidine **1** with compound **3d** via Schiff base reaction under reflux condition as shown in **Scheme 3.7**. The target sensor **J2B** was achieved in 75% yield.
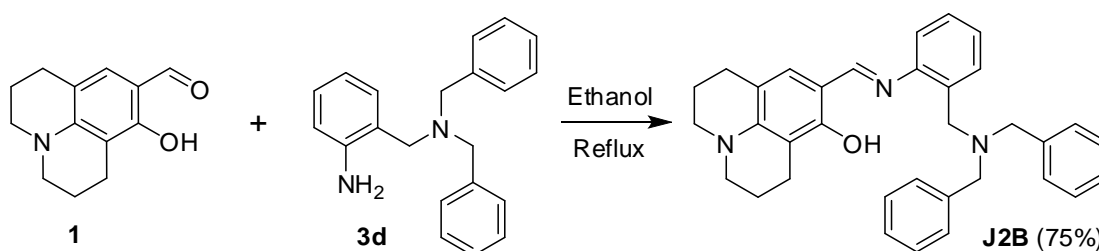
Scheme 3.7 The synthesis of **J2B.**

Sensor **J2B** was characterized by ^{1}H NMR and confirmed its existence by HRMS. According to ^{1}H NMR spectrum (**Figure 3.41)**, the imine proton e was observed as singlet peak at 8.22 ppm and the signals of proton l, m and n at benzyl group were found at 7.35, 7.24, 7.17 ppm, respectively. The HRMS result of **J2B** showed the molecular ion peak at of the positive charge of [J2B+H] at *m/z* = 502.2851 (**Figure 3.42)**.
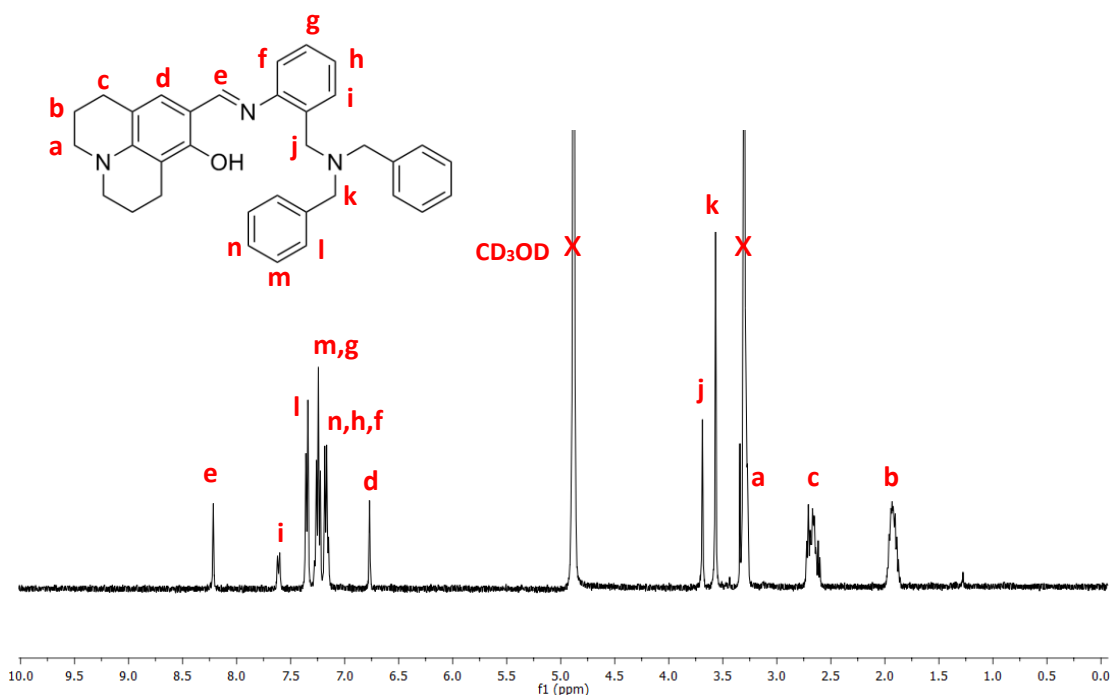
Figure 3.41 ^{1}H NMR spectrum (400 MHz) of **J2B**.
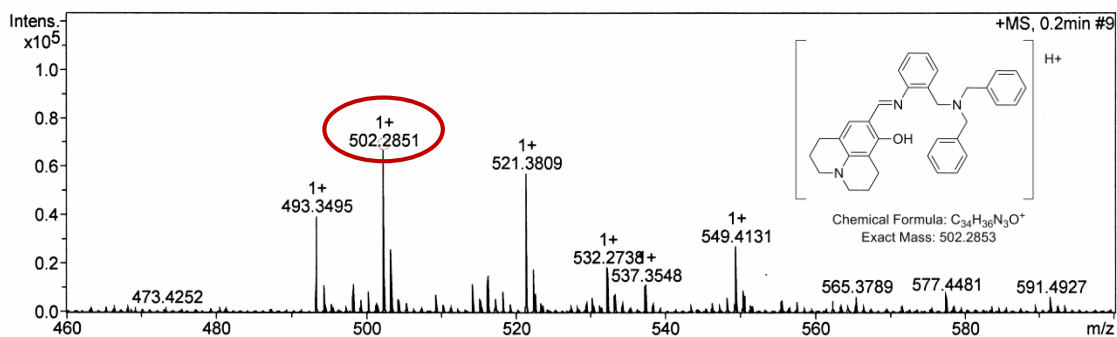
Figure 3.42 HR mass spectrum of **J2B**.

3.5.13 Photophysical and sensing properties of J2B

According to the photophysical property of **J2B** (**Table 3.2**), the maximum absorption in 10% H_2O/methanol and 5% H_2O/DMSO were observed at 368 and 375 nm, respectively. The molecular extinction coefficients (ε) were calculated as 1.58 x 10^4 in 10% H_2O/methanol and 2.03 x 10^4 in 5% H_2O/DMSO. As similar to **J2P**, sensor **J2B** did not exhibit any fluorescence signal under both solvent conditions.

Table 3.2 The photophysical properties of **J2B**.

Absorption		Emission		Appearance of **J2B** (50 µM) under day light	Appearance of **J2B** (50 µM) under black light
λ_{ab} (nm)	ε ($M^{-1}cm^{-1}$)	λ_{em} (nm)	Φ_F[*]		
368[a] 375[b]	1.58x10^{4a} 2.03x10^{4b}	N/A	N/A		

[*] Quinine sulfate in 0.1 M H_2SO_4 (Φ = 0.54) was used as the reference.

[a] Experiment data achieved in mixed solvent of 10% H_2O/methanol.

[b] Experiment data achieved in mixed solvent of 5% H_2O/DMSO

N/A = not available

The sensing applications of **J2B** were studied under the same conditions with **J2P**. The selectivity of **J2B** in 10% H_2O/methanol (**Figure 3.43**) was achieved at 15 minutes after the addition of metal ion (10.0 equiv.) to 10 µM of **J2B**, the 46-folds (Φ_F = 0.114) of fluorescence intensity at 495 nm of **J2B** was observed in the presence of Al^{3+} with an excitation wavelength (λ_{ex}) of 368 nm (**Figure 3.44**) whereas the fluorescence signal did not significantly change upon the addition of other metal ions under the same condition.
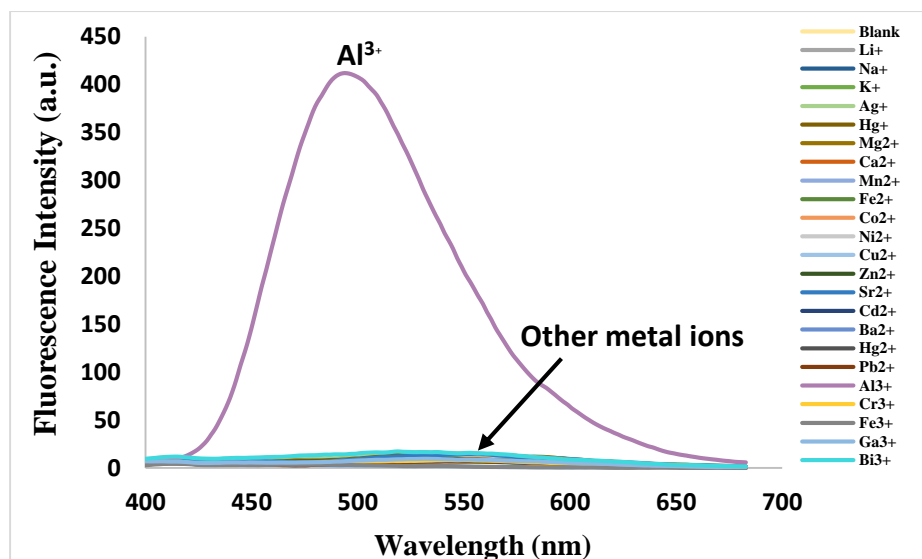
Figure 3.43 Fluorescence spectra of **J2B** (10 µM in 10% H_2O/methanol) after the addition of 10.0 equiv. of Li^+, Na^+, K^+, Ag^+, Hg^+, Mg^{2+}, Ca^{2+}, Mn^{2+}, Fe^{2+}, Co^{2+}, Ni^{2+}, Cu^{2+}, Zn^{2+}, Sr^{2+}, Cd^{2+}, Ba^{2+}, Hg^{2+}, Pb^{2+}, Al^{3+}, Cr^{3+}, Fe^{3+}, Ga^{3+} and Bi^{3+}. The fluorescence spectra were investigated at 15 minutes after the addition of metal ion with λ_{ex} = 368 nm

Figure 3.44 (a) Fluorescence signal ratio (I/I_o)-1 of **J2B** (10 µM in 10% H_2O/methanol) after addition of each metal ion (10.0 equiv.) with λ_{ex} = 368 nm and λ_{em} = 495 nm. (b) The photograph under black light of **J2B** upon addition of each metal ion (10.0 equiv.).

Furthermore, the fluorescence responses of **J2B** toward metal ion under the solvent condition of 5% H_2O/DMSO (**Figure 3.45**). The fluorescence signal at 475 nm that significantly enhanced around 10-folds (Φ_F = 0.078) toward only Mg^{2+} (**Figure 3.46**) while using the excitation wavelength of 375 nm.
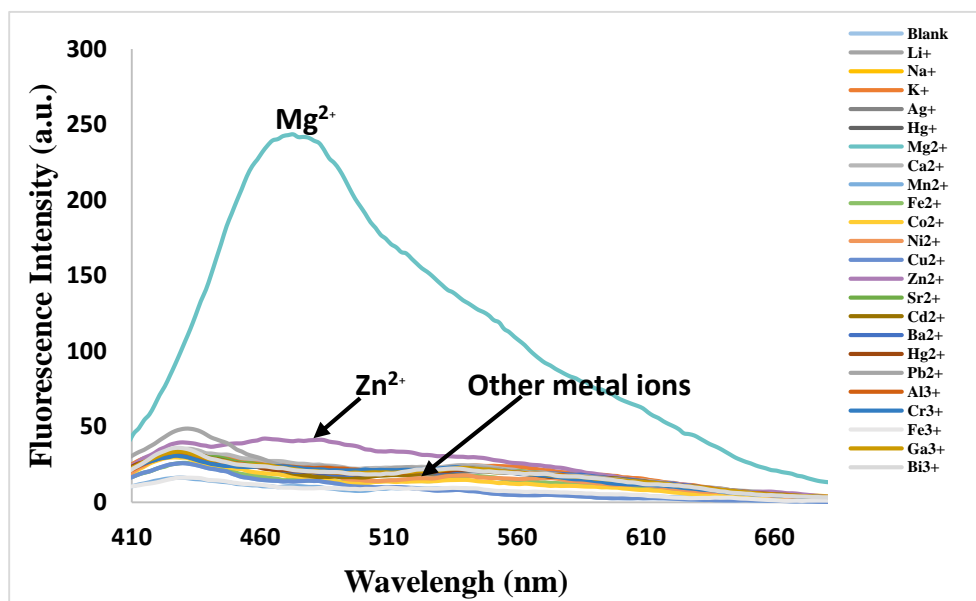
Figure 3.45 Fluorescence spectra of **J2B** (10 μM in 5% H_2O/DMSO) after the addition of 10.0 equiv. of Li^+, Na^+, K^+, Ag^+, Hg^+, Mg^{2+}, Ca^{2+}, Mn^{2+}, Fe^{2+}, Co^{2+}, Ni^{2+}, Cu^{2+}, Zn^{2+}, Sr^{2+}, Cd^{2+}, Ba^{2+}, Hg^{2+}, Pb^{2+}, Al^{3+}, Cr^{3+}, Fe^{3+}, Ga^{3+} and Bi^{3+}. The fluorescence spectra were investigated after the addition of metal ion with λ_{ex} = 375 nm.
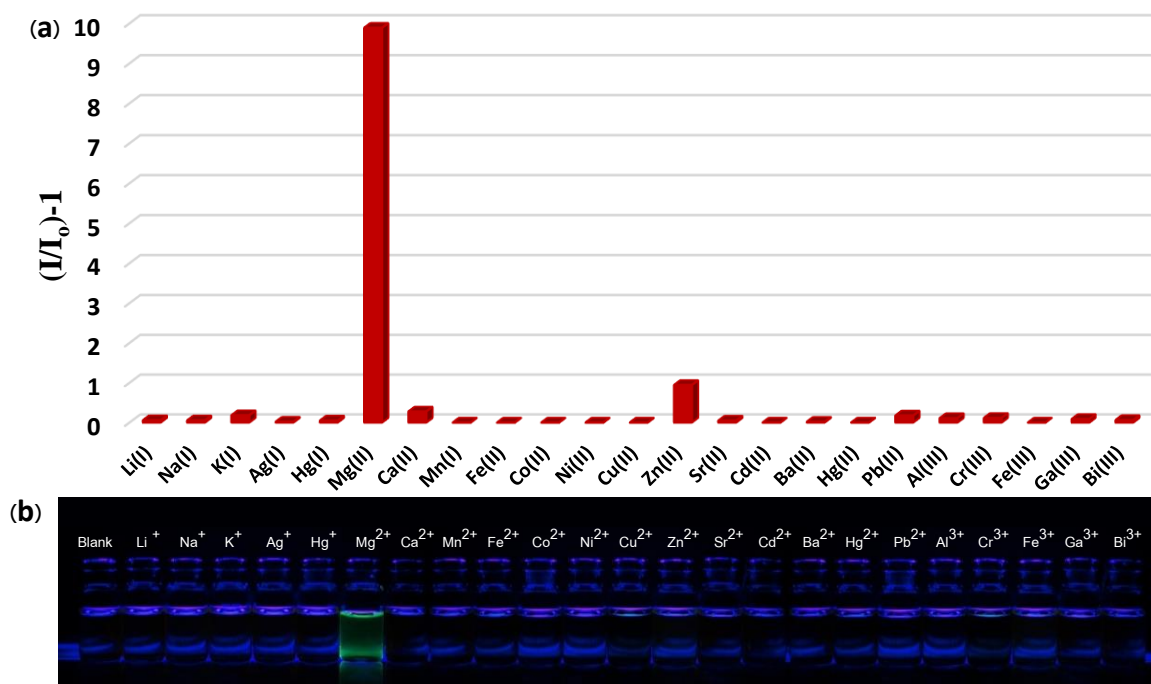
Figure 3.46 (a) Fluorescence signal ratio (I/I$_o$)-1 of **J2B** (10 μM in 10% H$_2$O/methanol) after addition of each metal ion (10.0 equiv.) with λ_{ex} = 375 nm and λ_{em} = 475 nm. (b) The photograph under black light of **J2B** upon addition of each metal ion (10.0 equiv.).

According to the selectivity study of **J2B** in both solvent conditions by UV-Visible spectroscopy, the results shows that in presence of Al^{3+}, Cu^{2+} and Fe^{3+} under solvent condition of 10% H$_2$O/methanol (**Figure 3.47a**), the absorption band of **J2B** at 368 nm was decreased and significantly red shifted, On the other hand, the maximum absorption of **J2B** at 368 nm significantly increased in the presence of Cr^{3+}.

In case of 5% H2O/DMSO, the absorption band of **J2B** slightly shifted to the rad region around 40 nm upon the addition of Cu^{2+} (**Figure 3.47b**) however the absorption band had not significantly change in presence of other metal ion under the same condition. Nevertheless, the naked-eye observation found that the color of **J2B** compared with the blank (control system) in each solvent condition did not significantly change.
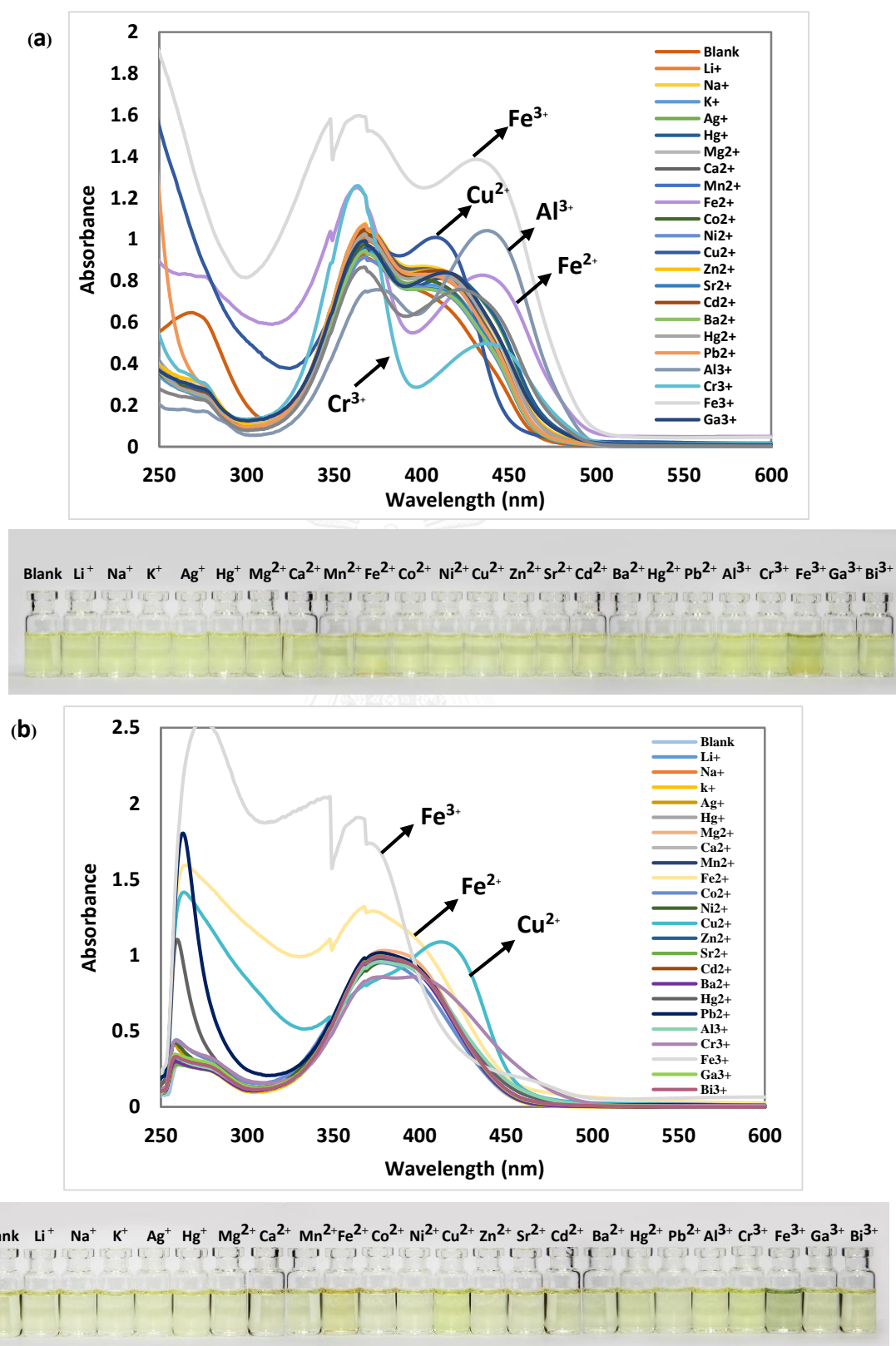
Figure 3.47 Absorption spectra and appearances under day light of **J2B** (50 µM) after addition of metal ions (10.0 equiv.) in (a) 10% H_2O/methanol and (b) 5% H_2O/DMSO.

The fluorescence titration between **J2B** and Al^{3+} in 10% H_2O/methanol showed the continuous increase of fluorescence intensity upon the addition of 0.2-1.0 equiv. of Al^{3+} before the complete enhancement at 1.0 equiv. of Al^{3+} (**Figure 3.4**8). Likewise, the fluorescence signal of **J2B** in 5% H_2O/DMSO increased along with the increased amount of Mg^{2+} and completely enhanced at 1.0 equiv. Mg^{2+} (**Figure 3.4**9).
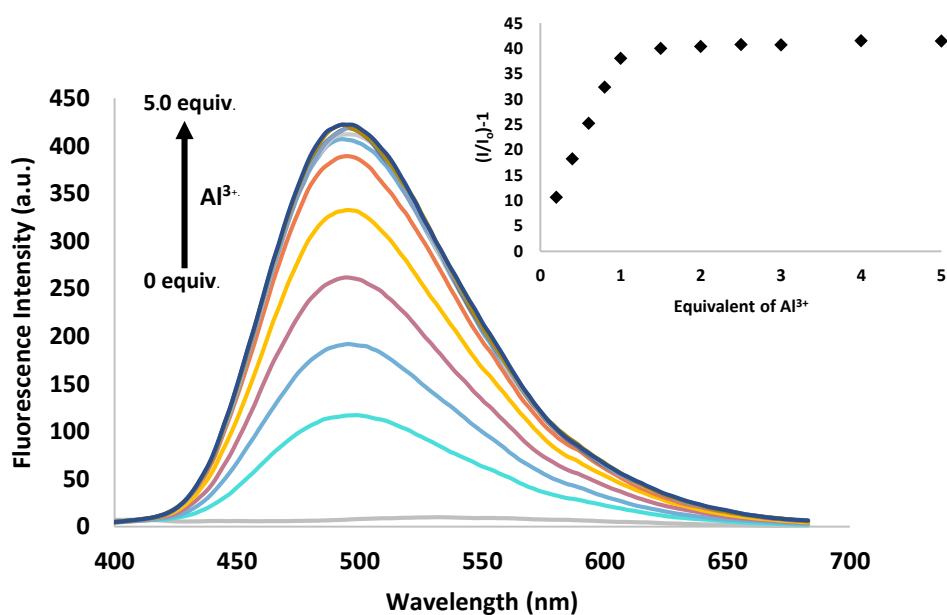
Figure 3.48 Fluorescence change of **J2B** (10 µM) with the addition of Al^{3+} (0-5.0 equiv.) under 10% H_2O/methanol using the excitation wavelength (λ_{ex}) at 368 nm.
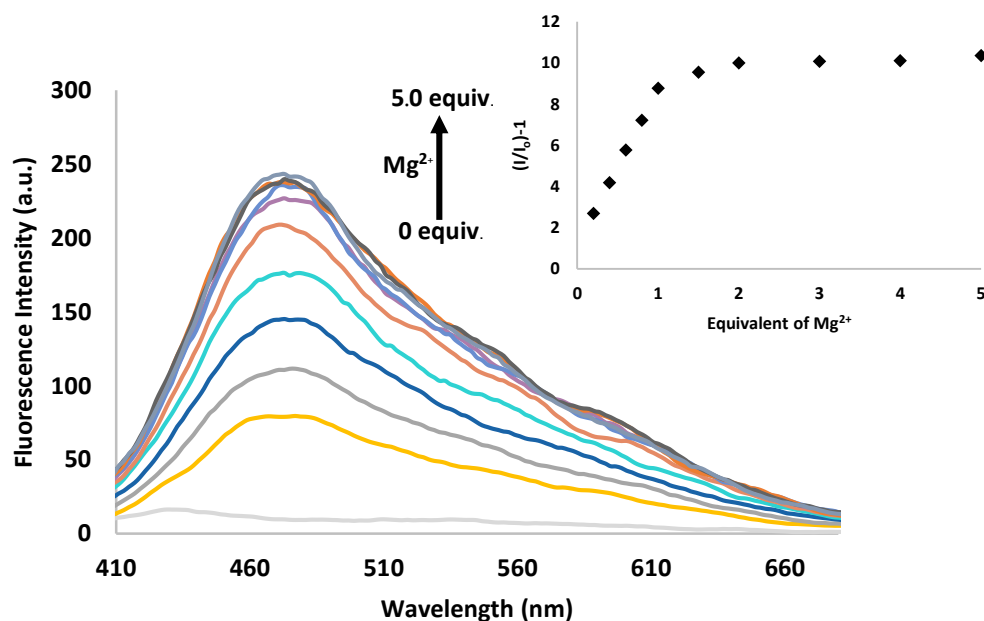
Figure 3.49 Fluorescence change of **J2B** (10 µM) with the addition Mg^{2+} (0-5.0 equiv.) under 5% H_2O/DMSO using the excitation wavelength (λ_{ex}) at 375 nm.

The Benesi-Hildebrand plots give a linear response for metal ion concentration range of 0.2-0.9 µM Al^{3+} (R^2 = 0.9925) (**Figure 3.50**) and 0.2-0.8 µM Mg^{2+} (R^2 = 0.9955) (**Figure 3.51**). The association constant (K_a) for the complexation of **J2B**-Al^{3+} and **J2B**-Mg^{2+} were calculated as 1.40 x 10^5 M^{-1} and 1.67 x 10^4 M^{-1}, respectively.
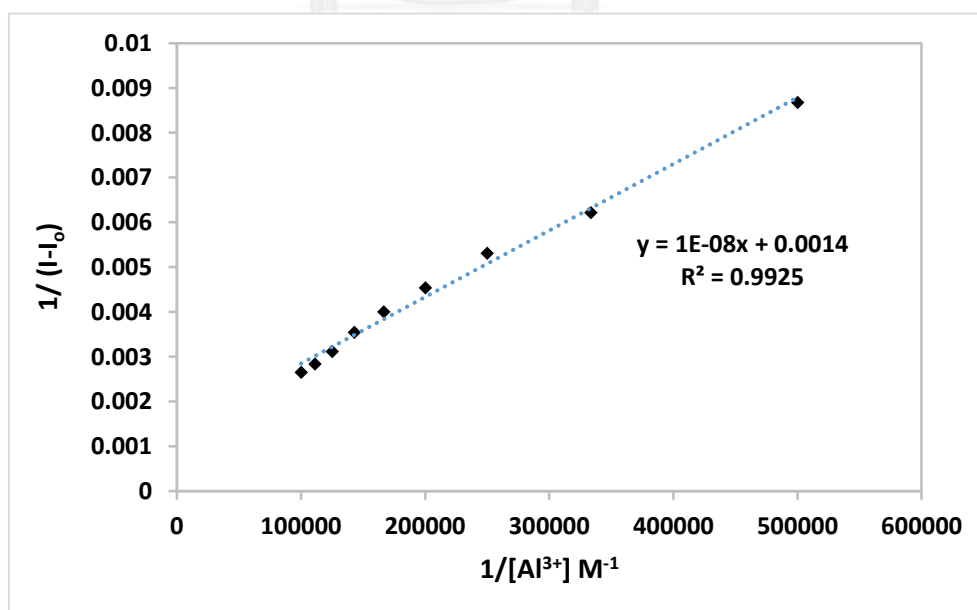
Figure 3.50 Benesi–Hildebrand plot of **J2B**-Al^{3+}.
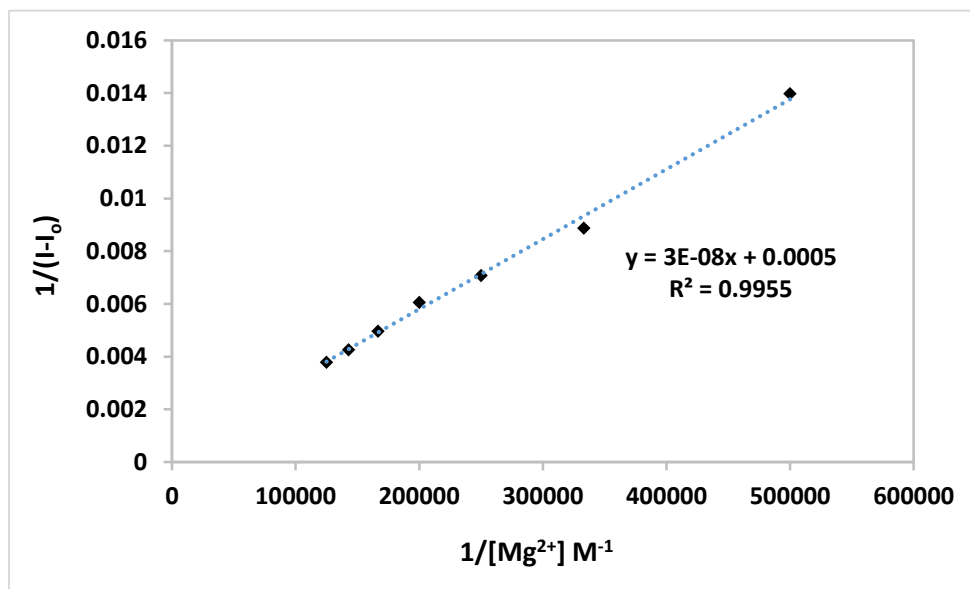
Figure 3.51 Benesi–Hildebrand plot of **J2B**-Mg^{2+}.

In order to determine the detection limit of **J2B**, the stock solution of **J2B** in methanol and DMSO were diluted to 1.0 μM for Al^{3+} detection and 10 μM for Mg^{2+} detection, respectively. The fluorescence titration profile provides the linear range of aluminum concentration between 0.2 and 0.9 μM with R^2 = 0.9988 (**Figure 3.52**) and magnesium concentration between 2.0 and 9.0 μM with R^2= 0.9907 (**Figure 3.53**). The detection limit was calculated as 0.75 μM for Al^{3+} detection and 6.47 μM for Mg^{2+} detection, respectively. The detection limit of both Al^{3+} and Mg^{2+} is much lower than the allowable concentration limit of Al^{3+} and Mg^{2+} in drinking water established by WHO.
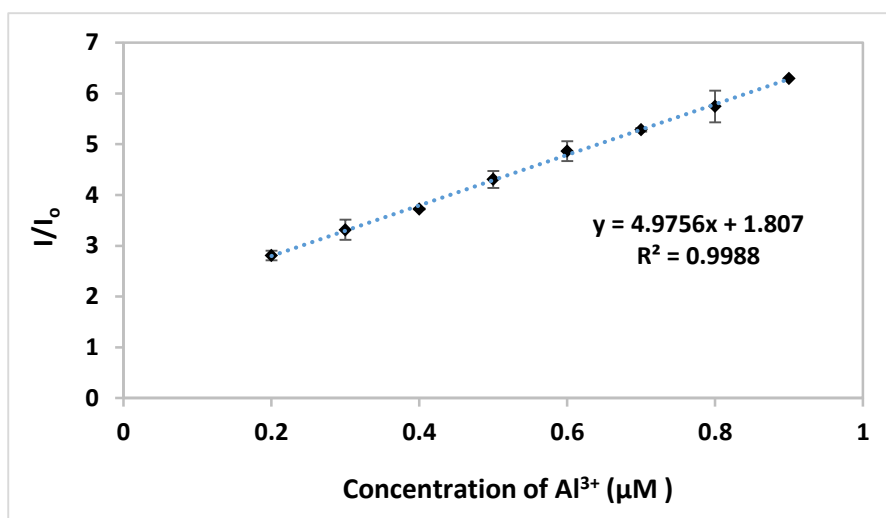
Figure 3.52 Calibration curves of fluorescence intensity ratio of **J2B** to Al^{3+} concentration.
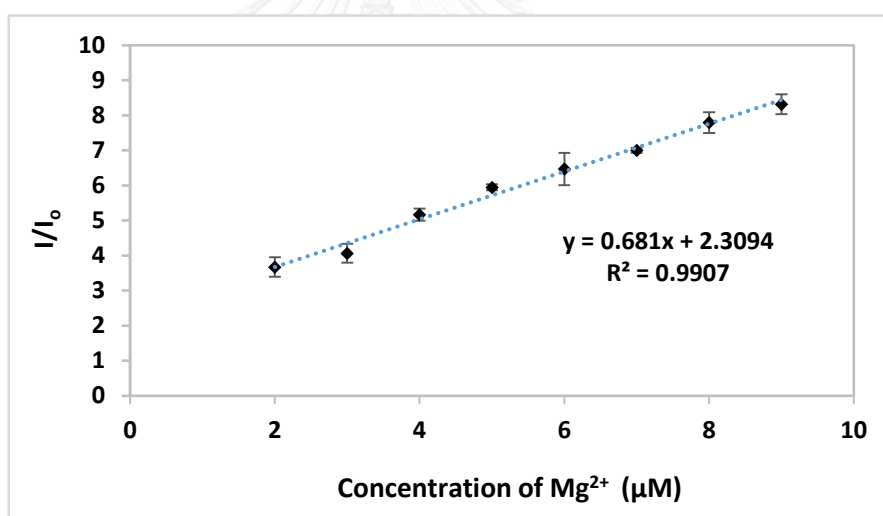
Figure 3.53 Calibration curves of fluorescence intensity ratio of **J2B** to Mg^{2+} concentration.

Job's method was operated to determine the stoichiometric complexation between **J2B** and metal ion. In cased of aluminum detection, the results were collected under the solvent condition as 10% H_2O/methanol and using the maximum fluorescence intensity at 495 nm to plot and calculate. The maximum coordination point on Job's plot of **J2B**-Al^{3+} was observed at 0.5 of X_a (Mole fraction of Al^{3+})

corresponding to 1:1 stoichiometric coordination between **J2B** and Al^{3+} (**Figure 3.54**). As the same token, Job's plot of **J2B**-Mg^{2+} was achieved under the solvent condition of 5% H_2O/DMSO with the maximum emission intensity of the complex at 475 nm (**Figure 3.55**). The results demonstrated that the stoichiometric complexation of **J2B**-Mg^{2+} was calculated as 1:1.
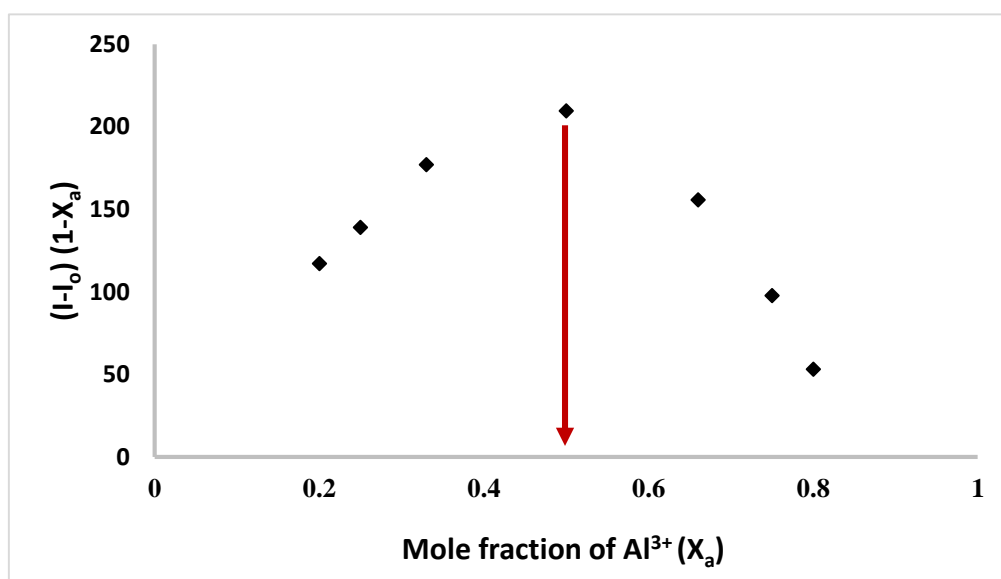
Figure 3.54 Job's plot examined between **J2B** and Al^{3+} by fluorescence responses.
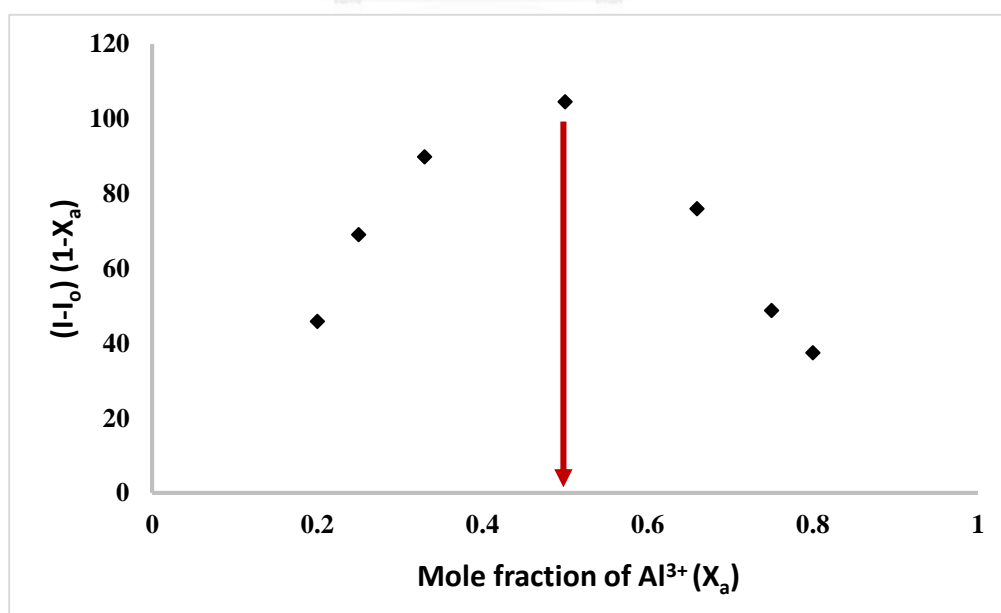
Figure 3.55 Job's plot examined between **J2B** and Mg^{2+} by fluorescence responses.

Moreover, the mass spectrum of **J2B**-Al^{3+} complex was carried out using ESI-MS analysis (**Figure 3.56**). According to the results, the molecular ion peak was observed at m/z = 622.8 corresponding to the exact mass of $[Al(NO_3) \cdot (J2B+H) \cdot CH_3OH]^+$ and demonstrating the 1:1 stoichiometric coordination of **J2B**-Al^{3+}.
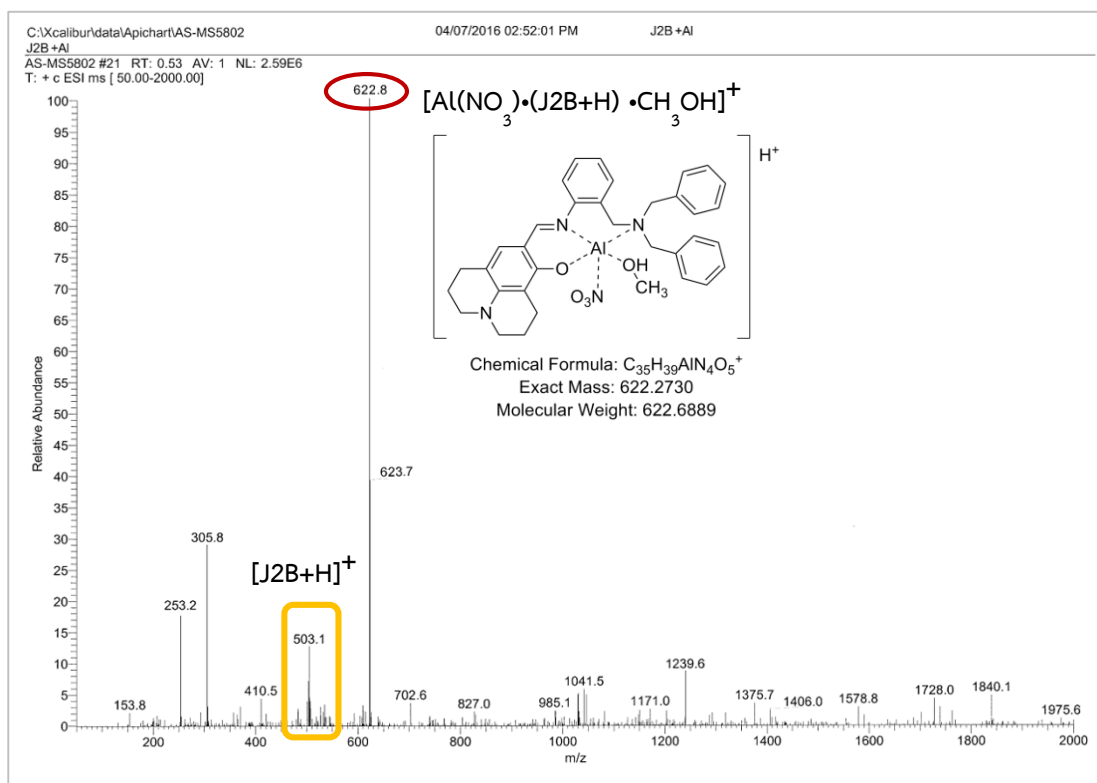
Figure 3.56 ESI-MS of **J2B**-Al^{3+}.

Table 3.3 Comparison of photophysical and sensing properties between **J2P** and **J2B**.

			Fluorescent sensor	
			J2P	**J2B**
Absorption	10% H$_2$O/MeOH	λ_{ab}(nm)	380	368
		ε (M^{-1}cm^{-1})	1.45 x 10^4	1.58x10^4
	5% H$_2$O/DMSO	λ_{ab}(nm)	390	375
		ε (M^{-1}cm^{-1})	1.37 x 10^4	2.03x10^4
Emission	Al^{3+} detection (10% H$_2$O/MeOH)	λ_{ex}(nm)	380	368
		λ_{em}(nm)	490	495
		K$_a$	2.25 x 10^5	1.40 x 10^5
		Φ_F	0.156	0.124
		LOD (μM)	0.17	0.75
		Appearance under black light*	J2P+Al^{3+}	J2B+Al^{3+}
	Mg^{2+} detection (5% H$_2$O/DMSO)	λ_{ex}(nm)	390	375
		λ_{em}(nm)	478	475
		K$_a$	4.00 x 10^4	1.67 x 10^4
		Φ_F	0.096	0.078
		LOD (μM)	1.32	6.47
		Appearance under black light*	J2P+Mg^{2+}	J2B+Mg^{2+}
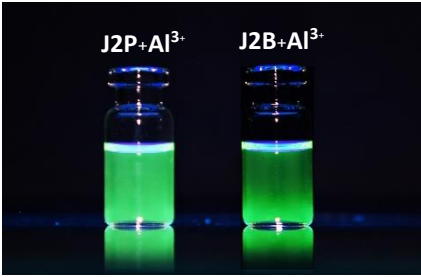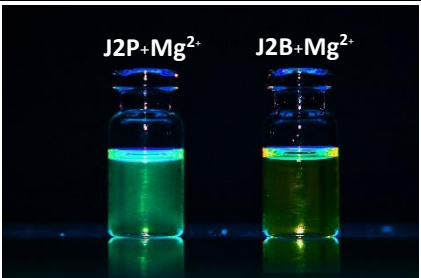
* 10 μM of **J2P** and **J2B** in presence of 10.0 equiv. of Al^{3+} and Mg^{2+}.

To clarify the coordination position between sensor **J2P** and metal ion, sensor **J2B** was designed and synthesis. According to photophysical and sensing properties, **J2B** is able to provide the good fluorescence response toward both Al^{3+} and Mg^{2+} as similar to **J2P**. Consequently, the efficiency of two fluorescent sensors need to be compared as shown in **Table 3.3**. These two fluorescent sensors composed of the same components such as an aromatic ring however **J2P** containing two nitrogen atoms at the pyridine ring that causing not only the higher absorption band of **J2P** but also the solubility in both methanol and DMSO. On the other hand, the sensing efficient of **J2P** seem to be better than **J2B** especially the fluorescence quantum yield (Φ_F) and limit of detection.

CHAPTER IV

CONCLUSION

4.1 Conclusion

In conclusion, the series of fluorescent probe **J2P**, **J3P** and **J4P** containing 8-hydroxyjulolidine derivative as a fluorophore linked with DPA derivative substituted on aniline ring at different position as a control part were successfully developed and synthesized. The structural confirmation of target compounds was achieved by using ^{1}H NMR, ^{13}C NMR and HRMS technique. According to the study of photophysical properties, the maximum absorption of compound **J2P**, **J3P** and **J4P** under mixed solvent condition of H_2O/methanol (1:9, v/v) were observed at 380, 415 and 420 nm, respectively, resulting from the difference in planarity of each molecule. The molar extinction coefficients (**ε**) were calculated as 1.45 x 10^4, 2.06 x 10^4 and 2.68 x 10^4 M^{-1}, respectively. Meanwhile, the maximum absorption band under the condition of H_2O/DMSO (5:95, v/v) of **J2P**, **J3P** and **J4P** were investigated at 390, 397 and 398 nm along with the **ε** values as 1.37 x 10^4, 2.50 x 10^4 and 3.42 x 10^4 M^{-1}, respectively. However, all compounds did not exhibit any emission signal in both solvent conditions. The fluorescent sensor **J2P** was proven to have a good selectivity toward Al^{3+} in H_2O/methanol (1:9, v/v). The fluorescence signals were investigated at 490 nm with the fluorescence quantum yield (Φ_F) of 0.156. The association constant (K_a) of **J2P**-Al^{3+} and detection limit (LOD) were calculated as 2.25 x 10^5 M^{-1} and 0.17 µM. When the condition was changed to H_2O/DMSO (5:95, v/v), the fluorescence enhancement of **J2P** was observed at 478 nm in the presence of Mg^{2+} (Φ_F = 0.096). The K_a and LOD value of **J2P**-Al^{3+} were calculated as 4.00 x 10^4 M^{-1} and 1.32 µM. As the ^{1}H NMR titration results, the imine nitrogen atom, oxygen atom from hydroxyl group as well as nitrogen atom at tertiary amine from DPA moiety ware used in the coordination between **J2P** and both metal ions but the two nitrogen atoms at pyridine rings at DPA are not involved in the chelation. The CHEF effect was proposed for the fluorescence

enhancing mechanism of **J2P** occurring through the inhibition of PET, ESIPT and also isomerization of imine bond.

4.2 Suggestion for the future work

According to the results, the fluorescent probe **J2P** was designed by using DPA derivative as a control part expecting the two nitrogen atoms at pyridine ring might help to bind with metal ion but they did not involve in the coordination of **J2P**-metal ion. The DPA group directly help to increase the solubility of **J2P** in methanol and DMSO. On the other hand, the steric effect of this group might cause the long fluorescence enhancing time. To prove this hypothesis, a simple compound **J2A** containing the primary amine group instead of DPA need to be further developed and studied its sensing properties comparing the results with **J2P**.
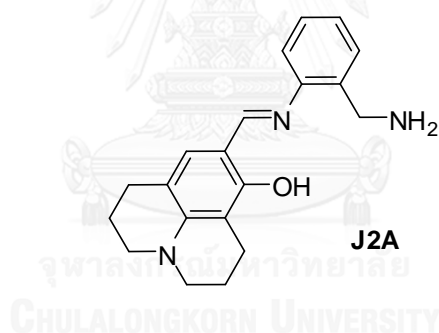
REFERENCES

[1]   Pinkus, G. Ueber die Einwirkung von Trimethylenchlorbromid auf einige
        aromatische Amine und Amide. Chemische Berichte 25(1892): 2798.

[2]   Gompel, J. V., Schuster, G. B. Chemiluminescence of Organic Peroxides:
        Intramolecular Electron-Exchange Luminescence from a Secondary Perester.
        Journal of Organic Chemistry 52(1987): 1465-1468.

[3]   Ghoshal, A., Sarkar, A. R., kumaran, R. S., Hegde, H., Manickam, G.,
        Jayashankaran, J. A facile stereoselective synthesis of julolidine hybrid analogs
        via domino knoevenagel intramolecular hetero Diels–Alder reaction.
        Tetrahedron Letters 53(2012): 1748-1752.

[4]   Huang, H., Zhou, Y., Liu, H. Recent advances in the gold-catalyzed additions
        to C–C multiple bonds. Beilstein Journal of Organic Chemistry 7(2011): 897-
        936.

[5]   Kim, B., Park, S. W., Lee, D., Kwon, I. K., Kim, J. P. Synthesis of Novel
        Hemicyanine Dyes for Color Compensating Film in Plasma Display Panels.
        Bulletin of the Korean Chemical Society 35(8) (2014): 2453-2459.

[6]   Vejdelek, Z., Protiva, M. Potential antidepressants and tranquillizers: Synthesis
        of some 9-(aminoalkoxy)-2,3,6,7-tetrahydro-1H,5H-benzo[ij] quinolizines and 1-
        (substituted amino)-3-(1-naphthoxy)-2-propanols Collect. Chemical
        Communications 55(1990): 1290-1926.

[7]   Yang, Y., Liu, F., Wang, H., Zhang, M., Xu, H., Bo, S., Liu, J., Qiu, L., Zhen, Z., Liu,
        X. Synthesis and characterization of a novel second-order nonlinear optical
        chromophore based on a new julolidine donor. Physical Chemistry Chemical
        Physics 16(2014): 20209-20215.

[8]   Lee, K. H., Park, M. H., Kim, S. M., Kim, Y. K., Yoon, S. S. Modified Julolidine-
        Containing Emitters for Red Organic Light-Emitting Diodes. Japanese Journal of
        Applied Physics 49(8) (2010): 15-18.

[9]   Glass, D. B., Weissberger, A. Julolidine. Organic Syntheses 3(1955): 504.

[10]   Labed, A., Jiang, F., Labed, I., Lator, A., Peters, M., Achard, M., Kabouche, A., Kabouche, Z., Sharma, G. V. M., Bruneau, C. Iridium-Catalyzed Sustainable Access to Functionalized Julolidines through Hydrogen Autotransfer. ChemCatChem 7(2015): 1090-1096.

[11]   Kauffinan, J. M., Imbesi, S. J. Synthesis of julolidine derivatives. Organic Preparations and Procedures International 33(2001): 603-613.

[12]   Katritzky, A., Rachwal, B., Rachwal, S. Convenient Synthesis of Julolidines Using Benzotriazole Methodology J. Journal of Organic Chemistry 61(1996): 3117-3126.

[13]   Yuan, L., Lin, L., Song, J., Yang, Y. Development of an ICT-based ratiometric fluorescent hypochlorite probe suitable for living cell imaging. Chemical Communications 47(2011): 12691-12693.

[14]   Zhang, S., Fan, J., Zhang, S., Wang, J., Wang, D., Du, J., Peng, X. Lighting up fluoride ions in cellular mitochondria with a highly selective and sensitive fluorescent probe. Chemical Communications 50(2014): 342-345.

[15]   Na, Y. J., Hwanf, I. H., Jo, H., Y., Lee, S. A., Park, G. J., Kim, C. Fluorescent chemosensor based-on the combination of julolidine and furan for selective detection of zinc ion. Inorganic Chemistry Communications 35(2013): 342-345.

[16]   Choi, Y. W., Park, G. J., Na, Y. J., Jo, H. Y., Lee, S. A., You, G., R., Kim, C. A single schiff base molecule for recognizing multiple metal ions: A fluorescence sensor for Zn(II) and Al(III) and colorimetric sensor for Fe(II) and Fe(III). Sensors and Actuators B: Chemical 194(2014): 343-352.

[17]   Lee, J. J., Park, G. J., Kim, Y. S., Lee, S. Y., Lee, H. J. A water-soluble carboxylic-functionalized chemosensor for detecting Al^{3+} in aqueous media and living cells: Experimental and theoretical studies. Biosensors and Bioelectronics 69(2015): 226-229.

[18]   Lee, S. A., You, G. R., Choi, Y. W., Jo, H. Y., Kim, A. R., Noh, I., Kim, S., Kim, Y., Kim, C. A new multifunctional Schiff base as fluorescence sensor for Al^{3+} and colorimetric sensor for CN^- in aqueous media: an application to bioimaging. Dalton Transactions 43(2014): 6650-6659.

[19]   Kim, S., Noh, J. Y., Kim, K. Y., Kim, J. H., Kang, H. K., Nam, S. W., Kim, S. H., Park, S., Kim, C., Kim, J. Salicylimine-Based Fluorescent Chemosensor for Aluminum Ions and Application to Bioimaging. Inorganic Chemistry 51(2012): 3597-3602.

[20]   Song, E. J., Park, G. J., Lee, J. J., Lee, S., Noh, I., Kim, Y., Kim, S. J., Kim, C., Harrison, R. C. A fluorescence sensor for Zn^{2+} that also acts as a visible sensor for Co^{2+} and Cu^{2+}. Sensors and Actuators B: Chemical 213(2015): 268-275.

[21]   Li, Y., Liao, C., Huang, S., Xu, H., Zheng, B., Du, J., Xiao, D. A selective fluorescent probe based on bis-Schiff base for "turn-on" detection of Al^{3+} and cysteine by different mechanisms. RSC Advances 6(2016): 25420-25426.

[22]   Zyryanov, G. V., Palacios, M. A., Anzenbacher, P. Simple Molecule-Based Fluorescent Sensors for Vapor Detection of TNT. Organic Letters 10(2008): 3681-3684.

[23]   Yapici, I., Lee, K. S. S., Berbasova, T., Nosrati, M., Jia, X., Vasileiou, C., Wang, W., Santos, E. M., Geiger, J. H., Borhan, B. "Turn-On" Protein Fluorescence: In Situ Formation of Cyanine Dyes. Journal of the American Chemical Society 137(2015): 1073-1080.

[24]   Pickup, J. C., Hussain, F., Evans, N., D., Rolinski, O. J., Birch, D. J. S. Fluorescence-based glucose sensors. Biosensors and Bioelectronics 20(2005): 2555-2565.

[25]   Lakowicz, J. R. Principles of Fluorescence Spectroscopy; 3rd ed.;John Wiley & Sons Inc., Kluwer. (2006):

[26]   Wu, J., Liu, W., Ge, J., Zhang, H., Wang, P. New Sensing mechanisms for design of fluorescent chemosensors emerging in recent year. Chemical Society Reviews 40(2011): 3483-3495.

[27]   Jung, H. S., Verwilst, P., Kim, W. Y., Kim, J. S. Fluorescent and colorimetric sensors for the detection of humidity or water content. Chemical Society Reviews 45(2016): 1242-1256.

[28]   Vollmer, F., Rettig, W. Fluorescence loss mechanism due to large-amplitude motions in derivatives of 2,2′-bipyridyl exhibiting excited-state intramolecular proton transfer and perspectives of luminescence solar concentrators. Journal of Photochemistry and Photobiology A 95(1996): 143-155.

[29]   Catalan, J., Valle, J. C. Correction. Toward the Photostability Mechanism of Intramolecular Hydrogen Bond Systems. The Photophysics of 1'-Hydroxy-2'-acetonaphthone. Journal of the American Chemical Society 115(1993): 4321-4325.

[30]   Khan, A. U., Kasha, M. Singlet molecular oxygen in the Haber-Weiss reaction. Proc. Natl. Proceedings of the National Academy of Sciences 26(1994): 12365-12367.

[31]   Sytnik, A., Kasha, M. Proc. Excited-state intramolecular proton transfer as a fluorescence probe for protein binding-site static polarity. Proceedings of the National Academy of Sciences 18(1994): 8627-8630.

[32]   Guallar, V., Batista, V. S., Miller, W. H. Semiclassical molecular dynamics simulations of intramolecular proton transfer in photoexcited 2-(2' -hydroxyphenyl)-oxazole. Journal of Chemical Physics 113(21) (2000): 9510-9522.

[33]   Das, S. K., Dogra, J. Intramolecular Excited State Proton Transfer of 2-(2'-Hydroxyphenyl)benzimidazole in Nonionic Micelles: Tweens. Journal of Colloid and Interface Science 205(1998): 443-453.

[34]   Jayabharathi, J., Thanikachalam, V., Jayamoorthy, K., Srinivasan, N. Synthesis, spectral studies and solvatochromism of some novel benzimidazole derivatives - ESIPT process. Spectrochimica Acta Part A: Molecular and Biomolecular Spectroscopy 105(2013): 223-228.

[35]   Pandey, A., Kumar, A., Vishwakarma, S., Upadhyay, K. K. A highly specific 'turn-on' fluorescent detection of Mg^{2+} through a xanthene based fluorescent molecular probe. RSC Advances 6(2016): 6724-6729.

[36]   Goswami, S., Manna, A., Paul, S., Aich, K., Das, A. K., Chakraborty, S. Dual channel selective fluorescence detection of Al(III) and PPi in aqueous media with an "off–on–off" switch which mimics molecular logic gates (INHIBIT and EXOR gates). Dalton Transactions 42(2013): 8078-8085.

[37]   Meng, Q., Liu, H., Cheng, S., Cao, C., Rem, J. A novel molecular probe sensing polynuclear hydrolyzed aluminum by chelation-enhanced fluorescence. Talanta 99(2012): 464-470.

[38]   Lee, H., Lee, H. R. J. H., Handcock, R. D. Mechanism of "Turn-on" Fluorescent
        Sensors for Mercury(II) in Solution and Its Implications for Ligand Design.
        Inorganic Chemistry 51(2012): 10904-10915.

[39]   Jung, H. S., Ko, K. C., Lee, J. H., Kim, S. H., Bhuniya, S., Lee, J. Y., Kim, Y., Kim, S.
        J., Kim, J. S. Rationally Designed Fluorescence Turn-On Sensors: A New Design
        Strategy Based on Orbital Control. Inorganic Chemistry 49(2010): 8552-8557.

[40]   Fan, L., Li, T., Wang, B., Yang, Z., Liu, C. A colorimetric and turn-on fluorescent
        chemosensor for Al(III) based on a chromone Schiff-base. Spectrochimica Acta
        Part A: Molecular and Biomolecular Spectroscopy 118(2014): 760-764.

[41]   Qiu, B., Cao, L., Hu, R., Zhang, X., Yu, T., Chen, J., Yang, G., Li, Y. A colorimetric
        and ratiometric fluorescence sensor for sensitive detection of fluoride ions in
        water and toothpaste. RSC Advances 6(2016): 49158-49163.

[42]   Dai, N., Kool, E. T. Fluorescent DNA-based enzyme sensors. Chemical Society
        Reviews 40(2011): 5756-5770.

[43]   Minami, T., Esipenko, N. A., Zhang, B., Isaacs, L., Anzenbacher, P. ''Turn-on''
        fluorescent sensor array for basic amino acids in water. Chemical
        Communications 50(2014): 61-63.

[44]   Klockow, J. L., Hettie, K. S., Glass, T. E. ExoSensor 517: A Dual-Analyte
        Fluorescent Chemosensor for Visualizing Neurotransmitter Exocytosis. ACS
        Chemical Neuroscience 4(2013): 1334-1338.

[45]   Hettie, K. S., Liu, X., Gillis, K. D., Glass, T. E. Selective Catecholamine
        Recognition with NeuroSensor 521: A Fluorescent Sensor for the Visualization
        of Norepinephrine in Fixed and Live Cells. ACS Chemical Neuroscience
        4(2013): 918-923.

[46]   Dis, J. A. Aluminum and Alzheimer's disease: after a century of controversy, is
        there a plausible link?. Journal of Alzheimer's Disease 23(4) (2011): 567-598.

[47]   Kim, S. H., Choi, H. S., Kim, J., Lee, S. J., Quang, D. T., Kim, J. S. Novel
        optical/electrochemical selective 1, 2, 3-triazole ring-appended chemosensor
        for the Al3+ ion. Organic Letters 12(3) (2010): 560-563.

[48]   Wolf, F. I., Torsello, A., Fasanella, S., Cittadini, A. Cell physiology of
        magnesium. Molecular Aspects of Medicine 24(2003): 11-26.

[49]   Schmitz, C., Perraud, A., Johnson, C. O., Inabe, K., Smith, M. K., Penner, R.,
        Kurosaki, T., Fleig, A., Scharenberg, A. M. Regulation of vertebrate cellular
        Mg2+ homeostasis by TRPM7. Cell 114(2003): 345-351.

[50]   Sinha, S., Koner, R. R., Kumar, S., Mathew, J., V., M. P., Kazi, I., Ghosh, S. Imine
        containing benzophenone scaffold as an efficient chemical device to detect
        selectively Al^{3+}. RSC Advances 3(2013): 345-351.

[51]   Das, S., Goswami, S., Aich, K., Ghoshal, K., Quah, C. K., Bhattacharyya, M., Fun,
        H. ESIPT and CHEF based highly sensitive and selective ratiometric sensor for
        Al^{3+} with imaging in human blood cells. New Journal of Chemistry 39(2015):
        8582-8587.

[52]   Guo, A., Zhu, R., Ren, Y., Dong, J., Feng, L. A "turn-on" fluorescent
        chemosensor for aluminum ion and cell imaging application. Spectrochimica
        Acta Part A: Molecular and Biomolecular Spectroscopy 153(2016): 530-534.

[53]   Boonkitpatarakul, K., Wang, J., Niamnont, N., Liu, B., Mcdonald, L., Pang, Y.,
        Sukwattanasinitt, M. Novel Turn-On Fluorescent Sensors with Mega Stokes
        Shifts for Dual Detection of Al^{3+} and Zn^{2+}. ACS Sensors 1: 144-150.

[54]   Wang, G., Qin, J., Fan, L., Li, C., Yang, Z. A turn-on fluorescent sensor for highly
        selective recognition of Mg^{2+} based on new Schiff's base derivative. Journal of
        Photochemistry and Photobiology A: Chemistry 314(2016): 29-34.

[55]   Kao, M., Chen, T., Cai, Y., Hu, C., Liu, Y., Jhong, Y. A turn-onSchiff-base
        fluorescence sensor for Mg^{2+} ion and its practical application. Journal of
        Luminescence 169(2016): 156-160.

[56]   Noh, J. Y., Kim, S., Hwang, I. H., Lee, G. Y., Kang, J., Kim, S. H., Min, J., Park, S.,
        Kim, C., Kim, J. Solvent-dependent selective fluorescence assay of aluminum
        and gallium ions using julolidine-based probe. Dyes and Pigments 99(2013):
        1016-1021.

[57]   Park, G. J., Na, Y. J., Jo, H. Y., Lee, S. A., Kim, A. R., Noh, I., Kim, C. A single
        chemosensor for multiple analytes: fluorogenic detection of Zn^{2+} and OAc^{-}
        ions in aqueous solution, and an application to bioimaging. New Journal of
        Chemistry 38(2014): 2587-2594.

[58]   Ballesteros, E., Moreno, D., Gómez, T., Rodríguez, T., Rojo, J., Garíca-Valverde, M., Torroba, T. A New Selective Chromogenic and Turn-On Fluorogenic Probe for Copper(II) in Water-Acetonitrile 1:1 Solution. Organic Letters 11(2009): 1272-1369.

[59]   Xue, L., Liu, C., Liang, H. Highly Sensitive and Selective Fluorescent Sensor for Distinguishing Cadmium from Zinc Ions in Aqueous Media. Organic Letters 11(2009): 1655-1658.

[60]   Du, P., Lippard, S. J. A Highly Selective Turn-On Colorimetric, Red Fluorescent Sensor for Detecting Mobile Zinc in Living Cells. Inorganic Chemistry 49(2010): 10753-10755.

[61]   Du, H., Fuh, R. A., Li, J., Corkan, A., Lindsey, J. S. Photochem CAD: A Computer-aided design and research tool in photochemistry. Photochemistry and Photobiology 68(1998): 141-142.

[62]   Fery-Forgues, S., Lavabe, D. Are fluorescence quantum yields so tricky to measure a demonstration using familiar stationery products. Journal of Chemical Education 76(1999): 1260-1264.

[63]   Slater, J. C. Atomic Radii in Crystals. Journal of Chemical Physics 41(10) (1946): 3199-3204.

[64]   Valeur, B., Leray, I. design principles of Fluorescent molecular sensors for cation recognition. Coordination Chemistry Reviews 205(1) (2000): 3-40.

[65]   Barceló, J., Poschenrieder, C. Fast root growth responses, root exudates, and internal detoxification as clues the mechanisms of aluminium toxicity and resistance: a review. Environmental and Experimental Botany 48(1) (2002): 75-92.

[66]   Han, T., Feng, X., Tong, B., Shi, J., Chen, L., Zhi, J., Dong, Y. A novel "turn-on" fluorescent chemosensor for the selective detection of Al^{3+} based on aggregation-induced emission. Chemical Communications 48(3) (2012): 416-418.

[67]   Kumar, M., Puri, A. A review of permissible limits of drinking water. Indian. Journal of Occupational and Environmental Medicine 16(1) (2012): 40-44.

[68]   Cannan, R. K., Kibrick, A. Complex Formation between Carboxylic Acids and Divalent Metal Cations. <u>Journal of the American Chemical Society</u> 60(10) (1938): 2314-2320.

APPENDIX
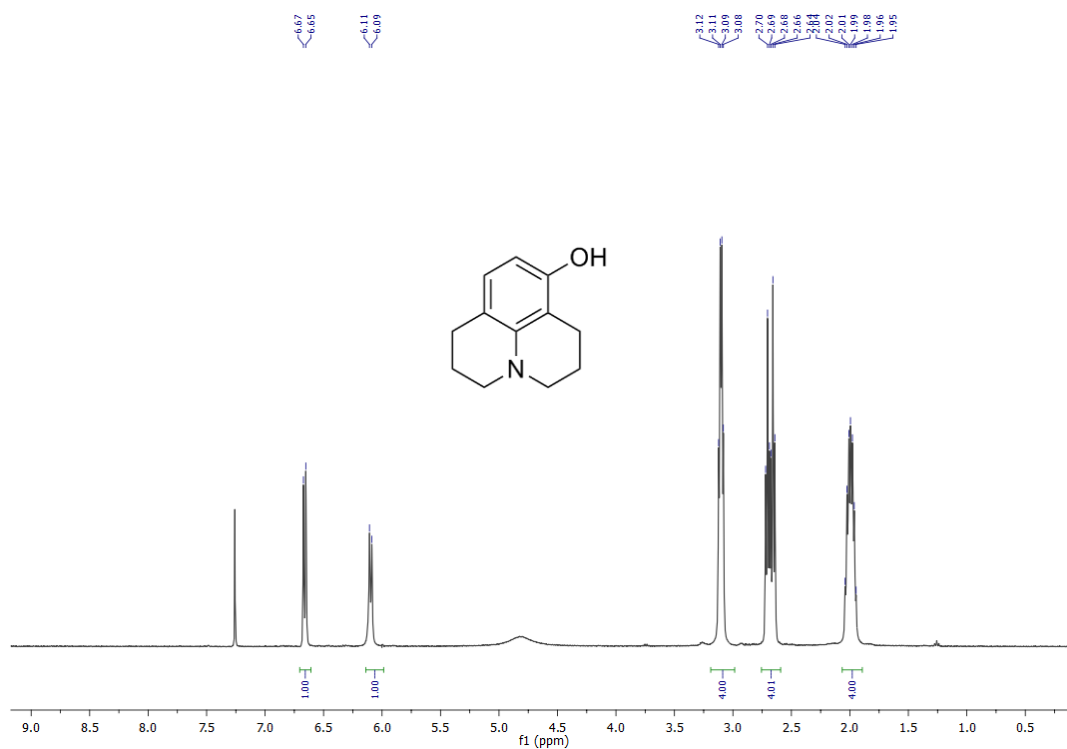
Figure A1 The ^{1}H NMR of 1,2,3,5,6,7-hexahydropyrido[3,2,1-ij]quinolin-8-ol (**JD-OH**) in CDCl$_3$.
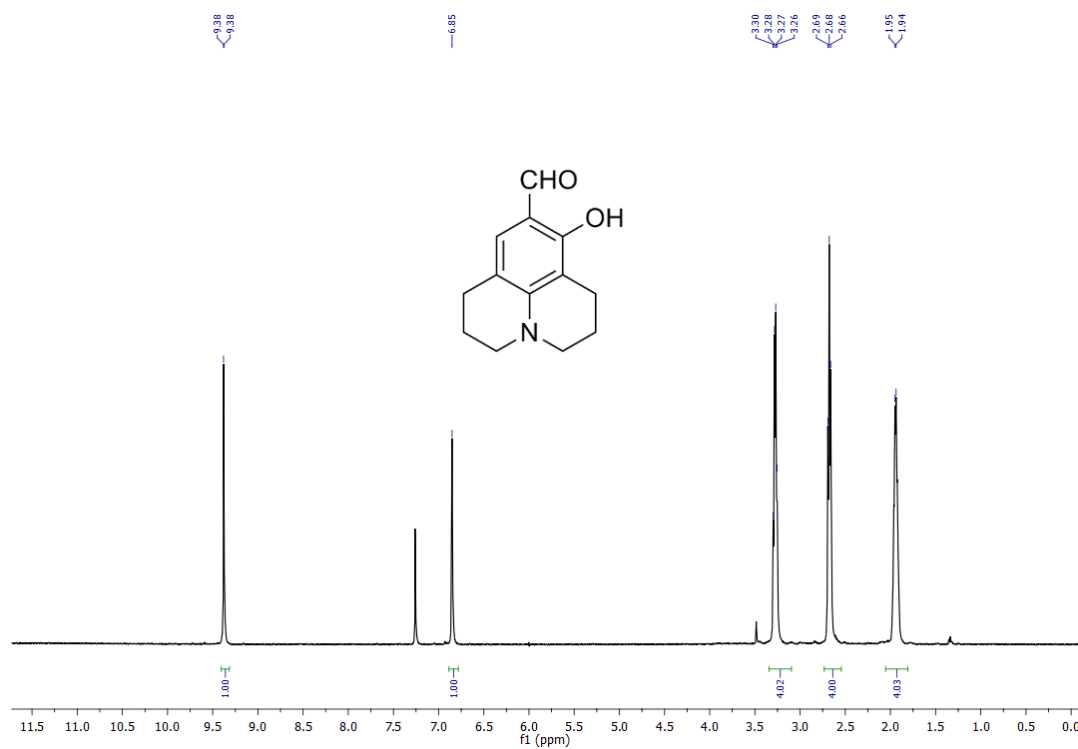
Figure A2 The ^{1}H NMR 8-hydroxy-1,2,3,5,6,7-hexahydropyrido[3,2,1-ij]quinoline-9-carbaldehyde (julolidine **1**) in CDCl$_3$.

Figure A3 The ^{1}H NMR of 2-[Bis(2-pyridyl methyl)aminomethyl]nitrobenzene (**2a**) in CDCl$_3$.

Figure A4 The ^{1}H NMR of 2-[Bis(2-pyridylmethyl)aminomethyl]aniline (**3a**) in CD$_3$OD.
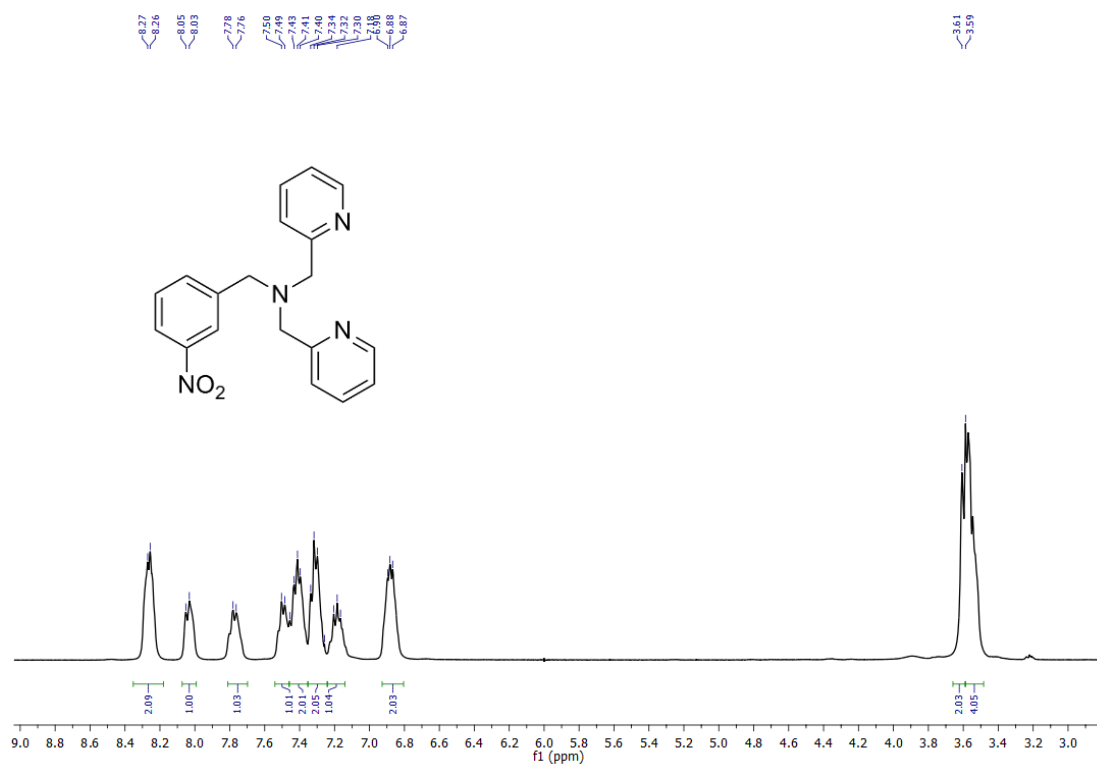
Figure A5 The ^{1}H NMR of 3-[Bis(2-pyridylmethyl)aminomethyl]nitrobenzene (**2b**) in CDCl$_3$.
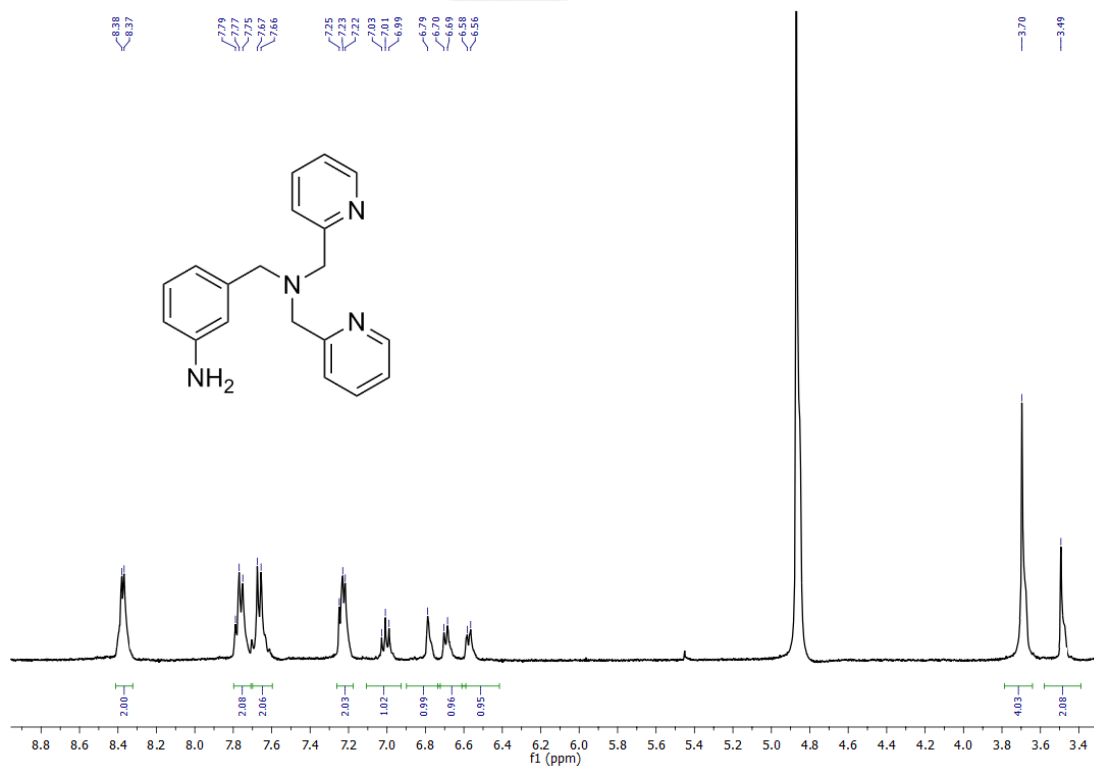
Figure A6 The ^{1}H NMR of 3-[Bis(2-pyridylmethyl)aminomethyl]aniline (**3b**) in CD$_3$OD.
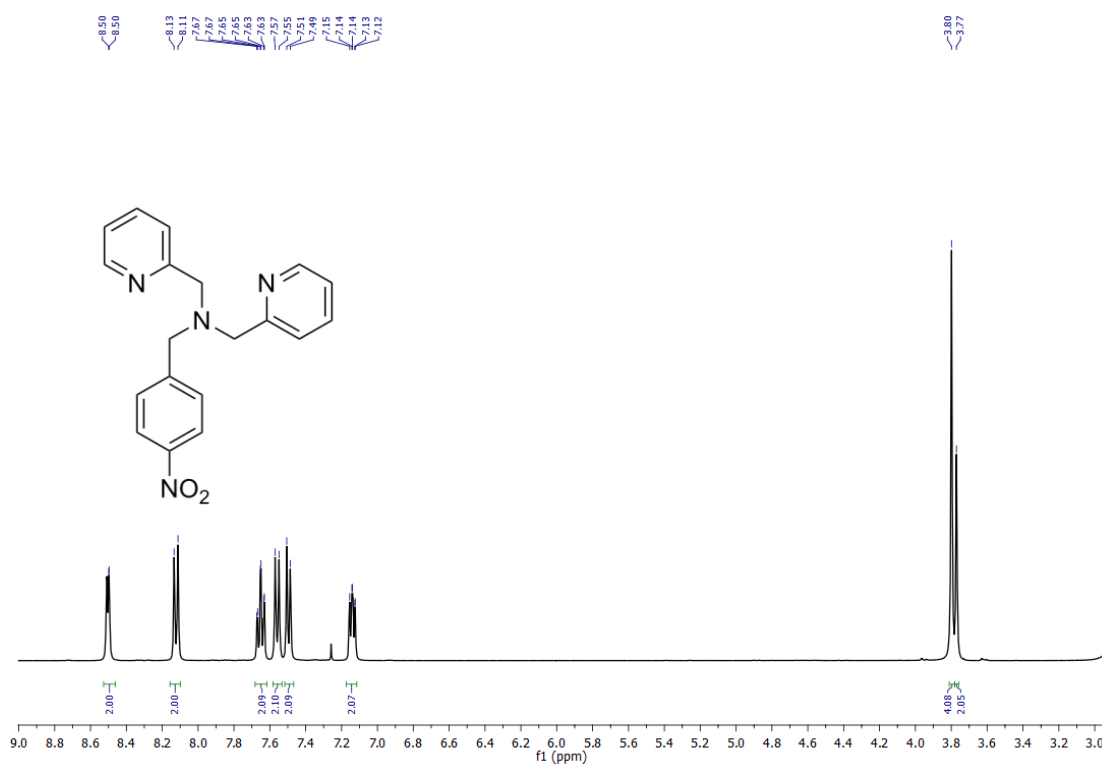
Figure A7 The ^1H NMR of 4-[Bis(2-pyridylmethyl)aminomethyl]nitrobenzene (**2c**) in CDCl₃.
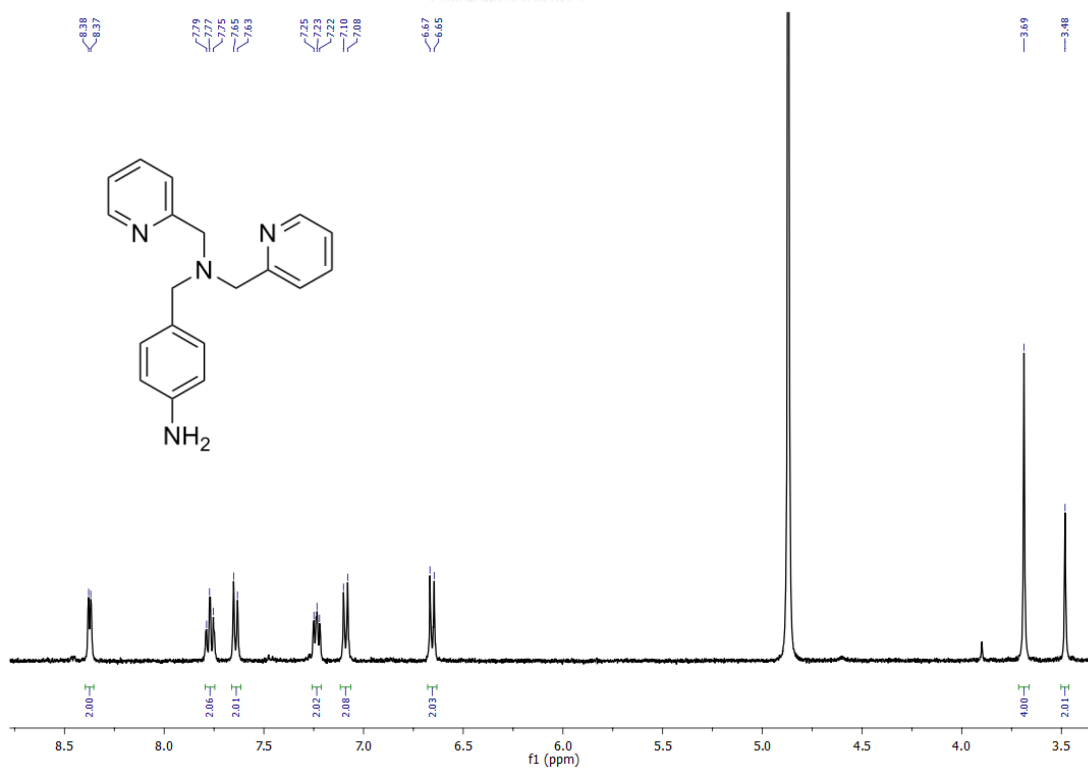
Figure A8 The ^1H NMR of 4-[Bis(2-pyridylmethyl)aminomethyl]aniline (**3c**) in CD₃OD.
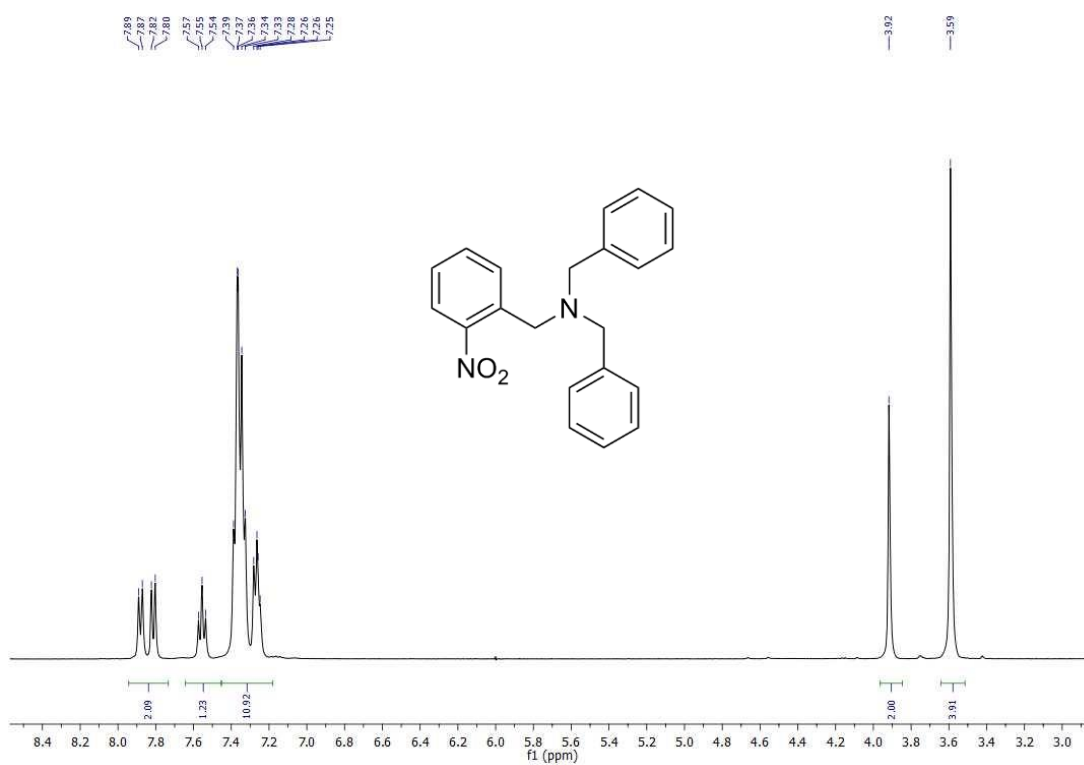
Figure A9 The ^{1}H NMR of *N,N*-dibenzyl-1-(2-nitrophenyl)methanamine (**2d**) in CDCl$_3$.
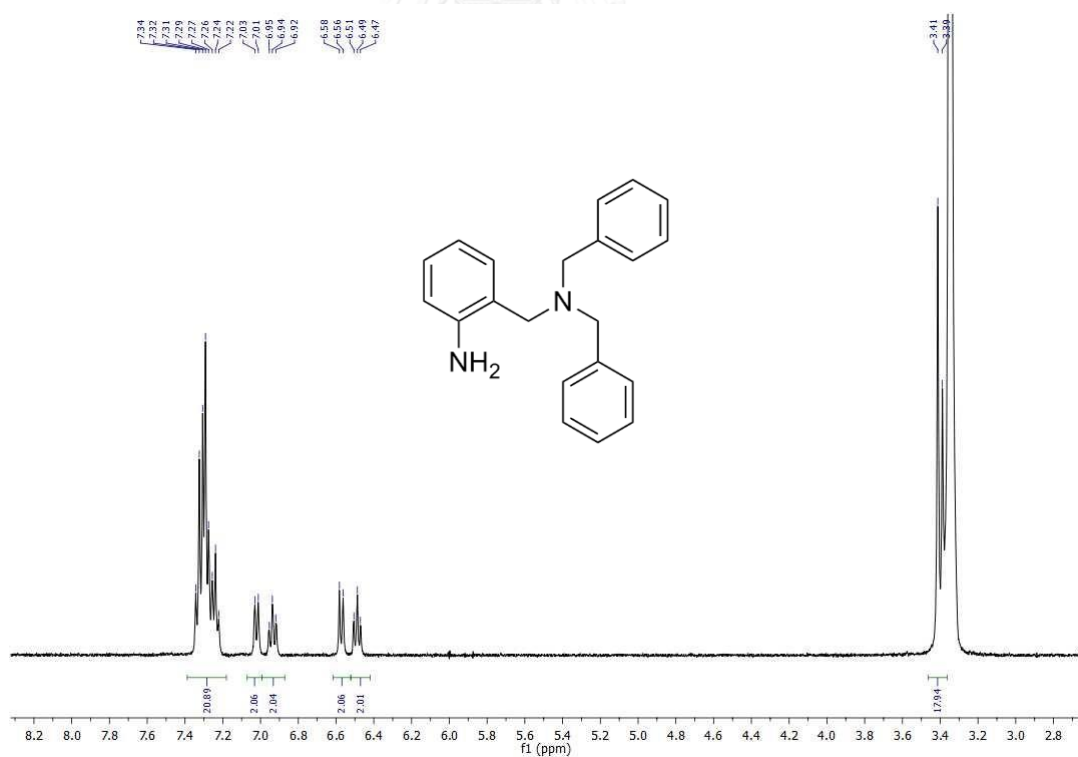
Figure A10 The ^{1}H NMR of 2-((dibenzylamino)methyl)aniline (**3d**) in DMSO-*d$_6$*.
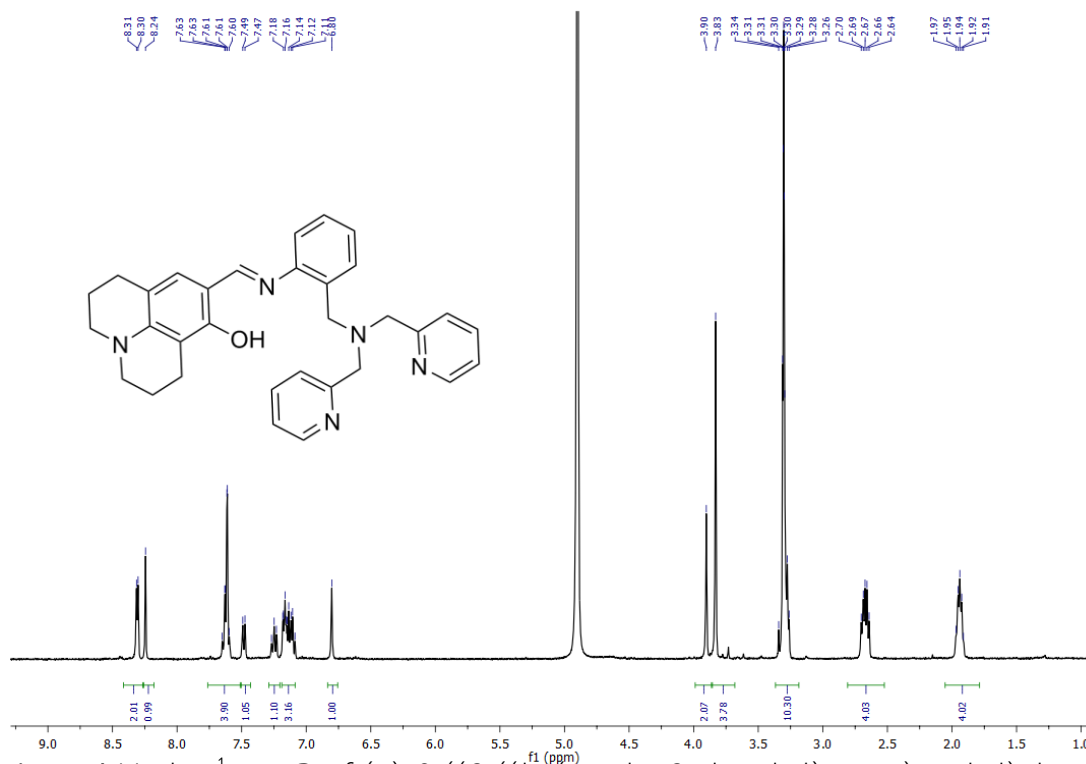
Figure A11 The ^{1}H NMR of (E)-9-((2-((bis(pyridin-2-ylmethyl)amino)methyl)phenyl imino)methyl)-1,2,3,5,6,7 hexahydropyrido[3,2,1-ij]quinolin-8-ol (**J2P**) in CD$_3$OD.
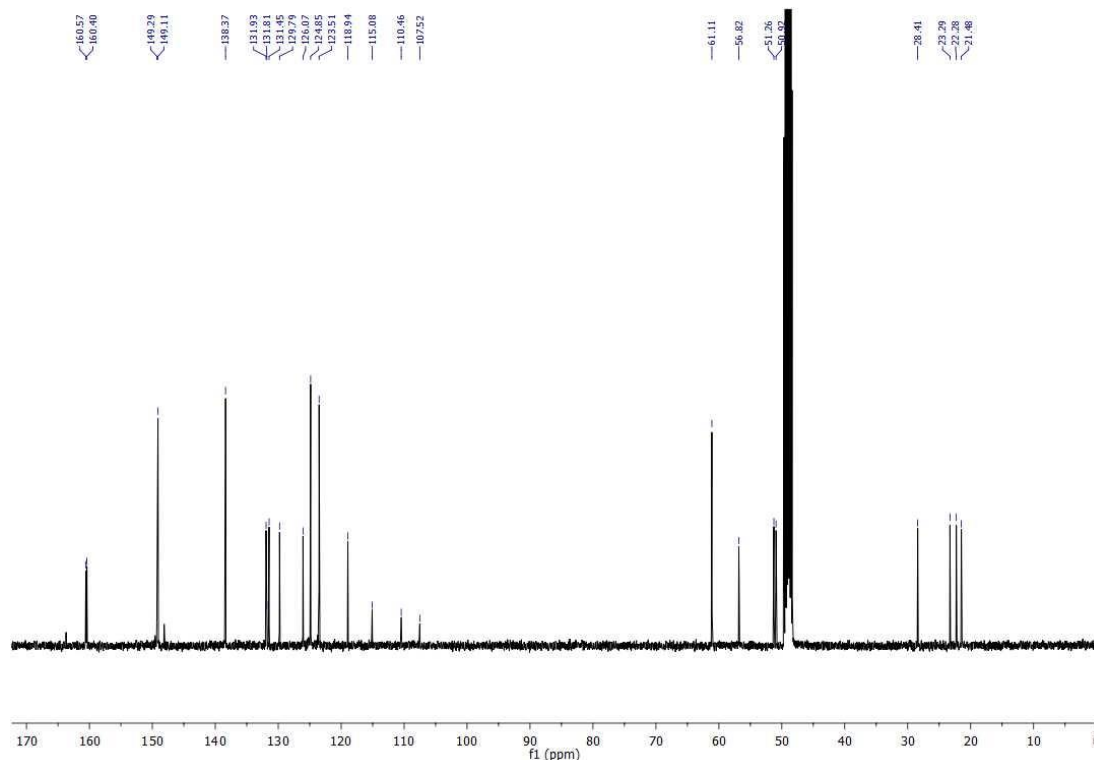
Figure A12 The ^{13}C NMR of (E)-9-((2-((bis(pyridin-2-ylmethyl)amino)methyl)phenyl imino)methyl)-1,2,3,5,6,7 hexahydropyrido[3,2,1-ij]quinolin-8-ol (**J2P**) in CD$_3$OD.
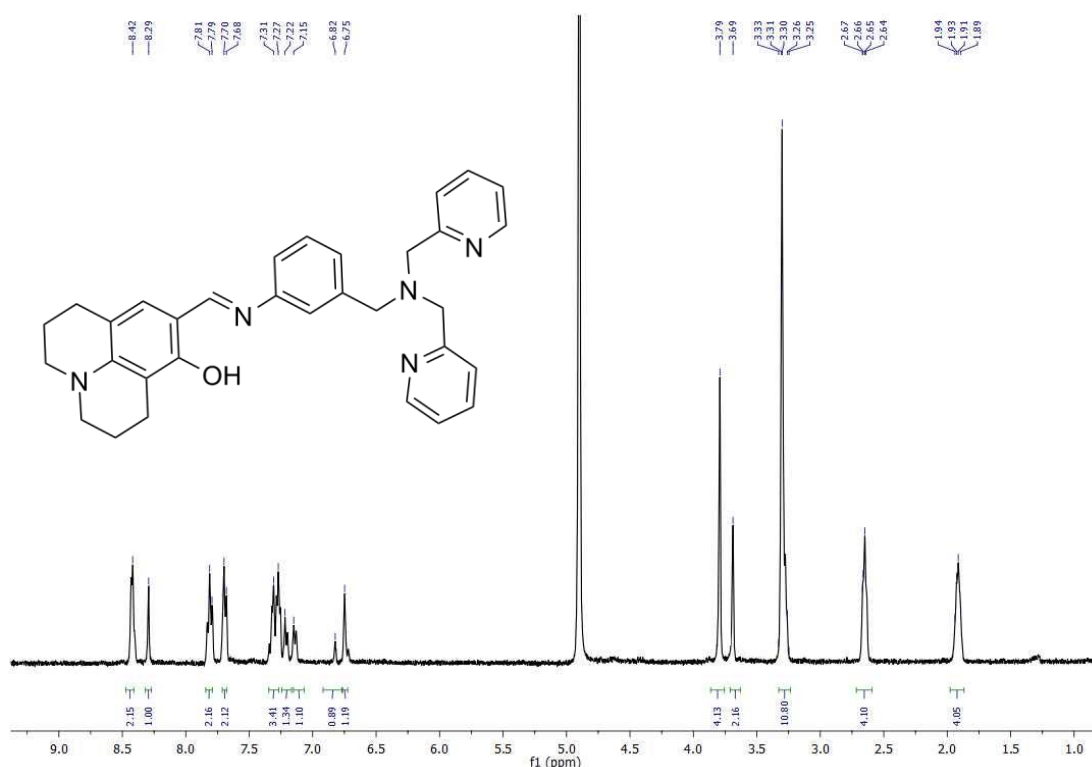
Figure A13 The ^{1}H NMR of (E)-9-((3-((bis(pyridin-2-ylmethyl)amino)methyl)phenyl imino)methyl)-1,2,3,5,6,7-hexahydropyrido[3,2,1-ij]quinolin-8-ol (**J3P**) in CD$_3$OD.
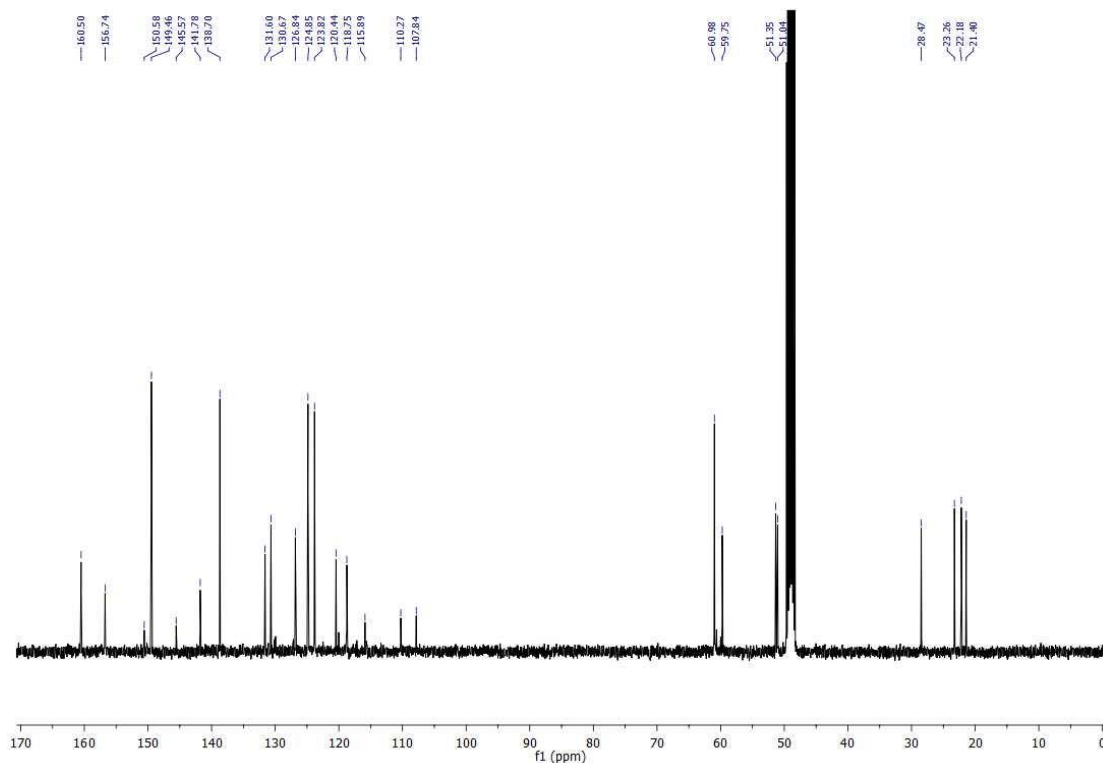
Figure A14 The ^{13}C NMR of (E)-9-((3-((bis(pyridin-2-ylmethyl)amino)methyl)phenyl imino)methyl)-1,2,3,5,6,7-hexahydropyrido[3,2,1-ij]quinolin-8-ol (**J3P**) in CD$_3$OD.
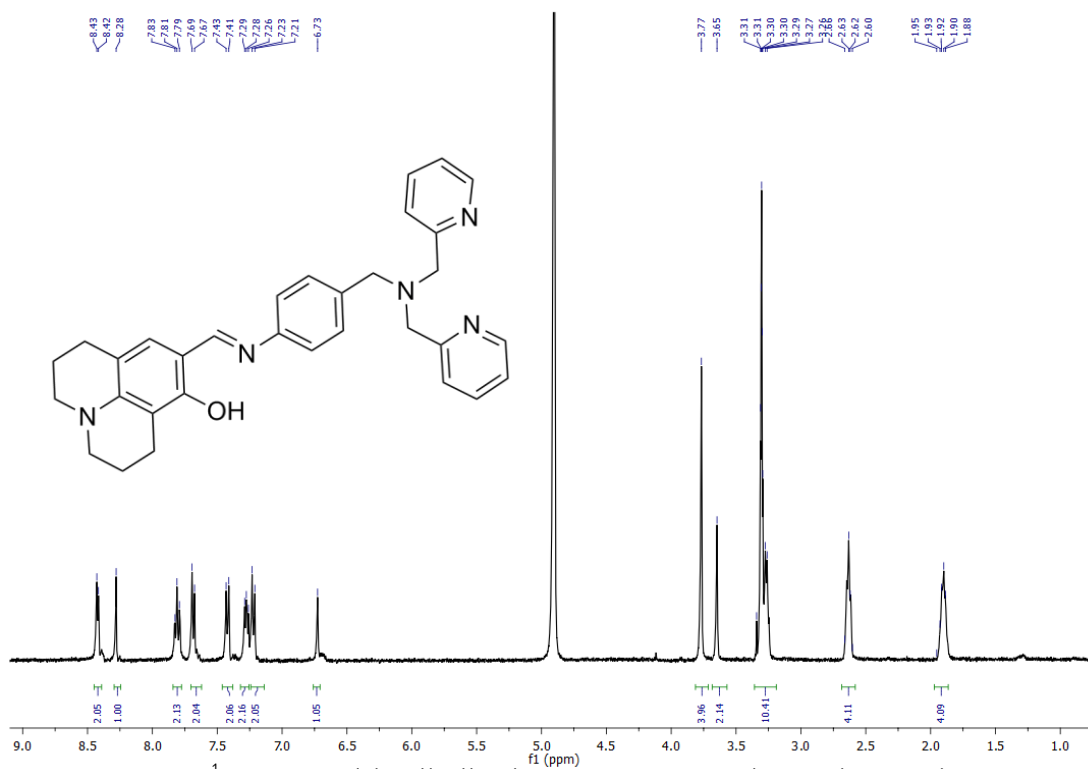
Figure A15 The ^{1}H NMR of (E)-9-((4-((bis(pyridin-2-ylmethyl)amino)methyl)phenyl imino)methyl)-1,2,3,5,6,7-hexahydropyrido[3,2,1-ij]quinolin-8-ol (**J4P**) in CD$_3$OD.
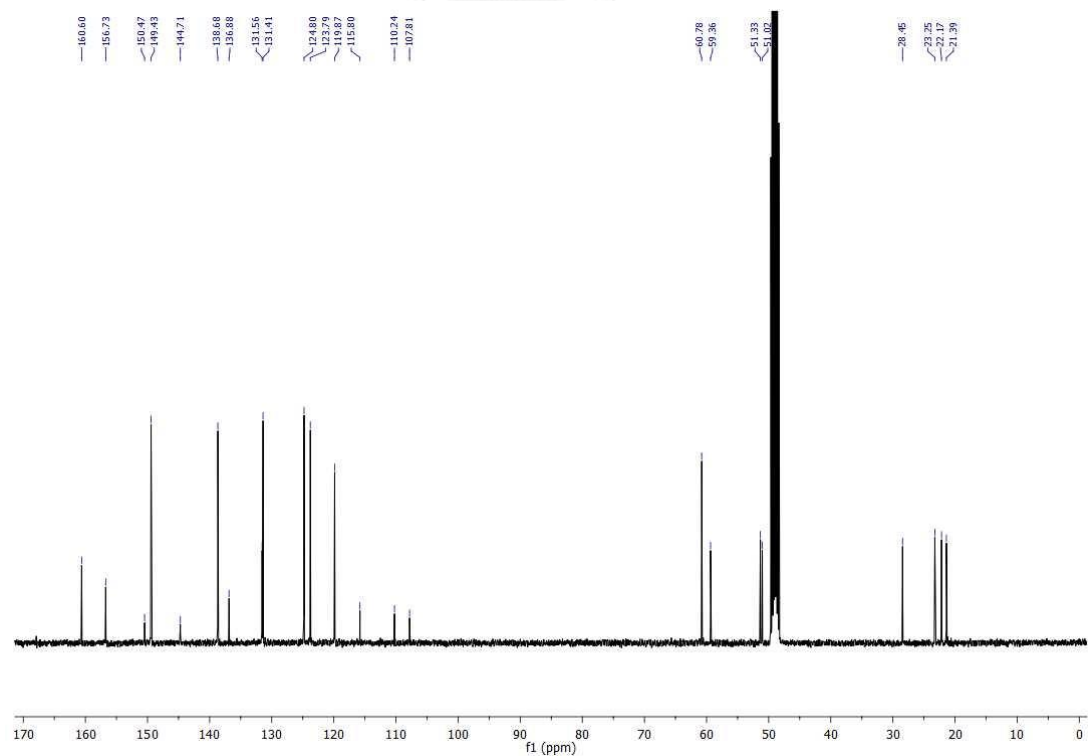
Figure A16 The ^{13}C NMR of (E)-9-((4-((bis(pyridin-2 ylmethyl)amino)methyl)phenyl imino)methyl)-1,2,3,5,6,7-hexahydropyrido[3,2,1-ij]quinolin-8-ol (**J4P**) in CD$_3$OD.
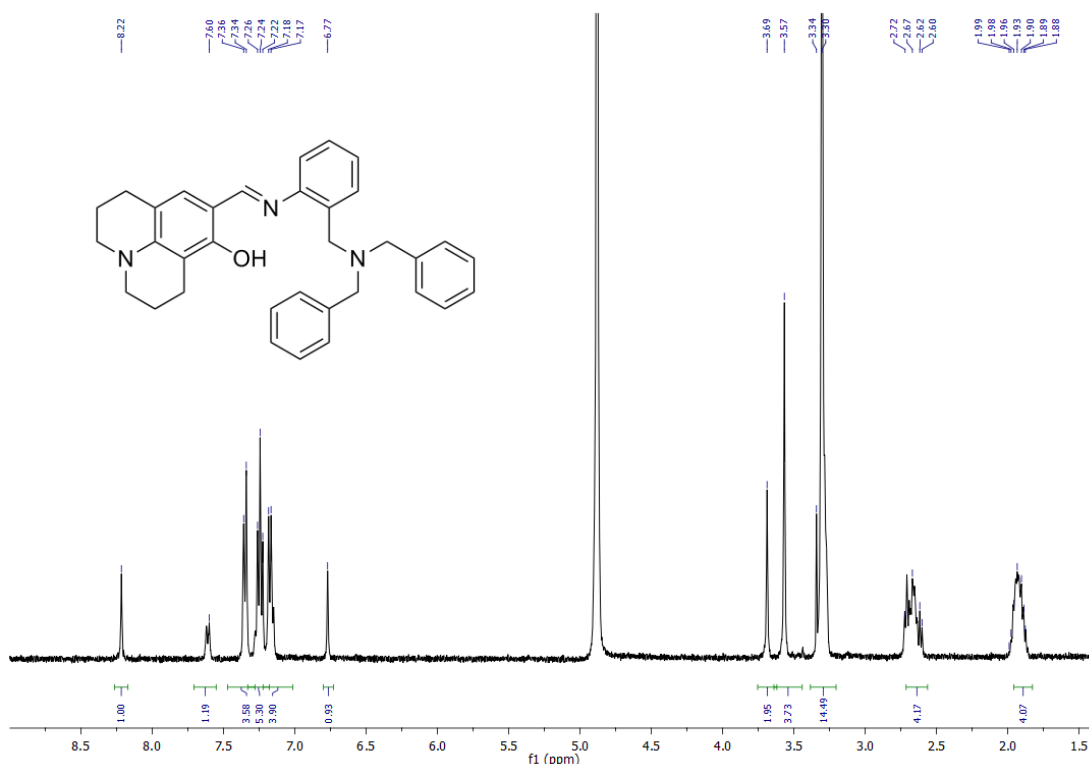
Figure A17 The ^{1}H NMR of (E)-9-((2-((dibenzylamino)methyl)phenylimino)methyl)-1,2,3,5,6,7-hexahydro-pyrido[3,2,1-ij]quinolin-8-ol (**J2B**) in CD$_3$OD.
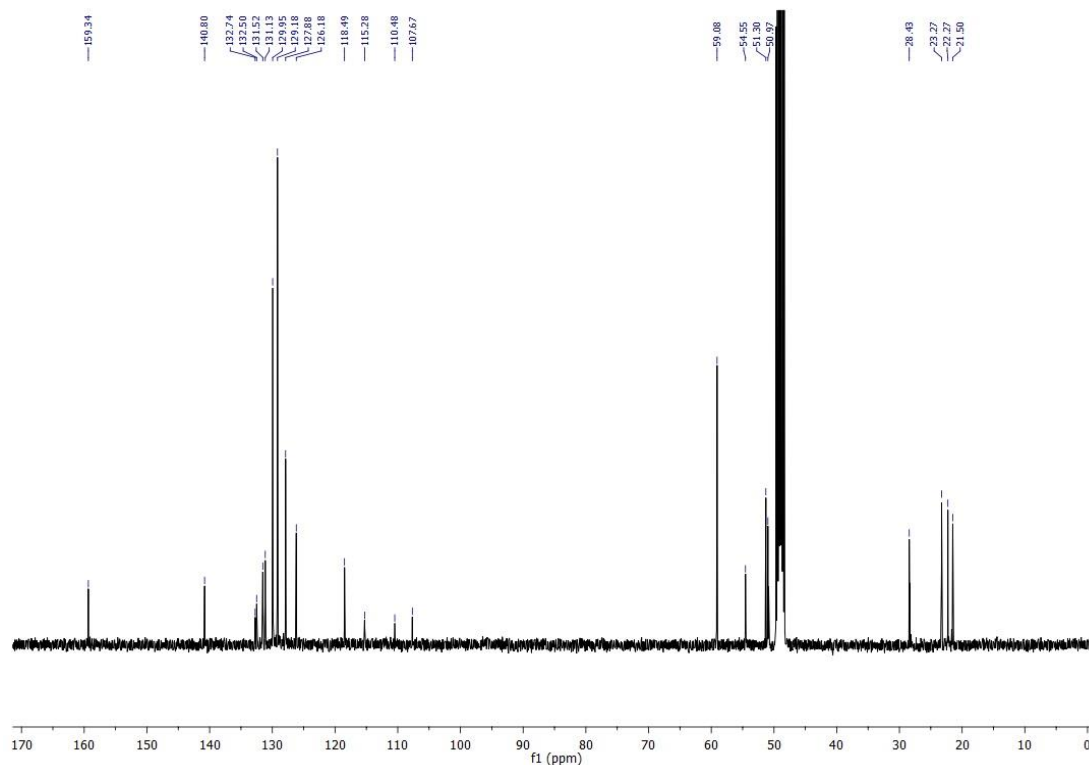
Figure A18 The ^{13}C NMR of (E)-9-((2-((dibenzylamino)methyl)phenylimino)methyl)-1,2,3,5,6,7-hexahydro-pyrido[3,2,1-ij]quinolin-8-ol (**J2B**) in CD$_3$OD.

Mass Spectrum SmartFormula Report

Analysis Info

Analysis Name	D:\Data\Vachiraporn\ESI\VA-HRMS-05. (pos).d	Acquisition Date	11/2/2015 12:36:16 PM
Method	tune_wide.m	Operator	RU
Sample Name	JD-2DP	Instrument	micrOTOF 8213750.10411
Comment			

Acquisition Parameter

Source Type	ESI	Ion Polarity	Positive	Set Nebulizer	0.4 Bar
Focus	Not active			Set Dry Heater	180 °C
Scan Begin	50 m/z	Set Capillary	4500 V	Set Dry Gas	4.0 l/min
Scan End	3000 m/z	Set End Plate Offset	-500 V	Set Divert Valve	Waste

Meas. m/z	# Ion Formula	m/z	err [ppm]	Mean err [ppm]	rdb	N-Rule Conf	e⁻	mSigma	Std I	Std Mean m/z	Std I VarNo rm	Std m/z Diff	Std Comb Dev
504.275798	1 C32H34N5O	504.275787	0.0	0.3	18.5	ok even		4.0	6.8	0.8	3.8	0.9	842.7
	2 C31H38NO5	504.274450	-2.7	-2.2	13.5	ok even		10.7	17.2	1.4	5.7	1.1	925.8
	1 C32H34N5O	504.275787	0.0	0.3	18.5	ok even		4.0	6.8	0.8	3.8	0.9	842.7
	2 C31H38NO5	504.274450	-2.7	-2.2	13.5	ok even		10.7	17.2	1.4	5.7	1.1	925.8
	1 C30H35N5NaO	504.273381	4.8	-4.5	15.5	ok even		11.4	20.9	2.4	7.4	0.9	842.7
	2 C29H39NNaO5	504.272044	-7.4	-7.0	10.5	ok even		21.9	35.7	3.6	11.3	1.1	917.9
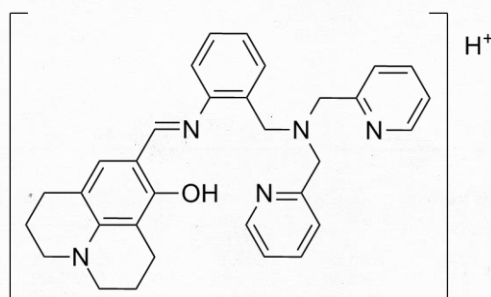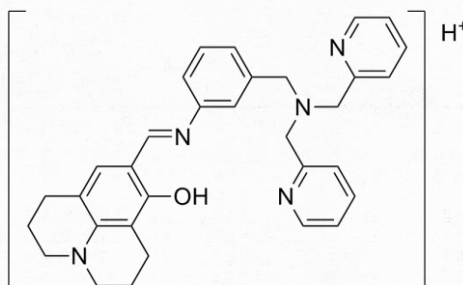
Chemical Formula: $C_{32}H_{34}N_5O^+$
Exact Mass: 504.2758

Figure A19 The HRMS of (E)-9-((2-((bis(pyridin-2-ylmethyl)amino)methyl)phenyl imino)methyl)-1,2,3,5,6,7 hexahydropyrido[3,2,1-ij]quinolin-8-ol (**J2P**)

Figure A20 The HRMS of (E)-9-((3-((bis(pyridin-2-ylmethyl)amino)methyl)phenyl imino)methyl)-1,2,3,5,6,7 hexahydropyrido[3,2,1-ij]quinolin-8-ol (**J3P**)

Mass Spectrum SmartFormula Report

Analysis Info

		Acquisition Date	11/2/2015 12:31:26 PM
Analysis Name	D:\Data\Vachiraporn\ESI\VA-HRMS-04. (pos).d		
Method	tune_wide.m	Operator	RU
Sample Name	JD-4DP	Instrument	micrOTOF 8213750.10411
Comment			

Acquisition Parameter

Source Type	ESI	Ion Polarity	Positive	Set Nebulizer	0.4 Bar	
Focus	Not active			Set Dry Heater	180 °C	
Scan Begin	50 m/z	Set Capillary	4500 V	Set Dry Gas	4.0 l/min	
Scan End	3000 m/z	Set End Plate Offset	-500 V	Set Divert Valve	Waste	

Meas. m/z	#	Ion Formula	m/z	err [ppm]	Mean err [ppm]	rdb	N-Rule Conf	e⁻	mSigma	Std I	Std Mean m/z	Std I VarNo rm	Std m/z Diff	Std Comb Dev
526.258855	1	C33H36NO5	526.258800	-0.1	0.3	16.5	ok	even	6.0	8.2	0.4	3.7	0.8	677.5
	2	C34H32N5O	526.260137	-2.4	2.7	21.5	ok	even	8.7	13.1	1.4	4.6	0.6	842.7
	3	C29H32N7O3	526.256114	5.2	-5.1	17.5	ok	even	15.8	24.2	2.7	7.6	0.3	937.5
	1	C33H36NO5	526.258800	-0.1	0.3	16.5	ok	even	6.0	8.2	0.4	3.7	0.8	677.5
	2	C34H32N5O	526.260137	-2.4	2.7	21.5	ok	even	8.7	13.1	1.4	4.6	0.6	842.7
	3	C29H32N7O3	526.256114	5.2	-5.1	17.5	ok	even	15.8	24.2	2.7	7.6	0.3	937.5
	1	C32H33N5NaO	526.257731	-2.1	-1.9	18.5	ok	even	3.9	6.1	1.0	2.5	0.6	842.7
	2	C31H37NNaO5	526.256394	-4.7	-4.3	13.5	ok	even	15.1	21.9	2.3	7.0	0.8	975.3
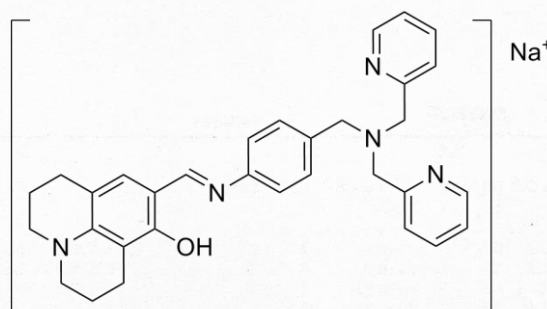
Chemical Formula: C$_{32}$H$_{33}$N$_5$NaO$^+$
Exact Mass: 526.2577

Bruker Compass DataAnalysis 4.1   printed: 11/2/2015 7:33:25 PM   by: RU   1 of 1

Figure A21 The HRMS of (E)-9-((4-((bis(pyridin-2-ylmethyl)amino)methyl)phenyl imino)methyl)-1,2,3,5,6,7 hexahydropyrido[3,2,1-ij]quinolin-8-ol (**J4P**)

Mass Spectrum SmartFormula Report

Analysis Info

| | | | | Acquisition Date | 6/12/2016 5:09:04 PM |

Analysis Name   D:\Data\Apichart\ESI\AS-HRMS 325 (pos).d

Method   tune_wide.m

Sample Name   J2B

Comment

Operator   RU

Instrument   micrOTOF   8213750.10411

Acquisition Parameter

Source Type	ESI	Ion Polarity	Positive	Set Nebulizer	0.4 Bar
Focus	Not active			Set Dry Heater	180 °C
Scan Begin	50 m/z	Set Capillary	4500 V	Set Dry Gas	4.0 l/min
Scan End	3000 m/z	Set End Plate Offset	-500 V	Set Divert Valve	Waste

Intens. x10^5   +MS, 0.2min #9

1+ 502.2851
1+ 521.3809
1+ 493.3495
1+ 549.4131
1+ 532.2738 +537.3548
473.4252
565.3789 577.4481 591.4927
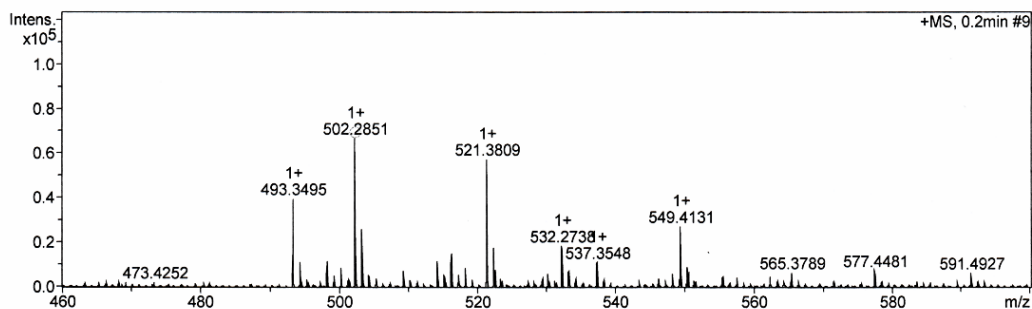
Meas. m/z	#	Ion Formula	m/z	err [ppm]	Mean err [ppm]	rdb	N-Rule Conf	e⁻	mSigma	Std I a	Std Mean m/z	Std I VarNo rm	Std m/z Diff	Std Comb Dev
502.285148	1	C34H36N3O	502.285289	-0.3	0.8	18.5	ok	even	6.7	9.6	0.6	5.2	0.8	636.9
	2	C32H37N3NaO	502.282884	4.5	-4.0	15.5	ok	even	16.7	25.4	2.0	8.8	0.8	842.7
	3	C29H36N5O3	502.281266	7.7	-7.3	14.5	ok	even	28.8	44.1	3.7	14.3	0.6	935.7
	1	C32H37N3NaO	502.282884	4.5	-4.0	15.5	ok	even	16.7	25.4	2.0	8.8	0.8	842.7
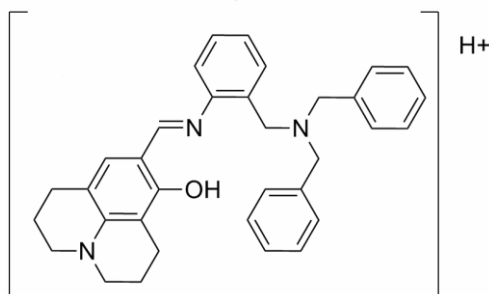
Chemical Formula: $C_{34}H_{36}N_3O^+$

Exact Mass: 502.2853

Bruker Compass DataAnalysis 4.1   printed: 6/12/2016 5:41:59 PM   by: RU   1 of 1

Figure A22 The HRMS of (E)-9-((2-((dibenzylamino)methyl)phenylimino)methyl)-1,2,3,5,6,7-hexahydro-pyrido[3, 1-ij]quinolin-8-ol (**J2B**)

VITA

Mr. Thanaphong Lertpiriyasakulkit was born on May 28th, 1990 in Nakhon Ratchasima, Thailand. He received a Bachelor's Degree of Science, majoring in chemistry, from faculty of Science, Chulalongkorn University in 2012. He had been a graduate student in the program of Prtrochemistry and Polymer Science, Faculty of Science, Chulalongkorn University as well as become a member of Material Advancement via Proficient Synthesis group (MAPS) under supervision of Assistant Professor Dr. Anawat Ajavakom. He had got the proceeding along with the poster presentation of his research in Pure and Applied Chemistry International Conference (PACCON 2016) then completed a Master's Degree in Prtrochemistry and Polymer Science in academic year 2015.

His present address is 10/36 Ladprao 10, Lardrao road, Jompol, Jatujak, Bangkok, Thailand 10900.